National Library of Canada

Acquisitions and Bibliographic Services Branch

395 Wellington Street
Ottawa, Ontario
K1A 0N4

Bibliothèque nationale du Canada

Direction des acquisitions et des services bibliographiques

395, rue Wellington
Ottawa (Ontario)
K1A 0N4

Your file Votre référence

Our file Notre référence

NOTICE

The quality of this microform is heavily dependent upon the quality of the original thesis submitted for microfilming. Every effort has been made to ensure the highest quality of reproduction possible.

If pages are missing, contact the university which granted the degree.

Some pages may have indistinct print especially if the original pages were typed with a poor typewriter ribbon or if the university sent us an inferior photocopy.

AVIS

La qualité de cette microforme dépend grandement de la qualité de la thèse soumise au microfilmage. Nous avons tout fait pour assurer une qualité supérieure de reproduction.

S'il manque des pages, veuillez communiquer avec l'université qui a conféré le grade.

La qualité d'impression de certaines pages peut laisser à désirer, surtout si les pages originales ont été dactylographiées à l'aide d'un ruban usé ou si l'université nous a fait parvenir une photocopie de qualité inférieure.

Canada

Speckle Noise Reduction of Synthetic Aperture Radar Imagery using Kalman Filters

by

Gary W. Geling

A thesis submitted to the
School of Graduate Studies and Research
in partial fulfillment of the requirements for the degree of

Masters of Applied Science

Ottawa-Carleton Institute for Electrical Engineering
Department of Electrical Engineering
Faculty of Engineering
University of Ottawa
July 1995

National Library of Canada

Acquisitions and Bibliographic Services Branch

395 Wellington Street
Ottawa, Ontario
K1A 0N4

Bibliothèque nationale du Canada

Direction des acquisitions et des services bibliographiques

395, rue Wellington
Ottawa (Ontario)
K1A 0N4

Your file Votre référence

Our file Notre référence

ISBN 0-612-07796-9

Canada

UNIVERSITÉ D'OTTAWA
UNIVERSITY OF OTTAWA

ABSTRACT

Synthetic aperture radar(SAR) imagery is gaining increased usage as more systems become available and more applications are being developed. An "unfortunate" problem with SAR imagery is the high level of noise, often called speckle. The speckle effects reduce the utility of SAR imagery a great deal. This thesis will address the causes of speckle and many of the current methods that are used to reduce the speckle noise. Kalman filtering methods will then be adapted for use on SAR imagery taking into account the special properties of this type of filter and images.

ACKNOWLEDGEMENT

I wish to express my sincere gratitude to my supervisor, Dr. Dan Ionescu, for his constant guidance, encouragement, and support throughout my research.

I thank the Department of National Defence for funding my education leave so that I might pursue further research and the Canadian Centre of Remote Sensing for the support of this study through the provision of ERS-1 image data under DSS contract #18SR23413-2-7100.

I would like to thank the faculty and staff of the Department of Electrical Engineering, University of Ottawa, for their kindness and support.

Above all I would like to thank my friends and family for their constant support and especially my wife, Carrie, for her love and caring. She and our new baby, James, have kept me happy and sane when all else seemed dull and dreary.

Contents

List of Tables

List of Figures

Notation

Various symbols, superscripts, subscripts, and abbreviations used frequently in this thesis are summarized below. All notation is fully defined where it first arises in the text.

Symbols

$\mathcal{I}_{16}$	Integers quantized to 16 bits.
$\mathcal{E}(\ )$	The mathematical expectation.
$x(i,j)$	The state values of the image.
$\mathbf{X}$	Block state space value of image.
$y(i,j)$	The observed values of the image.
$\mathbf{Y}$	Block state space value of observed image.
$\mathbf{I}$	Identity matrix
$\zeta^o(\mathbf{R})$	Mean backscatter received from transmitted radar.
$P(\ )$	Probability distribution.
$Z(t)$	Innovation/Estimation error.
K	Kalman gain.
$\mathcal{L}$	Parameter estimation gain.

$P^{(i)}$	Error Covariance of Kalman Filter.
$\mathcal{R}$	Approximation of Hessian of quadratic norm.
R_z	Covariance of innovation process.
C_o	Coefficient of variation.
C_r	Contrast Ratio.

Greek Letters

γ/Γ	Multiplicative observation noise
ψ/Ψ	Multiplicative dynamic process noise
μ_x	The mean of the value x
σ_x^2	Statistical variance of x
Σ_a	Estimation derivative
Φ	Parameter vector
Δ	Gradient
κ	Derivative of Kalman Gain
λ	Forgetting Factor

Special Symbols

$\bar{x}$	The mean of the value x
$\hat{x}$	The estimate of the value x
z^{-1}	Spatial shift operator

Acronyms and Definitions

2-D	Two Dimensional
AR	Auto-regressive
ABKF	Adaptive Block Kalman Filter
ENL	Equivalent Number of Looks
SAR	Synthetic Aperture Radar.
RUPK	Reduced Update Kalman filter
NSHP	Non-Symmetric Half Plane
LSI	Linear Space Invariant
RPE	Recursive Parameter Estimation
EKF	Extended Kalman Filter
MAP	Maximum A Posteriori

MMSE	Minimum Mean Square Error
LLMMSE	Localy Linear Minimum Mean Square Error
SNR	Signal to Noise Ratio

Chapter 1

Introduction

In this thesis Kalman filtering techniques are applied to reduce speckle noise in synthetic aperture radar(SAR) images. Synthetic aperture radar images suffer from speckle noise that greatly impair their utilization. Current filtering techniques for the processing of SAR imagery are examined. Existing two-dimensional Kalman filter based techniques are also examined. Problems with existing Kalman filter techniques are identified and several variations are derived. These modified Kalman filters are implemented and compared with both previous Kalman filtering techniques and one of the most common speckle reduction methods, the Lee filter.

1.1 Rationale

The observation of the Earth from some safe high ground has always been an important task from the earliest times in human history. The high ground has been extended from trees to early observation balloons, reconnaissance aircraft, and finally to cameras in space. This desire to view the earth has extended to the observation of things in ways that could never be achieved with our own eyesight. Observation using radiation invisible to the human eye is also becoming very important. It is the ability of radar imagery to penetrate most atmospheric barriers to observation that makes it very desirable. The capability of synthetic aperture radar (SAR) images to give reasonable detail from hundreds of miles above the Earth's surface in all weather conditions makes it absolutely essential to many who study the Earth's surface[9].

As we use different parts of the electro-magnetic spectrum to observe the earth, we often loose sight of how these differ from our normal sight capabilities. SAR imagery is typically very difficult to interpret for this reason. The most significant difficulty in using SAR imagery is the high degree of noise that is found in the images. It is not uncommon for an image to contain as much noise as information. In images such as SAR, this noise is referred to as speckle noise.

The speckle noise present in SAR imagery results in the poor performance of many existing techniques for the detection of edges [31],[17], and the classification of regions[35],[23],[15],[42]. The utility of SAR images may be greatly improved by

the removal of this speckle noise. Speckle noise is created in an image by both the properties of the illuminating radar beam and the objects being imaged. Due to the complexity of the SAR image formation process and the complexity of the scenes that are imaged, the process of removing the noise can be extremely difficult. Some people have taken simple assumptions about the properties of the image and developed ad-hoc/simple methods for noise reduction. Many others have derived statistical models of SAR imagery and used these to develop methods of reducing the high noise levels caused by the properties of the illuminating radar beam and the objects being imaged. Speckle noise is most commonly modeled as a noise term multiplied by the input signal, ie. multiplicative noise, when the speckle is said to be "fully developed". Methods have also been developed that attempt to take advantage of the statistics available from the image itself and approximate an image formation process that is used to determine how to remove the noise.

One such method that utilizes the image statistics is Kalman filtering. Kalman filtering is commonly used to determine linear approximations to dynamic systems in the presence of noise. The advantages of Kalman filters include the ability to determine an optimal estimate in the mean squared error, the ability to adapt to changing conditions in the input using the input statistics, and the ability to measure filter performance by monitoring several filter values such as the gain matrix. It is possible to model the SAR image as a two dimensional dynamic process such that each pixel is related to all the previous pixels. Using this model and a description of the noise in the system, a Kalman filter can be used to filter the image and reduce the noise present. In many instances, the noise statistics of an image are considered

unchanging over the entire image, ie. globally stationary. It is possible to also consider the noise as being only consistent over subregions or locally stationary. Azimi-Sadjadi et al [5] developed a Kalman filter for speckle noise reduction in SAR images.

When using the Kalman filter or any other filter with an auto-regressive model, it is not always known what the relationship between the current location is to the following locations. In these cases, it is necessary to estimate the parameters for the state transition. One method for estimating the parameters of an unknown system when using the Kalman filter is the extended Kalman filter. A method developed by Ljung and Söderström[37] called recursive parameter estimation(RPE), was adapted by Azimi-Sadjadi et al [5] for use in Kalman filtering for speckle noise reduction.

This thesis covers the application of Kalman filtering and recursive parameter estimation for the reduction of speckle noise in synthetic aperture radar images. Different Kalman filtering techniques are developed to better process the SAR imagery for speckle reduction. The adaptive-block Kalman filter(ABKF) given by Azimi-Sadjadi[5] is modified so that the multiplicative noise statistics are considered only locally stationary. This allows the filter to model regions where the multiplicative noise assumption does not hold. The filter is also adaptive over the whole image so that changes in the image model that are due to large variations in the image, such as over urban areas, can still be filtered. The problem of filtering non-homogeneous regions is also approached from two different directions. One method involves incorporating an adaptive additive noise term in the system dynamic equations to

compensate for changes in the image at edge boundaries. A second method that is demonstrated involves the use of a multiplicative noise term in the system dynamic equation to follow sharp changes in highly dynamic regions such as urban areas. Finally, the methods used for the modified 2-D ABKF filter will be applied to a model using a full plane region of support instead of the half plane region of support. This use of the full plane model reduces the asymmetric distortions that result with the half plane model.

In this thesis it will be shown that the original assumptions made by Azimi-Sadjadi et al. were invalid for use in speckle reduction of complex images that did not remain statistically homogeneous. This caused the filter to become less stable over highly variable regions such as images of urban centres. The modifications made to the filter in this thesis resulted in better performance over these highly variable regions as well as improved performance near edge regions. The adaptation of all of these methods to the full plane model of the Kalman filter also resulted in much better performance due to the symmetric estimator. This overcame problems with the block effects of the non-symmetric half plane model. Several scientific criteria were used in evaluating the performance of the different Kalman filters and some of the existing standard speckle reduction techniques.

The thesis outlines the details of the development of modifications to existing Kalman filters to enhance their utility for processing SAR imagery. Chapter 2 introduces the models that have been developed to describe the image formation model of synthetic aperture radar images. Several current noise reduction methods

are introduced with a review of their capabilities, including the use of Kalman filtering for speckle noise reduction. Chapter 3 shows the development of Kalman filters to reduce speckle noise in SAR imagery. The dynamic model of the SAR image is defined and the Kalman equations for the quarter plane model are developed. The Kalman filter is adaptive over the entire image as a parameter estimation technique for the state transition parameters is included. Two alternate models, the half-plane and the full-plane, are described as well. Chapter 4 covers the implementation of the Kalman filters described in chapter 3. Modifications to the models given in chapter 3 are developed to improve the performance of the filters. Chapter 5 demonstrates the performance of the modified Kalman filters on both test and real images. The results are compared to results obtained from the original unmodified Kalman filter and some of the other techniques given in chapter 2 using both scientific criteria and subjective visual inspection. Chapter 6 presents the conclusions of the work and describes further work that may be carried out.

Chapter 2

SAR Image Processing

Demand for synthetic aperture radar (SAR) imaging has increased greatly recently due to the all-weather capability of a radar imaging system and the unique properties of the radar image. SAR imaging modes are being used for such systems as fighter aircraft, battle field surveillance(JSTARS), remote sensing aircraft(SAR-580), and spacecraft(Almaz, ERS-1, JERS-1, SIR-C/X, and Radarsat). The SAR image is created by measuring the reflected return from a region illuminated by a coherent radar. Thus, in radar imagery, the earth does not appear as white clouds, blue ocean and green vegetation, dependent on the sun angle[9]. Rather, the image is dependent on the geometrical properties of the surface and is further influenced by the presence of moisture. For example, it is difficult to determine the exact coastline in a SAR image because the scattering from the surface waves of the water equals or exceeds the surface scattering of the shoreline[31]. Hendry et al.[22] demonstrate the difficulty of viewing linear features in SAR images due to the variability of the

image that is dependent on the viewing geometry. The primary drawback of SAR imagery is the low signal to noise ratio due to the granular noise known as speckle. This limits the resolution of the image as well as its utility.

The largest source of noise in a SAR image, is the speckle noise that is caused by the interaction of the coherent imaging radar beam and the relatively rough surface being imaged [19]. For a typical single-look intensity image the signal to noise ratio is often as low as 1:1. Because of this speckle noise, typical image processing techniques experience great difficulty when applied to SAR imagery[35]. As an example, many segmentation schemes require prefiltering [15] or modified techniques that take into account the special requirements of SAR imagery [23],[42]. The problem is even greater when one attempts edge detection. Many specialized edge detection methods have been developed solely for application to SAR imagery [17],[54],[49],[10] and many prefiltering techniques developed are specifically modified to preserve edges in SAR imagery[51],[30].

An example of a single-look intensity image is given in Figure 2.1. The image is of the downtown region of Victoria, B.C. taken by ERS-1 in August 1993 and is marked on the map given in Figure 2.2. The dark region in the left third of the image is Victoria Harbour and the Victoria Arm. The bright region in the centre is a highly developed urban region. The image is 256x256 pixels, but is displayed here with non-square pixels due to the higher along-track sampling rate of the single-look image. This image illustrates how the speckle noise severely reduces the interpretability of the image. The large variations in the image make it difficult

to clearly identify region boundaries, and this problem is greatly exacerbated when computer algorithms are used. This image was chosen as a test image for this thesis for its great variability. Many processing algorithms assume homogeneous regions and have difficulty handling images that have such different regions.

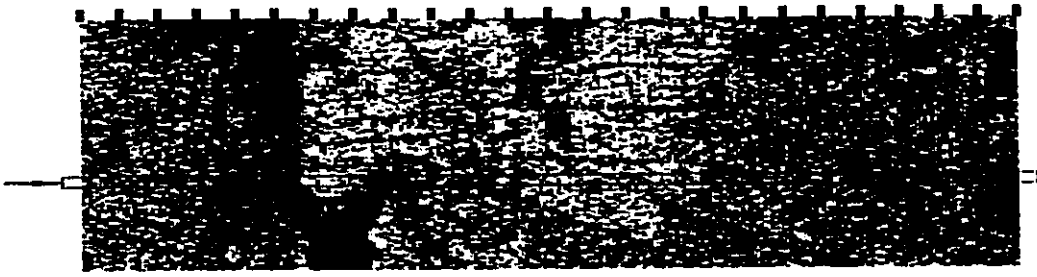

Figure 2.1: Single-Look Intensity Image of Victoria, B.C. from ERS-1.

Figure 2.2: Map of Victoria, B.C. Showing Area of SAR Image.

2.1 SAR image formation

A radar image is created by measuring the returning radiation from a coherent radar source. A coherent radar beam is emitted by the imaging platform and is absorbed and reflected by the target region. The portion of the beam that returns to the receiver is measured and used to create an "image" of the illuminated region. The electro-magnetic field equations used to express the transmission and reflection of the radar beam are linear in field intensity. Thus, radar systems are designed to be linear in voltage and the radar parameters are typically measured in terms of voltage rather than power. The resulting radar equation for SAR imagery is given as [13]

$$v_r(\mathbf{R}) = \int_{-\infty}^{\infty} h(\mathbf{R}|\mathbf{R}')\zeta(\mathbf{R}')dA' \tag{2.1}$$

where:

$v_r(\mathbf{R})$	is received complex voltage signal
$h(\mathbf{R}\|\mathbf{R}')$	is impulse response for the radar
$\zeta(\mathbf{R}')$	is the complex random scattering coefficient of the terrain
dA'	is the area element or resolution cell, and
$\mathbf{R}$	is an arbitrary space point

The image will consist of estimates of the scattering coefficient, $\zeta(\mathbf{R})$, which are referred to as $\hat{\zeta}(\mathbf{R})$. This results in the following image formation model:

$$\hat{\zeta}(\mathbf{R}) = \int_{-\infty}^{\infty} h^{-1}(\mathbf{R}|\mathbf{R}')v_r(\mathbf{R}')d\mathbf{R}' \tag{2.2}$$

Since the system is resolution limited by the processing algorithm, the area dA consists of many scattering elements. This results in $\hat{\zeta}(\mathbf{R})$ being a random process.

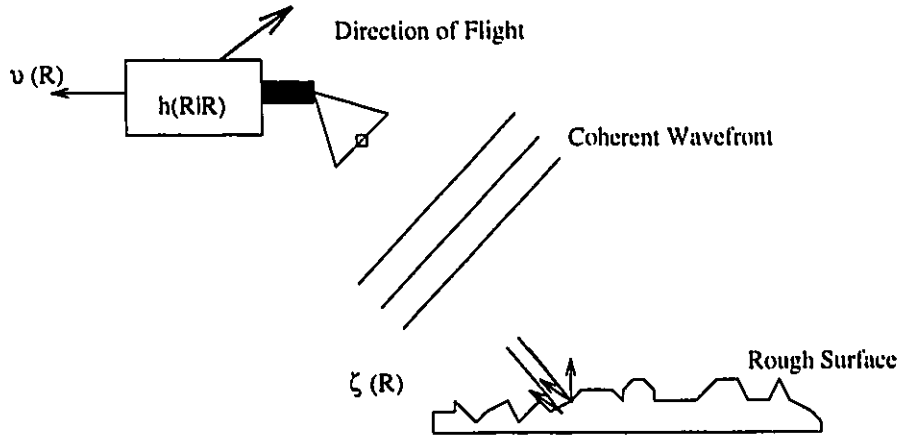

Figure 2.3: Illustration of SAR image formation

The radar back-scatter coefficient over the resolution cell, dA, is given as

$$\begin{aligned} \zeta_o(\mathbf{R}) &= \zeta(\mathbf{R})/dA \\ &= |\hat{\zeta}(\mathbf{R})|^2 \end{aligned} \tag{2.3}$$

The ensemble mean of these values is the expectation, $\mathcal{E}(\ )$ [44], and is referred to as the mean backscatter given as

$$\begin{aligned} \zeta^o(\mathbf{R}) &= \mathcal{E}(\zeta_o(\mathbf{R})) \\ &= \mathcal{E}(|\zeta(\mathbf{R})|^2) \end{aligned} \tag{2.4}$$

The difference between any particular measurement or realization of $\zeta_o(\mathbf{R})$ and $\zeta^o(\mathbf{R})$ is referred to as speckle noise.

Goodman [19] summarizes the speckle effect as a random walk phenomenon. In order for this to be valid, three assumptions must be true.

- the number of elementary contributions to the signal at one location is large,

- the amplitude and the phase of each elementary scatterer are statistically independent, and
- the phase of the elementary scatterer is uniformly distributed, ie. the surface is rough compared with the wavelength.

If all of the above assumptions are true, the speckle is called "fully developed" [40], and can be treated as strictly multiplicative noise in the observation equation as

$$y(i,j) = x(i,j) \cdot \gamma(i,j) \tag{2.5}$$

where:

$y(i,j) \in \|R\|$	is the observed image
$x(i,j) \in \|R\|$	is the actual image or state, and
$\gamma(i,j)$	is the multiplicative noise term.

The multiplicative noise assumption results in the distribution of the intensity, $P(I)$, being a negative exponential of the following form[55].

$$P(I) = \begin{cases} \frac{1}{I}\exp(\frac{-I}{I}), & I \geq 0 \\ 0, & \text{otherwise} \end{cases} \tag{2.6}$$

where the intensity is defined as

$$I = |\hat{\zeta}(\mathbf{R})|^2 \tag{2.7}$$

$$\sigma_I^2 = \bar{I} \tag{2.8}$$

In many cases, the amplitude of the image is used instead of the intensity. The distribution of this type of image is described as a Rayleigh distribution[44] and is

given by[55]

$$P(A) = \begin{cases} \frac{A}{\sigma_I^2} \exp(\frac{A^2}{2\sigma_I^2}), & A \geq 0 \\ 0, & \text{otherwise} \end{cases} \tag{2.9}$$

where

$$\begin{aligned} A &= |\hat{\zeta}(\mathbf{R})| \\ &= \sqrt{I} \qquad (2.10) \\ \bar{A} &= \sigma_I \sqrt{\frac{\pi}{2}} \qquad (2.11) \\ \sigma_A^2 &= (2 - \frac{\pi}{2})\sigma_I^2 \qquad (2.12) \end{aligned}$$

Note: σ_I^2 is the variance term found in (2.8). (2.13)

It is often the case in real SAR imagery that certain regions will be dominated by a single point reflector, or that the surface is not rough with respect to the wavelength. This becomes more likely as the resolution of these systems improves. In these cases, the assumption of strictly multiplicative behaviour of speckle is no longer valid and the image must be modeled in a different manner. This often requires weakening the multiplicative noise condition in the observation equation.

Aside from the multiplicative effect of the speckle, there is also additive noise in the processing of the SAR data through the matched inverse of the radar impulse response, $h(\mathbf{R}|\mathbf{R}')$. Although this term is typically small in SAR imagery, there are cases where the noise may influence the observed image.

It is assumed in many SAR speckle reduction procedures that the speckle noise in adjacent pixels is independent. It has been noted by Raney[47], that in real

cases of SAR imagery, this assumption is invalid and that the speckle measured in adjacent pixels must be considered correlated.

2.2 Speckle Noise Reduction

There exist several methods of speckle reduction, many of which will be summarized here in order of increasing complexity. One method of speckle reduction is multi-look processing. The image is sampled as several independent, lower resolution images or looks, which are then averaged together. Sampling is achieved by dividing the Doppler frequency spectrum into M segments and processing each segment independently. This method leads to a reduction in the speckle noise of intensity images by a factor of $1/\sqrt{M}$, where M represents the number of independent looks[19]. This results in the amplitude and the intensity of the image becoming gamma distributions[36].

$$P(I_M) = \begin{cases} \frac{M^M I^{M-1}}{(M-1)!\sigma_I^{2M}} \exp^{\frac{-MI}{\sigma_I^2}}, & I \geq 0 \\ 0, & \text{otherwise} \end{cases} \tag{2.14}$$

where

$$I_M = \text{the intensity image after M look processing} \tag{2.15}$$

$$\bar{I_M} = \sigma_I^2 \tag{2.16}$$

$$\sigma_{I_M}^2 = \sigma_I^2/M \tag{2.17}$$

Multi-look processing is very common, due to its reduction of the processing

complexity by $1/M$. However, it reduces the resolution of the image by $1/M$ while improving the signal to noise ratio by $1/\sqrt{M}$, and does not take into consideration the spatially varying statistics of speckle over the image. Also, the additive noise from these independent samples is added, which may bias the image and reduce the gain in signal noise reduction by a value less than $\sqrt{M}$[13].

Since speckle noise is considered multiplicative in nature for fully developed speckle, homomorphic filtering has been used as suggested in Jain[25]. This method involves a non-linear transform to a domain where the multiplicative noise may be treated as additive noise and removed. The corrected image is then retrieved using a corresponding inverse transform. The process is illustrated in Figure 2.4. The most common homomorphic transform for multiplicative noise is the log operation. Multiplicative terms in the normal domain become additive in the logarithmic domain. Thus, noise may be removed using an additive noise model in the logarithmic domain. The restored image is recovered by taking the exponent of the cleaned logarithmic image. Durand et al.[15] analysed several filters including homomorphic versions of the box filter, and the homogeneous block filter. They found that the non-homomorphic filters performed better on real SAR imagery despite the more appropriate multiplicative noise model used.

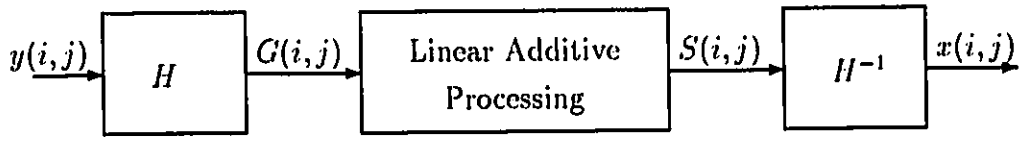

Figure 2.4: Homomorphic Filtering Process

Another speckle reduction method that does not use a model of the SAR image

is the Crimmins geometric filter[12]. The Crimmins filter uses a morphological process referred to as the complementary eight-hull algorithm to "fill in the narrow valleys and break down the narrow peaks". This algorithm utilizes the correlation between the speckle of adjacent pixels and results in a smoothed image. However, the Crimmins geometric filter does not take into account the multiplicative nature of the speckle noise. Thus, the noise at higher intensities will remain while the values at lower intensities will be overly smoothed. It also requires that the image be detected and mapped to a relatively small dynamic range to work reasonably well.

One simple speckle reduction filter is the Lee-sigma filter[33]. The Lee-sigma filter uses an estimate of the variance of the image for a multiplicative model of the speckle noise. A $(2n+1) \times (2m+1)$ window about the current pixel is defined. The central pixel of the window is assigned the average grey level of those pixels in the window that are within an intensity range defined by twice the multiplicative noise standard deviation from the centre pixel's grey level.

$$\delta_{k,l} = \begin{cases} 1, & if(1-2\sigma_\gamma)y_{k,l} \leq y_{k,l} \leq (1+2\sigma_\gamma)y_{k,l} \\ 0, & otherwise \end{cases} \tag{2.18}$$

$$\hat{x}_{i,j} = \frac{\sum_{k=i-n}^{i+n}\sum_{l=j-m}^{j+m}\delta_{k,l}y_{k,l}}{\sum_{k=i-n}^{i+n}\sum_{l=j-m}^{j+m}\delta_{k,l}} \tag{2.19}$$

where:

$\hat{x}$ is the estimate of the original image,

y is the observed image, and

σ_γ is the multiplicative noise variance.

This filter is based on the fact that 95.5% of all values are within two sigma of the mean in a Gaussian distribution. However, the assumption of a local gaussian distribution is often not valid for SAR imagery.

Lee also derived very popular statistical filters using data models for both additive and multiplicative noise [32], [34]. The Lee statistical filter for multiplicative noise assumes the noise-corrupted image is described as

$$y_{i,j} = x_{i,j}\gamma_{i,j} \tag{2.20}$$

where:

$y_{i,j}$ is the observed image

$x_{i,j}$ is the desired original image, and

$\gamma_{i,j}$ is the multiplicative noise.

A linear approximation to the image model in Equation 2.20 is given such that

$$\hat{y}_{i,j} = Ax_{i,j} + B\gamma_{i,j} + C \tag{2.21}$$

and A,B, and C are nonrandom variables. In order to ensure an unbiased estimate the value of C must be constrained such that

$$C = \bar{x}_{i,j}\bar{\gamma}_{i,j} - A\bar{x}_{i,j} - B\bar{\gamma}_{i,j} \tag{2.22}$$

This results in a linear approximation of the form

$$\hat{y}_{i,j} = x_{i,j}\bar{\gamma}_{i,j} + \bar{x}_{i,j}(\gamma_{i,j} - \bar{\gamma}_{i,j}) \tag{2.23}$$

which is optimal in the mean square error of $(\hat{y} - y)$. Approximating the necessary terms using local statistics gives a filter of the following form:

$$\bar{x}_{i,j} = \frac{\bar{y}_{i,j}}{\bar{\gamma}} \tag{2.24}$$

$$\sigma_{x\ i,j}^2 = \frac{\sigma_{y\ i,j}^2 + \bar{y}^2}{\sigma_\gamma^2 + \bar{\gamma}^2} - \bar{x}_{i,j}^2 \tag{2.25}$$

$$k_{i,j} = \frac{\bar{\gamma}\sigma_{x\ i,j}^2}{\bar{x}_{i,j}^2\sigma_\gamma^2 + \bar{\gamma}^2\sigma_{x\ i,j}^2} \tag{2.26}$$

$$\hat{x}_{i,j} = \frac{\bar{y}_{i,j}}{\bar{\gamma}} + k_{i,j}(y_{i,j} - \bar{y}_{i,j}) \tag{2.27}$$

where $\bar{y}_{i,j}$ and $\sigma_{y\ i,j}$ are the first order image statistics calculated for the local window, $k_{i,j}$ is the gain, and $\hat{x}_{i,j}$ is the new image estimate at i,j.

In further work, Lee [36] uses a linear model where

$$\hat{x} = a\bar{x} + by \tag{2.28}$$

in which $\hat{x}$ is the mimimum mean square estimate, and a and b are chosen to minimize the mean square error. This results in a minimum mean square estimate of the form

$$\hat{x}_{i,j} = \bar{x}_{i,j} + k(y_{i,j} - \bar{y}_{i,j}) \tag{2.29}$$

where the gain term $k_{i,j}$ is

$$k_{i,j} = \sigma_{x\ i,j}^2/\sigma_{y\ i,j}^2 \tag{2.30}$$

The difference between this filter and the previous Lee filter is only in the calculation of the gain term. Lee found that there was little difference between the two filters when using 4-look amplitude images, but the newer Lee filter had significantly improved performance with single look intensity images over the original derivation.

The Lee statistical filter assigns a value to the central pixel that is between the mean of the given window and the observed value. As the local mean value gets larger or the ratio between the local variance and the local mean gets smaller, the

output tends to be closer to the mean. This filter was rated very favourably by Durand et al [15] and by Lee et al [36] in terms of performance and efficiency. The previous four filtering methods were also compared by Dewaele et al. [14]. They found that the Lee statistical filter performed well, but preferred the Crimmins filter for preserving edges. The primary drawback of the Lee statistical filter is the over-smoothing of edges. This effect can be seen in Figure 2.5 when compared to the original image in Figure 2.1. The single bright linear feature in Figure 2.5 in the harbour region in the left third of the image is actually two separate targets that have been smoothed together.

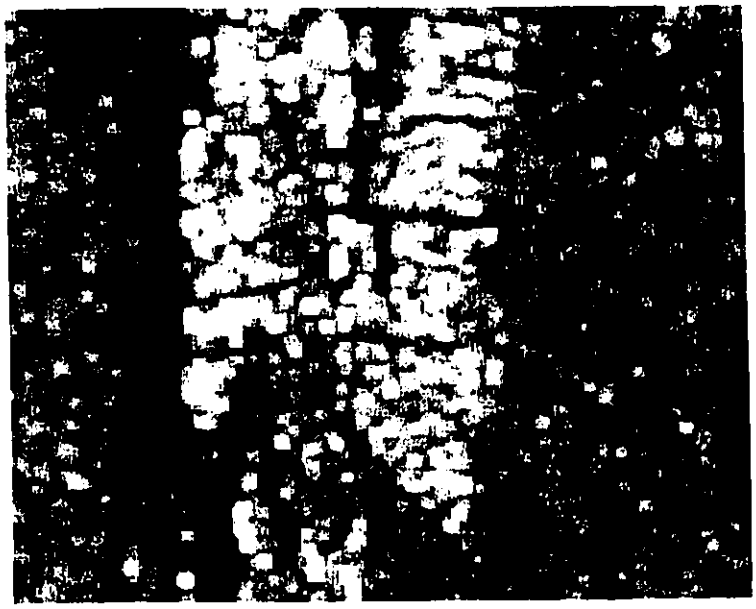

Figure 2.5: Results of Lee Statistical Filter(5x5) Applied to SAR Image

In order to overcome the problem of over-smoothing of the edges, Lee further refined the filter to use edge directed windows[30]. In this algorithm, eight non-square windows for eight edge orientations are created within a 7x7 window. The

local statistics are calculated using the windows for the edge model selected and then the Lee filter is applied. For homogenous regions, this performs similarly to the original Lee statistical filter, but gives much better performance near edge boundaries[36].

Arsenault [3] expressed the observed image as a result of the addition of the original signal and a signal dependent term.

$$y_{ij} = x_{ij} + K x_{ij} \eta \tag{2.31}$$

where:

K is a constant, and

η is a Gaussian noise source with zero mean and unity variance.

A homomorphic transformation of the form

$$G_{ij} = \frac{255}{\ln 256} \ln(x_{ij} + 1) \tag{2.32}$$

was applied to the data to convert the signal dependent noise to additive noise. The noise was then removed using the additive noise model given by Lee [32].

$$\hat{S}_{ij} = \bar{G}_{ij} + Q_{ij}(G_{ij} - \bar{G}_{ij}), \tag{2.33}$$

$$Q_{ij} = 1 - \frac{\sigma_i^2}{\sigma_w^2} \tag{2.34}$$

where:

$\hat{S}_{ij}$ is the estimate in the transformed domain,

Q_{ij} is the gain,

σ_i^2 is the image variance, and

σ_w^2 is the local window variance.

The image was then restored using an inverse transform of (2.32). However, Durand et al[15] found that this filter performed less satisfactorily than the extended multiplicative noise model derived by Lee [32] discussed above.

Kuan et al. [27] developed a locally linear minimum mean square error (LLMMSE) filter using a nonstationary mean, nonstationary variance model of the image. The resulting filter for signal dependent noise is the same as the Lee filter except for the k term which is given as

$$k_{i,j} = \frac{\bar{\gamma}\sigma^2_{xi,j}}{\bar{x}^2_{i,j}\sigma^2_\gamma + \bar{\gamma}^2\sigma^2_{xi,j} + \sigma^2_\gamma\sigma^2_{xi,j}} \tag{2.35}$$

Although this method is better optimized than Lee's method, the improvement in the results is usually reported as negligible [15], [40].

Kuan further developed a maximum *a posteriori*(MAP) method for gamma and Rayleigh distributions[28], two distributions which are often associated with multilook and amplitude SAR images. The MAP estimate of the image is obtained by maximizing the *a posteriori* probability density function, (2.37) with respect to x.

$$y_{ij} = \eta x_{ij} \tag{2.36}$$

$$P(x|y) = \frac{P(y|x)P(x)}{P(y)} \tag{2.37}$$

This method requires solving a cubic equation(2.38) for each pixel to determine the optimal MAP result for the given distribution.

$$-\hat{x}^2_{MAP\ ij}[\hat{x}_{MAP\ ij} - \bar{x}_{ij}] + \sigma^2_{x_{ij}}[y_{ij} - \hat{x}_{MAP\ ij}] = 0 \tag{2.38}$$

The LLMMSE filter is used to reduce the computational load of the MAP filter by solving for the cubic root only when the data changes significantly.

Frost et al.[16] developed a minimum mean square error (MMSE) filter for a stationary image model. The radar image is modeled as

$$y_{ij} = |x_{ij} \cdot \gamma_{ij}| * h_{ij} \tag{2.39}$$

The minimization of the mean square error results in the impulse response of the filter being given as

$$m'(t) = K_1 \exp(-K C_o^2 |t|) \tag{2.40}$$

where K_1 is a normalizing constant, K is the filter parameter and C_o is the locally derived coefficient of variation

$$C_o = \frac{\sigma_{y\ ij}}{\mu_{y\ ij}} \tag{2.41}$$

This filter performs fairly well in comparison to several of the others described above as illustrated by Shi and Fung [50], but it does fail to model additional additive noise as pointed out by Woods and Biemond [58]. Quelle and Boucher[46] combined the Frost model of SAR imagery with spectral estimation techniques to develop an adaptive Frost filter.

There exist many slight variations of the above filters. Lopes et al [40],[39],[38] have modified several of these filters to apply different criterion so that they are bounded to operate only in regions where the assumptions made in the filter design are valid. These modified filters use the local statistics to verify the assumption of multiplicative noise and vary the filter parameters when the assumption does not

appear valid. In [40], the coefficient of variation, C_v, is the criterion, while in [39], the contrast ratio, C_r, is the criterion. The contrast ratio, C_r, is defined as the ratio of the mean of two adjacent windows in the image. If the local variation of the image is small as determined by either of these criteria, then the region is homogeneous and the multiplicative speckle assumption is not used. If the criteria indicated that the variation of the image is too great to be accounted for by the image model, then the assumption of multiplicative speckle is also invalid and the value is left unfiltered. This results in greater averaging in homogenous regions while edge areas are left intact.

2.3 Kalman Filtering

In the previous section, each successive method involved a more complex model for speckle reduction. Images may also be modelled as a linear two dimensional autoregressive (AR) process[24]. Kalman filtering has been used extensively in processing of 1-D AR processes to achieve a linear estimate of the least square error solution[20]. The Kalman filter was extended to the 2-D case by Habibi [21]. However, the straight application of a Kalman filter to the 2-D case is difficult due to the large computational and spatial requirements.

The problem of large computational and spatial demands was first reduced when Woods et al. developed several filters, such as the reduced update Kalman filter (RUPK) [60] [57], that were efficient and could be used to process images that

were modelled as linear AR processes. These filters were expanded to include online parameter estimation[26], linear space invariant(LSI) blur correction[59], and multiple parallel models for edge preservation[53]. Roesser[48] also derived a single input, single output 2-D state space model that possessed a separable impulse response and divided the state into vertical and horizontal components. Zhang and Steenart[62] presented a high speed Kalman filter with LSI blur correction based on Roesser's model.

Azimi-Sadjadi and King[7] derived a general 2-D recursive multiple input, multiple output system based on the Roesser 2-D state space model. This system took advantage of special block structures to implement efficient 2-D filters by applying fast convolution methods[1]. The concept of a 2-D block processor was extended to Kalman filtering and applied to SAR imagery [4]. In order to model SAR imagery, the speckle noise was approximated by the inclusion of a multiplicative noise term in the equations. The 2-D block Kalman filter also included online parameter estimation based on local statistics. The adaptive nature of the online parameter estimation allowed the filter to be applied to a globally non-stationary image while assuming only local stationarity of the image within the blocks being processed, and global stationarity of the noise process[6]. Further modifications included the expansion of the region of support to a non-symmetric half plane block with special block attributes that increased the order of the filter[5].

The 2-D adaptive block Kalman filter(ABKF) was demonstrated to reduce speckle on relatively homogenous images. However, several simplifications were

made in order to reduce the computational work load for this algorithm. For the case of images with large non-homogenous regions such as urban regions or land/sea boundaries, these simplifications create difficulties. The main computational burden of the filter in [5] is the calculation of the derivative of the Kalman gain term for the parameter estimation. It was assumed that the gain would converge to its steady state value very quickly, and the gain was set to a constant value after an experimentally determined number of runs. The model also weighted the online parameter estimation so that the filter parameters would converge to global steady state values. The combination of selecting a steady state gain and using the steady state filter parameters removes the filter's adaptive capability, leading to blurring at edges and large block effects. The Kalman filter, as presented by Azimi-Sadjadi, also assumes a stationary multiplicative noise condition, ie. it assumes that the multiplicative noise statistics are constant over the entire image.

In the next chapter, the Kalman filter technique will be discussed and references to the improvements designed into this technique in order to apply it to SAR processes will be given.

Chapter 3

2D Kalman Filtering

The Kalman filter is a very powerful tool that can be applied to many problems to determine the optimal estimation of a system in the presence of noise. A dynamic model of a system is defined and the Kalman filter is applied to the model to estimate the system state variables. It is also possible to extend the Kalman filter so that it may estimate the parameters of the model of the system. One method for developing a dynamic model of a system is to approximate the system as an auto-regressive(AR) linear process[24]. This chapter will outline the development of some two dimensional AR processes that can be used to apply Kalman filter techniques to the speckle problem. Then various Kalman filters are derived for the different models and a parameter estimation technique is also outlined.

3.1 2-D AR state space model

Since an image is a two dimensional object, it is desirable to use a two dimensional model of the image. Each pixel of the image is represented by a value $x(i,j) \in |\mathcal{I}_{16}|$. The use of a dynamic linear process implies that the value of a single point, $x(i,j)$, can be calculated using a general 2D input-output model as given in (3.1) which uses a quarter-plane region of support of size $m \times n$. This single input-single output model must be converted into a state space model in order to be able to apply a Kalman filter.

$$\begin{aligned} x(i+1,j+1) &= a_{0,1}x(i+1,j) + a_{0,2}x(i+1,j-1) + \cdots a_{0,n-1}x(i+1,j-n+1) + \\ &\quad a_{1,0}x(i,j+1) + a_{1,1}x(i,j) + a_{1,2}x(i,j-1) + \cdots \\ &\quad \vdots \\ &\quad + a_{m-1,0}x(i-m+1,j+1) + a_{m-1,1}x(i-m+1,j) + \cdots \\ &\quad + a_{m-1,n-1}x(i-m+1,j-n+1) + bu(i+1,j+1) \qquad (3.1) \\ y(i+1,j+1) &= cx(i+1,j+1) + dv(i+1,j+1) \qquad (3.2) \end{aligned}$$

where:

x(i+1,j+1)	is the value of the system at location i+1,j+1,
y(i+1,j+1)	is the observed value of the system at location i+1,j+1,
a,b,c and d	are the parameters of the system,
u(i+1,j+1)	is the additive input noise, and
v(i+1,j+1)	is the additive observation noise.

The general scalar state space model for a two dimensional process has been given by Kurek [29]. In this model, the current state, X, is the result of the previous

states in both the i and j directions. The state model elements are defined as

$X(i,j)$	as the state
$Y(i,j)$	as the observed state
$U(i,j)$	as the additive state noise
$V(i,j)$	as the additive observation noise
$A_{\#}$	as the state transition matrices
$B_{\#}$	as the state transition matrices for the additive state noise
C	as the observation transition matrix, and
D	as the observation transition matrix for the observation noise.

Then, the general scalar state space model may be given as below[29].

$$\begin{aligned} X(i+1,j+1) &= A_0X(i,j) + A_1X(i+1,j) + A_2X(i,j+1) \\ &\quad + B_0U(i,j) + B_1U(i+1,j) + B_2U(i,j+1) \qquad (3.3) \\ Y(i,j) &= CX(i,j) + DV(i,j) \qquad (3.4) \end{aligned}$$

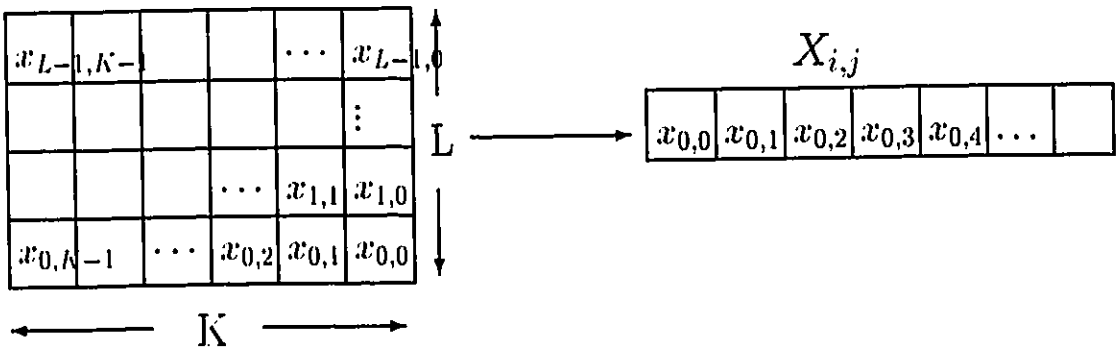

Figure 3.1: Example Mapping of 2-D blocks to Block Vector.

Azimi-Sadjadi and King [7] developed a block state realization of the 2-D AR process based on Roesser's model [48], which allows the extension of the scalar 2-D

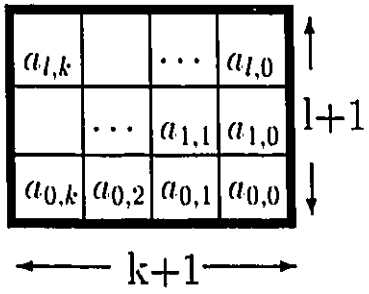

Figure 3.2: Example Mapping of Parameter Vector to Quarter Plane Region of Support.

state space model (single input-single output) to a multiple input-multiple output system. The input sequence, $x(i,j)$ is partitioned into non-overlapping blocks of dimension $K \times L$, where K is greater than the order of the filter in the vertical direction and L is greater than the order of the filter in the horizontal direction. These blocks are then mapped into a one dimensional vector to become block vectors, $X_{i,j}$. A diagram of this mapping is given in Figure 3.1. The 2D block is overlaid with the $(k+1) \times (l+1)$ region of support for the $x_{0,0}$ point that corresponds to the 2D input-output equation given in (3.1). A diagram of the mapping of the parameters to the region of support is given in Figure 3.2. The actual mapping of the block to the block vectors can be arranged to allow the most efficient implementation. For the quarter plane region of support, the block vectors are defined by Azimi-Sadjadi[4] as in (3.5),(3.6) and illustrated in Figure 3.3.

$$X_{i,j} = [X'_{iK}(jL+L-1), X'_{iK}(jL+L-2), \cdots, X'_{iK}(jL)]^T \quad (3.5)$$

$$X'_{iK}(m) = [x(iK,m), x(iK+1,m), \cdots, x(iK+K-1,m)] \quad (3.6)$$

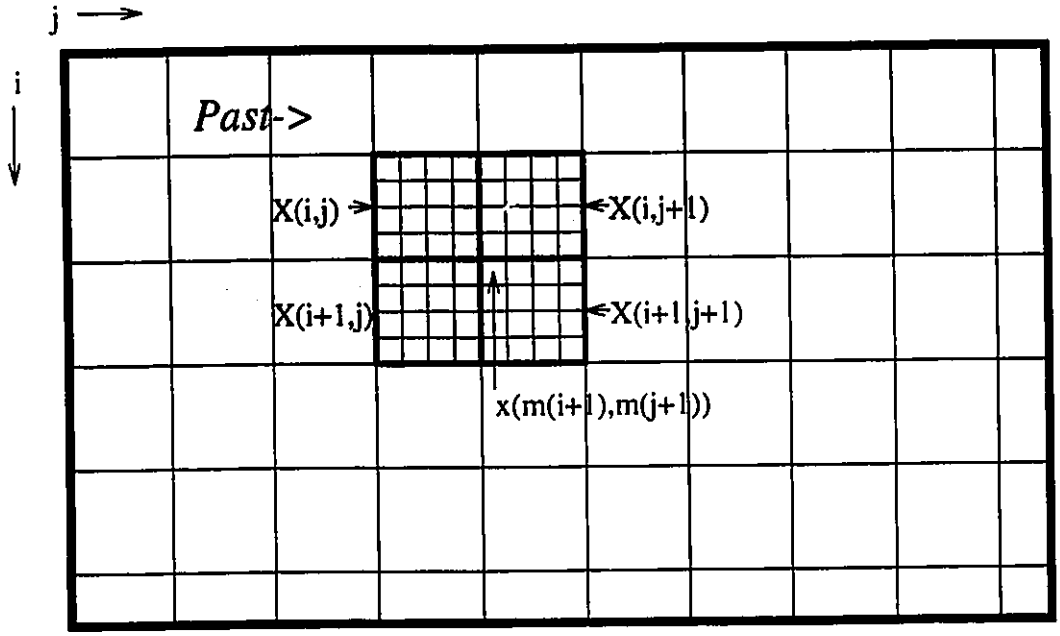

Figure 3.3: The quarter-plane region of support for a 2D AR model for images.

Depending on the region of support chosen, the current state is dependent on various neighbouring past state vectors. For the quarter plane case given in Figure 3.3, the state vector will be formed following [4] as

$$\mathbf{X}_{i,j} = [X^T_{i-1,j-1}\ X^T_{i-1,j}\ X^T_{i,j-1} X^T_{i,j}]^T \tag{3.7}$$

Combining the above state vector formulation, (3.7), and the 2-D general state space model, (3.3,3.4), it can be seen that the overlap in adjacent states results in a state equation of the form [5]:

$$\mathbf{X}_{i,j} = \mathbf{A}_0\mathbf{X}_{i,j-1} + \mathbf{A}_1\mathbf{X}_{i-1,j} + \mathbf{B}\mathbf{U}_{i,j} \tag{3.8}$$

where

$$\mathbf{A}_0 = \begin{bmatrix} 0 & \mathbf{I} & 0 & 0 \\ 0 & 0 & 0 & 0 \\ 0 & 0 & 0 & \mathbf{I} \\ 0 & A_0 & 0 & A_1 \end{bmatrix} \text{ and } \mathbf{A}_1 = \begin{bmatrix} 0 & 0 & 0 & 0 \\ 0 & 0 & 0 & \mathbf{I} \\ 0 & 0 & 0 & 0 \\ 0 & 0 & 0 & A_2 \end{bmatrix} \tag{3.9}$$

$$\mathbf{B} = [0\ 0\ 0\ B^T]^T$$

Since the models will be used for speckle reduction, a multiplicative noise term, Γ, is included in the observation equation (3.10). This Γ term is a result of the typical characterization of speckle noise as reviewed in the previous chapter and given in (2.5).

$$Y_{i,j} = C\Gamma_{i,j}X_{i,j} + V_{i,j} \tag{3.10}$$

3.2 Kalman Filter Equations

Using the block state space model given above, the block dynamic model equations for the Kalman filter can be defined[5].

$$X_{i,j} = \mathbf{A}_0\mathbf{X}_{i,j-1} + \mathbf{A}_1\mathbf{X}_{i-1,j} + \mathbf{B}\mathbf{U}_{i,j} \quad \textit{state transition} \tag{3.11}$$

$$Y_{i,j} = C\Gamma_{i,j}X_{i,j} + V_{i,j} \quad \textit{observation} \tag{3.12}$$

where the noise processes are Gaussian with the statistics as follows

$$\mathcal{E}[U_{i,j}] = 0 \quad \textit{process noise} \tag{3.13}$$

$$\mathcal{E}[U_{i,j}U_{i-k,j-l}^T] = \sigma_u^2\mathbf{I}\delta_{k,l} \tag{3.14}$$

$$\mathcal{E}[V_{i,j}] = 0 \qquad \textit{observation noise} \tag{3.15}$$

$$\mathcal{E}[V_{i,j}V_{i-k,j-l}^T] = \sigma_v^2\mathbf{I}\delta_{k,l} \tag{3.16}$$

$$\mathcal{E}[\Gamma_{i,j}] = \mu_\gamma \qquad \textit{multiplicative noise} \tag{3.17}$$

$$\mathcal{E}[\Gamma_{i,j}\Gamma_{i-k,j-l}^T] = \sigma_\gamma^2\mathbf{I}\delta_{k,l} + \mu_\gamma^2\mathbf{I} \tag{3.18}$$

Note that the various noise parameters, u, and v, are independent of the signal, $\mathbf{X}$, and are uncorrelated with respect to each other.

Using the block form of the filter and following Grewal and Andrews [20], the Kalman equations given in [5] can be derived as follows:

a priori estimate

$$\begin{aligned}\mathbf{X}_{i,j}^{(-)} &= \mathcal{E}[\mathbf{X}_{i,j}|\mathbf{X}_{i-1,j}^{(+)}, \mathbf{X}_{i,j-1}^{(+)}] \\ &= \mathbf{A}_0\mathbf{X}_{i,j-1}^{(+)} + \mathbf{A}_1\mathbf{X}_{i-1,j}^{(+)}\end{aligned} \tag{3.19}$$

a priori error covariance

$$\begin{aligned}P_{i,j}^{(-)} &= \mathcal{E}[(\mathbf{X}_{i,j} - \mathbf{X}_{i,j}^{(-)})(\mathbf{X}_{i,j} - \mathbf{X}_{i,j}^{(-)})^T] \\ &= \mathbf{A}_0P_{i,j-1}^{(+)}\mathbf{A}_0^T + \mathbf{A}_1P_{i-1,j}^{(+)}\mathbf{A}_1^T + \\ &\quad \mathbf{A}_0P_{i,j}^{(\times)}\mathbf{A}_1^T + \mathbf{A}_1P_{i,j}^{(\times)T}\mathbf{A}_0^T + \\ &\quad \mathbf{B}\sigma_u^2\mathbf{B}^T\end{aligned} \tag{3.20}$$

a priori error cross-covariance

$$\begin{aligned}P_{i,j}^{(\times)} &= \mathcal{E}[(\mathbf{X}_{i,j-1} - \mathbf{X}_{i,j-1}^{(+)})(\mathbf{X}_{i-1,j} - \mathbf{X}_{i-1,j}^{(+)})^T] \\ &= [\mathbf{I} - \mu_\gamma K_{i,j-1}C]A_1P_{i-1,j-1}^{(+)}A_0^T[\mathbf{I} - \mu_\gamma K_{i-1,j}C]^T\end{aligned} \tag{3.21}$$

innovation

$$\begin{aligned} Z_{i,j} &= \mathcal{E}[Y_{i,j} - Y_{i,j}^{(-)}] \\ &= Y_{i,j} - \mathcal{E}[C\Gamma_{i,j}X_{i,j}^{(-)} + V_{i,j}] \\ &= Y_{i,j} - \mu_\gamma C X_{i,j}^{(-)} \end{aligned} \tag{3.22}$$

gain calculation

$$\begin{aligned} R_{z\ i,j} &= \mathcal{E}[Z_{i,j}Z_{i,j}^T] \\ &= \mathcal{E}[(C\Gamma_{i,j}X_{i,j} + V_{i,j} - \mu_\gamma C X_{i,j}^{(-)}) \\ &\quad (C\Gamma_{i,j}X_{i,j} + V_{i,j} - \mu_\gamma C X_{i,j}^{(+)})^T] \\ &= \mu_\gamma^2 C P_{i,j}^{(-)} C^T + \sigma_v^2 \mathbf{I} + \sigma_\gamma^2(\sigma_{x\ i,j}^2 + \mu_{x\ i,j}^2)CC^T \end{aligned} \tag{3.23}$$

$$\begin{aligned} K_{i,j} &= \mathcal{E}[(X_{i,j} - X_{i,j}^{(-)})Z_{i,j}^T)R_{z\ i,j}^{-1} \\ &= \mu_\gamma P_{i,j}^{(-)} C^T R_{z\ i,j}^{-1} \end{aligned} \tag{3.24}$$

a posteriori estimate

$$X_{i,j}^{(+)} = X_{i,j}^{(-)} + K_{i,j}Z_{i,j} \tag{3.25}$$

a posteriori error covariance

$$\begin{aligned} P_{i,j}^{(+)} &= \mathcal{E}[(X_{i,j} - X_{i,j}^{(+)})(X_{i,j} - X_{i,j}^{(+)})^T] \\ &= (\mathbf{I} - \mu_\gamma K_{i,j}C)P_{i,j}^{(-)}(\mathbf{I} - \mu_\gamma K_{i,j}C)^T \\ &\quad + K_{i,j}C(\sigma_\gamma^2(\sigma_{x\ i,j}^2 + \mu_{x\ i,j}^2))C^T K_{i,j}^T + \sigma_v^2 K_{i,j}K_{i,j}^T \end{aligned} \tag{3.26}$$

$$= (\mathbf{I} - \mu_\gamma K_{i,j}C)P_{i,j}^{(-)} \tag{3.27}$$

The values of $\mu_{x_{i,j}}$ and $\sigma_{x\ i,j}^2$ must be estimated from the local statistics of the image.

3.3 Parameter Estimation

The Kalman filter requires that the filter parameters A, B, and C be defined. Unfortunately, it is very common for the matrices A and B to be unknown before the image is processed. The purpose of the filter for SAR imagery is to reduce the amount of noise that is present in the image. Thus, it will be assumed that the C matrix is known for this problem and is equivalent to the identity matrix. If there were any known systematic distortions in the imagery, these distortions could be placed in the C matrix as well. In order to determine the unknown Kalman filter parameters, a parameter estimation technique is required. The extended Kalman filter(EKF) is often proposed for parameter estimation[20]. Several methods for developing the estimation for the reduced update Kalman filter (RUPK) are summarized by Kaufman et al.[26]. A faster implementation of the parameter estimation for the RUPK is given by Tekalp et al. [52]. One of the difficulties with the EKF and its derivatives is its convergence properties[37]. The 1-D recursive prediction error(RPE) method derived by Ljung and Söderström[37] that is based on the stochastic Gauss-Newton approach includes extra features that aid in parameter convergence. The RPE technique will be used in this thesis as detailed in [5].

A recursive formula must be developed for the estimate of the parameters of the form [37]

$$\hat{\Phi}(t) = \hat{\Phi}(t-1) + \mathcal{L}(t)Z(t) \tag{3.28}$$

where

$\hat{\Phi}(t)$ is the vector containing the parameter estimates at time t.

$\mathcal{L}(t)$ is the gain for the parameter estimate, and

$Z(t)$ is the innovation or observation error as in (3.22).

In order to derive a model for parameter estimation, a criterion to be minimized is required. A quadratic criterion of the form

$$N(\Phi) = \mathcal{E}[\frac{1}{2} Z^T(t) \Pi^{-1} Z(t)] \tag{3.29}$$

where Π is a positive definite matrix, is often used [37],[5]. It is shown in [37] that the best choice for Π is the true prediction error covariance matrix. It is important to note that this form of criterion gives a substantial penalty for large errors and is sensitive to large measurement errors in the observed process[37].

For such a model of parameter estimation, the criterion may be minimized using the stochastic Newton method. The Newton method is generalized as a successive approximation process of the form

$$f(t+1) = f(t) + k \frac{h(t)}{\frac{d}{dt} h(t)} \tag{3.30}$$

where:

$f(t)$ is the solution,

$h(t)$ is the function being solved, and

k is a gain factor.

Applying this method to solve for the optimal solution to $N(\Phi)$, ie. solving $\frac{dN(\Phi)}{d\Phi} = 0$, gives an equation of the form [37]

$$\hat{\Phi}(t) = \hat{\Phi}(t-1) - \nu(t) \left[\frac{d^2}{d\Phi^2} N(\Phi) \right]^{-1} \left[\frac{d}{d\Phi} N(\Phi) \right]^T \tag{3.31}$$

$$= \hat{\Phi}(t-1) + \nu(t) \left[\frac{d^2}{d\Phi^2} N(\Phi) \right]^{-1} \Delta(t-1) \Pi^{-1} Z(t-1) \tag{3.32}$$

where

$\Delta(t)$ is the gradient of the observation error, and

$\nu(t)$ is a time decaying gain factor.

The second derivative, or Hessian, of the criterion can be approximated recursively using the following form [4]:

$$\mathcal{R}(t) \approx \frac{d^2}{d\Phi^2} N(\Phi) \tag{3.33}$$

$$\mathcal{R}(t) = \mathcal{R}(t-1) + \nu(t)[\Delta(t)\Pi^{-1}\Delta^T(t) - \mathcal{R}(t-1)] \tag{3.34}$$

The gradient of the observation error can be derived from the Kalman equations (3.22) [4] as

$$\begin{aligned} \Delta(\Phi, t) &= \left[\frac{d}{d\Phi} Y^{(-)}(\Phi, t)\right]^T \\ &= \left[\frac{d}{d\Phi} \mu_\gamma C X^{(-)}(\Phi, t)\right]^T \\ \Delta(\Phi, t) &= [(\mu_\gamma C \Sigma_b(\Phi, t)]^T \end{aligned} \tag{3.35}$$

where $\Sigma_b(\Phi, t)$ is the derivative of the *a priori* estimate from the Kalman filter (3.19).

$$\Sigma_b(\Phi, t) = \frac{d}{d\Phi} X^{(-)}(\Phi, t) \tag{3.36}$$

The calculation of (3.36) requires the derivative of the Kalman equations (3.19) - (3.27), and it should be noted that the calculation of the derivative of the gain function is computationally intensive[5].

The best estimate for the value Π has been shown to be the covariance of the innovation process $Z(t)$[37]. This covariance is the R_z term used in the formation of the Kalman filter as given in (3.23).

The formula for the calculation of the estimate of the Hessian given in (3.34) is very sensitive to round-off errors. It is desired that an alternative derivation be used that is more numerically stable. Towards this purpose a sequence, $\lambda(t)$, called the forgetting factor is defined. This factor is dependent on the gain sequence, $\nu(t)$, as follows [37]:

$$\lambda(t) = \frac{\nu(t-1)}{\nu(t)}[1 - \nu(t)] \tag{3.37}$$

Using this sequence and a new factor $\mathcal{P}(t)$ related to the Hessian by

$$\mathcal{P}(t) = \nu(t)\mathcal{R}^{-1}(t) \tag{3.38}$$

a form of the parameter gain function $\mathcal{L}(t)$ may be written that is more numerically stable[37].

$$\mathcal{L}(t) = \mathcal{P}(t-1)\Delta(t)[\Delta^T(t)\mathcal{P}(t-1)\Delta(t) + \lambda(t)R_z(t)]^{-1} \tag{3.39}$$

$$\mathcal{P}(t) = [\mathbf{I} - \mathcal{L}(t)\Delta^T(t)]\mathcal{P}(t-1)[\mathbf{I} - \Delta(t)\mathcal{L}^T(t)]/\lambda(t) + \mathcal{L}(t)R_z(t)\mathcal{L}^T(t) \tag{3.40}$$

$$\Phi(t) = [\Phi(t-1) + \mathcal{L}(t)Z(t)]_{DM} \tag{3.41}$$

The calculation of the gain must also be modified so that the parameter vector always results in a stable system as indicated by the mapping function in the right-hand side of (3.41) which has been marked as $[\,]_{DM}$ as specified in [37]. A common method to achieve this is to multiply the gain $\mathcal{L}(t)$ by a weighting factor that decreases from 1 to zero, and to select the greatest factor that results in a choice of parameters that yield to a stable system. The stability of the system may be verified by solving for the eigen values of the solution and ensuring that all are within the

unit circle [37]. A priori knowledge of the stable parameter space may also be used to force the parameters to remain in the region that guarantees a stable solution [2].

3.4 Online Parameter Estimation equations

The Kalman equations have been given in terms of two dimensions, while the parameter estimation is given in the one dimensional terms of the filter. The 2-D terms must be converted into a form compatible with the parameter estimation. Therefore, a parameter k is defined:

$$k = i * step_i + j * step_j;$$

where $step_i$ and $step_j$ are the number of iterations of the function that occur for each change in i and j respectively. For the block Kalman filter, $step_i$ is 1, and $step_j$ is equal to the number of blocks in one path across the image.

As well, it is necessary to define a sequence for the forgetting factor, $\lambda(t)$. The forgetting factor indicates the rate at which new information overrides the past. This factor should be a low value initially and should approach a value near 1 as the image is processed in order to achieve a stable result. The function

$$\lambda_k = \lambda_{ss} + \lambda_{rate}(\lambda_{k-1} - \lambda_{ss})$$

defines the forgetting factor [37], where λ_{ss} is the steady state value of λ, and λ_{rate} determines the rate at which the $\lambda(t)$ approaches λ_{ss}.

All of the equations required for the online parameter estimation may now be given in terms of the Kalman equations derived earlier [5, 37].

$$k = i * step_i + j * step_j \tag{3.42}$$

$$\lambda_k = \lambda_{ss} + \lambda_{rate}(\lambda_{k-1} - \lambda_{ss}) \tag{3.43}$$

$$\Delta_k^T(\Phi) = \mu_\gamma C \Sigma_{b(k)}(\Phi) \tag{3.44}$$

$$\mathcal{S}_k = \Delta_k^T(\Phi)\mathcal{P}_{k-1}\Delta_k(\Phi) + \lambda_k R_{z(k)} \tag{3.45}$$

$$\mathcal{L}_k = \mathcal{P}_{k-1}\Delta_k(\Phi)\mathcal{S}_k^{-1} \tag{3.46}$$

$$\mathcal{P}_k = \frac{1}{\lambda_k}(\mathbf{I} - \mathcal{L}_k\Delta_k^T(\Phi))\mathcal{P}_{k-1}(\mathbf{I} - \mathcal{L}_k\Delta_k^T(\Phi))^T + \mathcal{L}_k R_{z(k)}\mathcal{L}_k^T \tag{3.47}$$

$$\Phi_k = [\Phi_{k-1} + \mathcal{L}_k Z_k]_{\mathcal{D}_M} \tag{3.48}$$

$$\kappa_k = \frac{d}{d\Phi}K_k(\Phi) \tag{3.49}$$

$$\begin{aligned}\Sigma_{a(k)}(\Phi) &= \frac{d}{d\Phi}X_k^{(+)} \\ &= (\mathbf{I} - \mu_\gamma K_k(\Phi)C)\Sigma_{b(k)}(\Phi) + \kappa_k Z_k(\Phi)\end{aligned} \tag{3.50}$$

$$\begin{aligned}\Sigma_{b(k+1)}(\Phi) &= \frac{d}{d\Phi}X_k^{(-)} \\ &= \mathbf{A}(\Phi)\Sigma_{a(k)}(\Phi) + \frac{d\mathbf{A}(\Phi)}{d\Phi}X_{k-1}\end{aligned} \tag{3.51}$$

The initial conditions required for the parameter estimation are Φ_0, $\mathcal{R}_0$, λ_0, λ_{rate}, λ_{ss}, and $\Sigma_a(0)$.

3.5 Non-symmetric Half-plane ABKF

The 2-D ABKF equations were derived for the case of a quarter plane region of support as given in [4]. It is possible to develop a similar Kalman filter for different

block structures having other regions of support. For example Woods[60] defines a non-symmetric half plane region of support. Due to the inherent nature of scanning an image top to bottom, left to right, it is possible to declare all those regions to the left and above the current point as being in the past. Thus, it is possible to derive a causal filter that uses points in a non-symmetric window about the centre point, that extends upwards by the window size directly to the left, as well as above and to the right. The reduced update Kalman filter(RUPK) described in [60] used this non-symmetric half plane(NSHP) region of support. Also, Azimi-Sadjadi and Bannour[5] developed an adaptive block Kalman filter(ABKF) using this same region of support over a larger diagonal block. Several non-overlapping diagonal blocks are used to compose the state vector. The structure of the diagonal blocks is chosen to reduce the computational burden of the filtering and parameter estimation process[7],[1]. The structure of the diagonal blocks and an overlay of the NSHP region of support for one point are illustrated in Figure 3.4.

$$
\begin{aligned}
x(mi+1,nj+1) \;=\; & a_{0,1}x(mi+1,nj)+a_{0,2}x(mi+1,nj-1)+\cdots \\
& a_{0,n}x(mi+1,nj-n+1)+ \\
& a_{1,-n}x(mi,nj+1+n)+\cdots+a_{1,0}x(mi,nj+1)+ \\
& \cdots+a_{1,n}x(mi,nj-n+1)+ \\
& \vdots \\
& +a_{m-1,-n}x(mi-m+1,nj+1+n)+\cdots \\
& +a_{m-1,n}x(mi-m+1,nj-n+1)+ \\
& bu(i+1,j+1)
\end{aligned}
\tag{3.52}
$$

$$y(mi+1, nj+1) = cx(mi+1, nj+1) + v(mi+1, nj+1) \tag{3.53}$$

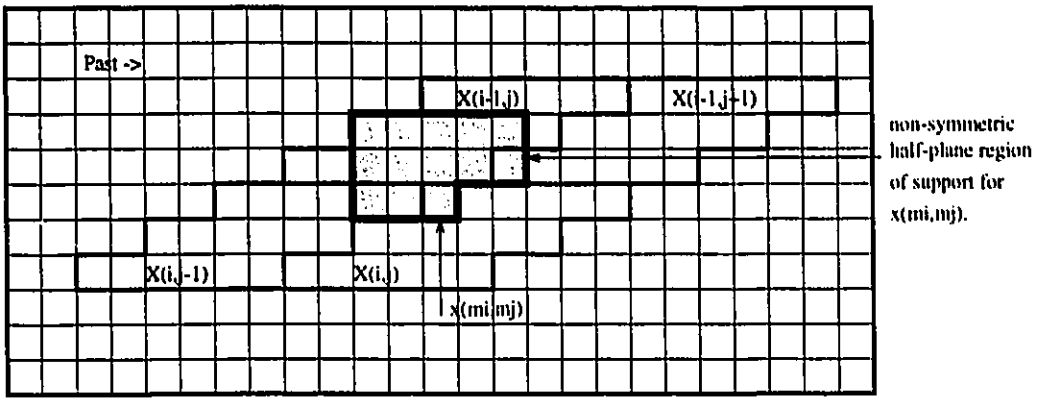

Figure 3.4: The NSHP region of support for the 2-D AR model for images

The mapping of the parameters within an NSHP region of support having $m = n = 2$ is illustrated in Figure 3.5 along with the mapping of the diagonal block onto the 1-D X vector.

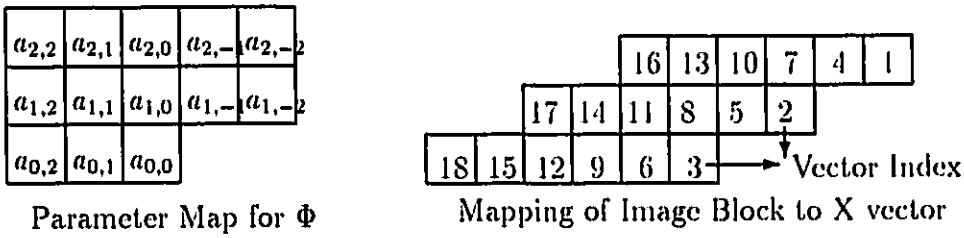

Figure 3.5: The Mapping of Parameters and Image Values to the NSHP Region of Support for $m = n = 2$.

Using the non-symmetric half plane region of support, the state vector $\mathbf{X}$ is changed to reflect the diagonal nature of the blocks in the following manner [5].

$$\mathbf{X}_{i,j} = [X_{i-1,j}^T \; X_{i-1,j+1}^T \; X_{i,j-1}^T X_{i,j}^T]^T \tag{3.54}$$

$$\mathbf{X}_{i,j} = \mathbf{A}_0 X_{i,j-1} + \mathbf{A}_1 X_{i-1,j+1} + \mathbf{B}\mathbf{U}_{i,j} \tag{3.55}$$

The A_0, A_1, and A_2 matrices need to change to reflect the different block state vector being used in the system dynamic equation.

$$\mathbf{A}_0 = \begin{bmatrix} 0 & \mathbf{I} & 0 & 0 \\ 0 & 0 & 0 & 0 \\ 0 & 0 & 0 & \mathbf{I} \\ 0 & A_0 & 0 & A_1 \end{bmatrix} \text{ and } \mathbf{A}_1 = \begin{bmatrix} 0 & 0 & 0 & 0 \\ 0 & 0 & 0 & \mathbf{I} \\ 0 & 0 & 0 & 0 \\ 0 & 0 & 0 & A_2 \end{bmatrix} \tag{3.56}$$

$$\mathbf{B} = [0\ 0\ 0\ B^T]^T$$

$$Y_{i,j} = C\Gamma_{i,j}X_{i,j} + V_{i,j} \tag{3.57}$$

Note that this results in a change in the parameters contained in the A and X matrices, but the remaining Kalman and parameter estimation equations remain unchanged. The mapping of the parameters within the A matrices for the case of $m = n = 2$ is given below.

$$A'_0 = \begin{bmatrix} a_{0,0} & 0 & 0 \\ a_{1,-2} & a_{0,0} & 0 \\ 0 & a_{1,-2} & a_{0,0} \end{bmatrix} A'_1 = \begin{bmatrix} a_{0,1} & 0 & 0 \\ a_{1,-1} & a_{0,1} & 0 \\ 0 & a_{1,-1} & a_{0,1} \end{bmatrix} A'_2 = \begin{bmatrix} a_{0,2} & 0 & 0 \\ a_{1,0} & a_{0,2} & 0 \\ a_{2,-2} & a_{1,0} & a_{0,2} \end{bmatrix}$$

$$A'_3 = \begin{bmatrix} 0 & 0 & 0 \\ a_{1,1} & 0 & 0 \\ a_{2,-1} & a_{1,1} & 0 \end{bmatrix} A'_4 = \begin{bmatrix} 0 & 0 & 0 \\ a_{1,2} & 0 & 0 \\ a_{2,0} & a_{1,2} & 0 \end{bmatrix}$$

$$A'_5 = \begin{bmatrix} 0 & 0 & 0 \\ 0 & 0 & 0 \\ a_{2,1} & 0 & 0 \end{bmatrix} A'_6 = \begin{bmatrix} 0 & 0 & 0 \\ 0 & 0 & 0 \\ a_{2,2} & 0 & 0 \end{bmatrix}$$

$$A_0'' = \begin{bmatrix} 0 & 0 & a_{1,-2} \\ 0 & 0 & 0 \\ 0 & 0 & 0 \end{bmatrix} A_1'' = \begin{bmatrix} 0 & 0 & a_{1,-1} \\ 0 & 0 & 0 \\ 0 & 0 & 0 \end{bmatrix} A_2'' = \begin{bmatrix} 0 & a_{2,-2} & a_{1,0} \\ 0 & 0 & a_{2,-2} \\ 0 & 0 & 0 \end{bmatrix}$$

$$A_3'' = \begin{bmatrix} 0 & a_{2,-1} & a_{1,1} \\ 0 & 0 & a_{2,-1} \\ 0 & 0 & 0 \end{bmatrix} A_4'' = \begin{bmatrix} 0 & a_{2,0} & a_{1,2} \\ 0 & 0 & a_{2,0} \\ 0 & 0 & 0 \end{bmatrix}$$

$$A_5'' = \begin{bmatrix} 0 & a_{2,1} & 0 \\ 0 & 0 & a_{2,1} \\ 0 & 0 & 0 \end{bmatrix} A_6'' = \begin{bmatrix} 0 & a_{2,2} & 0 \\ 0 & 0 & a_{2,2} \\ 0 & 0 & 0 \end{bmatrix}$$

$$A_{00} = \begin{bmatrix} A_0' & A_1' & A_2' & A_3' & A_4' & A_5' \\ 0 & A_0' & A_1' & A_2' & A_3' & A_4' \\ 0 & 0 & A_0' & A_1' & A_2' & A_3' \\ 0 & 0 & 0 & A_0' & A_1' & A_2' \\ 0 & 0 & 0 & 0 & A_0' & A_1' \\ 0 & 0 & 0 & 0 & 0 & A_0' \end{bmatrix} A_{01} = \begin{bmatrix} A_6' & 0 & 0 & 0 & 0 & 0 \\ A_5' & A_6' & 0 & 0 & 0 & 0 \\ A_4' & A_5' & A_6' & 0 & 0 & 0 \\ A_3' & A_4' & A_5' & A_6' & 0 & 0 \\ A_2' & A_3' & A_4' & A_5' & A_6' & 0 \\ A_1' & A_2' & A_3' & A_4' & A_5' & A_6' \end{bmatrix} \quad (3.58)$$

$$A_{10} = \begin{bmatrix} A_6'' & 0 & 0 & 0 & 0 & 0 \\ A_5'' & A_6'' & 0 & 0 & 0 & 0 \\ A_4'' & A_5'' & A_6'' & 0 & 0 & 0 \\ A_3'' & A_4'' & A_5'' & A_6'' & 0 & 0 \\ A_2'' & A_3'' & A_4'' & A_5'' & A_6'' & 0 \\ A_1'' & A_2'' & A_3'' & A_4'' & A_5'' & A_6'' \end{bmatrix} A_{11} = \begin{bmatrix} A_0'' & A_1'' & A_2'' & A_3'' & A_4'' & A_5'' \\ 0 & A_0'' & A_1'' & A_2'' & A_3'' & A_4'' \\ 0 & 0 & A_0'' & A_1'' & A_2'' & A_3'' \\ 0 & 0 & 0 & A_0'' & A_1'' & A_2'' \\ 0 & 0 & 0 & 0 & A_0'' & A_1'' \\ 0 & 0 & 0 & 0 & 0 & A_0'' \end{bmatrix} \quad (3.59)$$

$$A_0 = A_{00}^{-1} A_{10} \quad (3.60)$$

$$A_1 = A_{00}^{-1} A_{01} \tag{3.61}$$

$$A_2 = A_{00}^{-1} A_{11} \tag{3.62}$$

$$B = A_{00}^{-1} \tag{3.63}$$

3.6 Full Plane Kalman Filter

Kalman filtering is usually limited to the quarter plane or half plane regions of support in 2D image processing so that the filter remains causal [21],[48],[62],[60]. This limitation has the drawback of ignoring those pixels adjacent to the pixel being calculated that are in the "future" of the dynamic process, resulting in directionally biased estimates. Therefore, there are asymmetric distortions to the image that greatly detract from the image. Another limitation with the NSHP filter given above is that requires the states for the entire previous row processed to be saved. In order to reduce the problems of directional biasing and storage requirements of the filter, Citrin and Azimi-Sadjadi[11] also developed a semi-causal Kalman filter with a full plane region of support. The filter processes from left to right in strips without using the results of previous passes above the current pass. The mapping for the region of support for this filter is given in Figure 3.6. The full-plane Kalman filter is the combination of four Kalman filters, three employ causal regions of support while the fourth is semi-causal and is dependent on the output of the first three. The forward most block, $\mathbf{X}_6$, possesses a simplified quarter plane region of support for estimating its points. The upper and lower forward blocks also use a quarter plane region of support. The combined results from these three filters are applied

to calculate the final block using the full plane region of support. The full plane model, although requiring less storage, has a much greater complexity due to the four parallel filters, each with its own set of parameters. As well, fewer image points are processed per iteration of the filter for the same size region of support. These factors greatly increase the computational requirements of the full plane filter over those of the half plane filter.

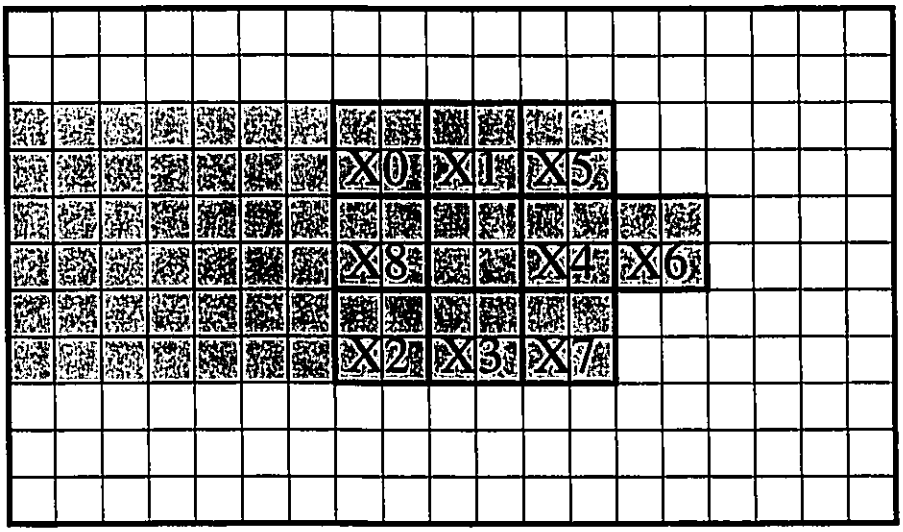

Figure 3.6: Full Plane region of support for 2-D AR image model.

In the original full plane Kalman filter [11], the system parameters were calculated *a priori* using the complete image statistics. The filter will be modified in this thesis to include the parameter estimation technique given by Ljung and Söderström [37]. The basic blocks of the full plane filter are given as in Figure 3.6. The image blocks on the trailing edge, $\mathbf{X}_0$, $\mathbf{X}_1$, $\mathbf{X}_2$, $\mathbf{X}_3$, and $\mathbf{X}_4$, are copied from the block to their right. The remaining blocks are calculated using the 2-D dynamic process equations.

$$\mathbf{X}_0 \Leftarrow \mathbf{X}_1 \tag{3.64}$$

$$\mathbf{X}_1 \Leftarrow \mathbf{X}_5 \tag{3.65}$$

$$\mathbf{X}_2 \Leftarrow \mathbf{X}_3 \tag{3.66}$$

$$\mathbf{X}_3 \Leftarrow \mathbf{X}_7 \tag{3.67}$$

$$\mathbf{X}_4 \Leftarrow \mathbf{X}_6 \tag{3.68}$$

$$A'_{06}\mathbf{X}_6 \Leftarrow A'_{66}\mathbf{X}_6 \tag{3.69}$$

$$A'_{05}\mathbf{X}_5 \Leftarrow A'_{54}\mathbf{X}_4 + A'_{55}\mathbf{X}_5 + A'_{56}\mathbf{X}_6 + A'_{57}\mathbf{X}_7 \tag{3.70}$$

$$A'_{07}\mathbf{X}_7 \Leftarrow A'_{74}\mathbf{X}_4 + A'_{75}\mathbf{X}_5 + A'_{76}\mathbf{X}_6 + A'_{77}\mathbf{X}_7 \tag{3.71}$$

$$A'_{08}\mathbf{X}_8 \Leftarrow A'_{80}\mathbf{X}_0 + A'_{81}\mathbf{X}_1 + \ldots + A'_{88}\mathbf{X}_8 \tag{3.72}$$

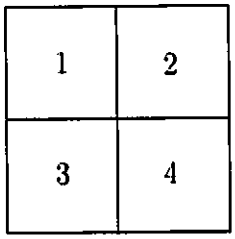

Figure 3.7: Example Mapping of 2-D blocks to Block Vector. Number corresponds to Location in X Vector.

The A' matrices are combined to calculate the state transition equations. One possible choice of input-output model parameters for the parameter estimations and the mapping to the full plane model for $m = 2$ is given below. The a_0 parameter is shown set to -1. The mapping of each X block to a vector is given in Figure 3.7. The mapping of each parameter to the local region of support for each block is given

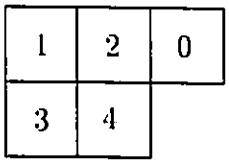

Mapping For X_6 1,2

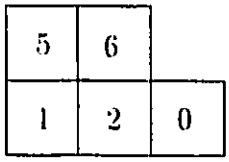

Mapping for X_6 3,4

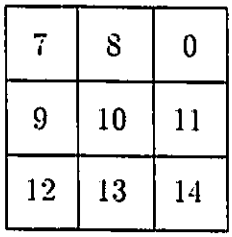

Mapping for X_5

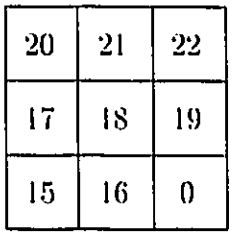

Mapping for X_7

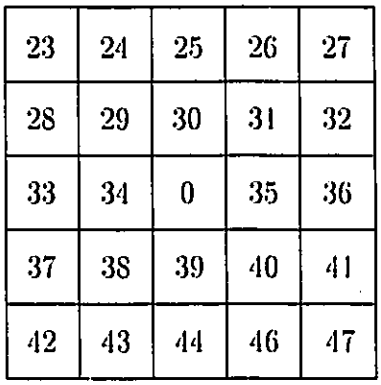

Mapping for X_8

Figure 3.8: Example Mapping FullPlane Parameters to Each Region of Support. Number corresponds to Location in Parameter Vector.

in Figure 3.8.

$$A'_{05} = \begin{bmatrix} -1 & 0 & a_{11} & 0 \\ a_8 & -1 & a_{10} & a_{11} \\ 0 & 0 & -1 & 0 \\ 0 & 0 & a_8 & -1 \end{bmatrix} \text{ and } A'_{55} = \begin{bmatrix} a_7 & a_8 & a_9 & a_{10} \\ 0 & a_7 & 0 & a_9 \\ 0 & 0 & a_7 & a_8 \\ 0 & 0 & 0 & a_7 \end{bmatrix}$$

$$A'_{54} = \begin{bmatrix} a_{12} & a_{13} & 0 & 0 \\ 0 & a_{12} & 0 & 0 \\ a_9 & a_{10} & a_{12} & a_{13} \\ 0 & a_9 & 0 & a_{12} \end{bmatrix} \text{ and } A'_{56} = \begin{bmatrix} a_{14} & 0 & 0 & 0 \\ a_{13} & a_{14} & 0 & 0 \\ a_{11} & 0 & a_{14} & 0 \\ a_{10} & a_{11} & a_{13} & a_{14} \end{bmatrix}$$

$$A'_{06} = \begin{bmatrix} -1 & 0 & 0 & 0 \\ a_2 & -1 & a_4 & 0 \\ 0 & 0 & -1 & 0 \\ a_6 & 0 & a_2 & -1 \end{bmatrix} \text{ and } A'_{66} = \begin{bmatrix} a_1 & a_2 & a_3 & a_4 \\ 0 & a_1 & 0 & a_3 \\ a_5 & a_6 & a_1 & a_2 \\ 0 & a_5 & 0 & a_1 \end{bmatrix}$$

$$A'_{07} = \begin{bmatrix} -1 & 0 & 0 & 0 \\ a_{16} & -1 & 0 & 0 \\ a_{19} & 0 & -1 & 0 \\ a_{18} & a_{19} & a_{16} & -1 \end{bmatrix} \text{ and } A'_{77} = \begin{bmatrix} a_{15} & a_{16} & 0 & 0 \\ 0 & a_{15} & 0 & 0 \\ a_{17} & a_{18} & a_{15} & a_{16} \\ 0 & a_{17} & 0 & a_{15} \end{bmatrix}$$

$$A'_{74} = \begin{bmatrix} a_{20} & a_{21} & a_{17} & a_{18} \\ 0 & a_{20} & 0 & a_{17} \\ 0 & 0 & a_{20} & a_{21} \\ 0 & 0 & 0 & a_{20} \end{bmatrix} \text{ and } A'_{76} = \begin{bmatrix} a_{22} & 0 & a_{19} & 0 \\ a_{21} & a_{22} & a_{18} & a_{19} \\ 0 & 0 & a_{22} & 0 \\ 0 & 0 & a_{21} & a_{22} \end{bmatrix}$$

$$A'_{08} = \begin{bmatrix} -1 & a_{35} & a_{39} & a_{40} \\ a_{34} & -1 & a_{38} & a_{39} \\ a_{30} & a_{31} & -1 & a_{21} \\ a_{29} & a_{30} & a_{34} & -1 \end{bmatrix} \text{ and } A'_{80} = \begin{bmatrix} a_{23} & a_{24} & a_{28} & a_{29} \\ 0 & a_{23} & 0 & a_{28} \\ 0 & 0 & a_{23} & a_{24} \\ 0 & 0 & 0 & a_{23} \end{bmatrix}$$

$$A'_{81} = \begin{bmatrix} a_{25} & a_{26} & a_{30} & a_{31} \\ a_{24} & a_{25} & a_{29} & a_{30} \\ 0 & 0 & a_{25} & a_{26} \\ 0 & 0 & a_{24} & a_{25} \end{bmatrix} \text{ and } A'_{82} = \begin{bmatrix} a_{42} & a_{43} & 0 & 0 \\ 0 & a_{42} & 0 & 0 \\ a_{38} & a_{39} & a_{42} & a_{43} \\ 0 & a_{38} & 0 & a_{42} \end{bmatrix}$$

$$A'_{83} = \begin{bmatrix} a_{44} & a_{45} & 0 & 0 \\ a_{43} & a_{44} & 0 & 0 \\ a_{39} & a_{40} & a_{44} & a_{45} \\ a_{38} & a_{39} & a_{43} & a_{44} \end{bmatrix} \text{ and } A'_{84} = \begin{bmatrix} a_{36} & 0 & a_{41} & 0 \\ a_{35} & a_{36} & a_{40} & a_{41} \\ a_{32} & 0 & a_{36} & 0 \\ a_{31} & a_{32} & a_{35} & a_{36} \end{bmatrix}$$

$$A'_{85} = \begin{bmatrix} a_{27} & 0 & a_{32} & 0 \\ a_{26} & a_{27} & a_{31} & a_{32} \\ 0 & 0 & a_{27} & 0 \\ 0 & 0 & a_{26} & a_{27} \end{bmatrix} \text{ and } A'_{87} = \begin{bmatrix} a_{46} & 0 & 0 & 0 \\ a_{45} & a_{46} & 0 & 0 \\ a_{41} & 0 & a_{46} & 0 \\ a_{40} & a_{41} & a_{45} & a_{46} \end{bmatrix}$$

$$A'_{88} = \begin{bmatrix} a_{33} & a_{34} & a_{37} & a_{38} \\ 0 & a_{33} & 0 & a_{37} \\ a_{28} & a_{29} & a_{33} & a_{34} \\ 0 & a_{28} & 0 & a_{33} \end{bmatrix}$$

$$\mathbf{A}_{66} = -A'_{06}{}^{-1} A'_{66} \tag{3.73}$$

$$\mathbf{A}_{54} = -A'_{05}{}^{-1} A'_{54} \tag{3.74}$$

$$\mathbf{A}_{55} = -A'_{05}{}^{-1} A'_{55} \tag{3.75}$$

$$\mathbf{A}_{56} = -A'_{05}{}^{-1} A'_{56} \tag{3.76}$$

$$\mathbf{A}_{57} = 0 \tag{3.77}$$

$$\mathbf{A}_{74} = -A'_{07}{}^{-1} A'_{74} \tag{3.78}$$

$$\mathbf{A}_{75} = 0 \tag{3.79}$$

$$\mathbf{A}_{76} = -A'_{07}{}^{-1} A'_{76} \tag{3.80}$$

$$\mathbf{A}_{77} = -A'_{07}{}^{-1} A'_{77} \tag{3.81}$$

$$\mathbf{A}_{80} = -A'_{08}{}^{-1} A'_{80} \tag{3.82}$$

$$\mathbf{A}_{81} = -A'_{08}{}^{-1} A'_{81} \tag{3.83}$$

$$\mathbf{A}_{82} = -A'_{08}{}^{-1} A'_{82} \tag{3.84}$$

$$\mathbf{A}_{83} = -A'_{08}{}^{-1} A'_{83} \tag{3.85}$$

$$\mathbf{A}_{84} = -A'_{08}{}^{-1} A'_{84} \tag{3.86}$$

$$\mathbf{A}_{85} = -A'_{08}{}^{-1} A'_{85} \tag{3.87}$$

$$\mathbf{A}_{86} = 0 \tag{3.88}$$

$$\mathbf{A}_{87} = -A'_{08}{}^{-1} A'_{87} \tag{3.89}$$

$$\mathbf{A}_{88} = -A'_{08}{}^{-1} A'_{88} \tag{3.90}$$

The dynamic equation for this filter is given as

$$\mathbf{X}_{i,j} = \mathbf{A}\mathbf{X}_{i,j-1} + \mathbf{B}\mathbf{U}_{i,j} \tag{3.91}$$

where

$$\mathbf{A} = \begin{bmatrix} 0 & \mathbf{I} & 0 & 0 & 0 & 0 & 0 & 0 & 0 \\ 0 & 0 & 0 & 0 & 0 & \mathbf{I} & 0 & 0 & 0 \\ 0 & 0 & 0 & \mathbf{I} & 0 & 0 & 0 & 0 & 0 \\ 0 & 0 & 0 & 0 & 0 & 0 & 0 & \mathbf{I} & 0 \\ 0 & 0 & 0 & 0 & 0 & 0 & \mathbf{I} & 0 & 0 \\ 0 & 0 & 0 & 0 & A_{54} & A_{55} & A_{56} & A_{57} & 0 \\ 0 & 0 & 0 & 0 & 0 & 0 & A_{66} & 0 & 0 \\ 0 & 0 & 0 & 0 & A_{74} & A_{75} & A_{76} & A_{77} & 0 \\ A_{80} & A_{81} & A_{82} & A_{83} & A_{84} & A_{85} & A_{86} & A_{87} & A_{88} \end{bmatrix} \tag{3.92}$$

The filter requires no history from each pass through the image, left to right. The filter processes only one strip at a time, using the data from three strips from the image. Only the centre strip from each scan through the image is saved.

In reviewing the development of the original ABKF by Azimi-Sadjadi [5], it can be seen that the derived Kalman filter is adaptive only in terms of a variable parameter system and even this condition is weakened when the filter is used to determine a steady state solution for both the Kalman gain and the parameters. The next chapter deals with the development of modified adaptive block Kalman filters for both the halfplane and fullplane cases. These filters will be modified so that they are truly adaptive over the entire image by evaluating the multiplicative noise assumption for each set of blocks processed. This will allow the filter to better

follow the large variations found in a "speckled" image of urban regions such as that found in the test image of Victoria, B.C..

Chapter 4

Modified Adaptive Block Kalman Filters

In the implementation of the ABKF as given by Azimi-Sadjadi [5],[37], several simplifications were made that had a negative impact on the noise reduction capabilities of the filter for SAR imagery. These simplifications were made in order to reduce the computation time and were based on the assumption that the image process possessed homogeneous statistics, ie. that the process was stationary. In this chapter, the simplifications used in the original half-plane ABKF will be reviewed and modifications to improve the performance of the filter will be proposed and developed. To improve filter performance, the assumption of stationary multiplicative noise will be modified to allow the multiplicative noise terms to vary over the image. Lastly, in order to more closely model the rapidly varying SAR image characteristics in the presence of several strong point reflectors, a dynamic model incorporating mul-

tiplicative noise in the state transition matrix will be derived and applied to SAR image processing.

4.1 Modifications to the Original Adaptive Block Kalman Filter

In the development of the original ABKF [5], it was assumed that the parameter relationships in the state transition matrix were constant, and that the Kalman gain would converge to a steady state value. In conducting tests on the ABKF, it was found that the parameters often converged to values not optimal for the entire image. In addition, the generating equation for the forgetting factor, λ , decreased the weighting of newer information to such a degree that the parameter vector remained constant after a short period of time. The Kalman gain was also assumed constant over the entire image and the "steady state" values were used after a relatively few number of iterations. For many real SAR images, these limitations are unacceptable. The optimal parameters will change for the different regions within the image, such as the water regions and the urban regions. The Kalman gain factor and parameters that are valid for darker water regions will certainly not be the best choice for a highly variable urban region.

The concept of a steady state Kalman gain for the multiplicative noise model is invalid when one considers the Kalman gain equation, (3.24). The R_z term includes a signal dependent term as shown in (3.23) and thus varies proportionally to the

local statistics as given in (4.1).

$$R_z \propto \sigma_\gamma^2(\sigma_{x\,i,j}^2 + \mu_{x\,i,j}^2) \tag{4.1}$$

For single look images where the multiplicative noise variance, σ_γ, is approximately one, this term is not negligible. To illustrate the importance of a variable gain term, consider the outlined region from the single look image of Victoria, B.C. given in Figure 2.1. The variability and mean of that portion of the SAR image of Victoria is evident in the scatter plot of the intensity of three adjacent rows of the image given in Figure 4.1. The effect of the local image mean and variance on the gain is illustrated by the variation of the norm of the Kalman gain over this portion of the image as shown in Figure 4.2. The gain tends to a low value over regions of high variability and high mean, such as those in the built-up urban area in the centre of the image, and is close to unity over regions with low variability and low mean, such as the water regions in the harbour that have almost no variation. The norm of the gain peaks at the boundary conditions of the image due to the use of a constant value for pixels that fall outside of the original image boundaries. As the figures show, the gain will be inversely proportional to the local mean and variance of the image. Azimi-Sadjadi[5] assumed these terms to be negligible. In the case of single look intensity images this is demonstrably not a valid assumption.

The parameter estimation process is controlled by the forgetting factor, λ. This factor limits the impact of new information on the calculation of the new parameter estimates at each step of the algorithm. Recall that the parameter forgetting factor,

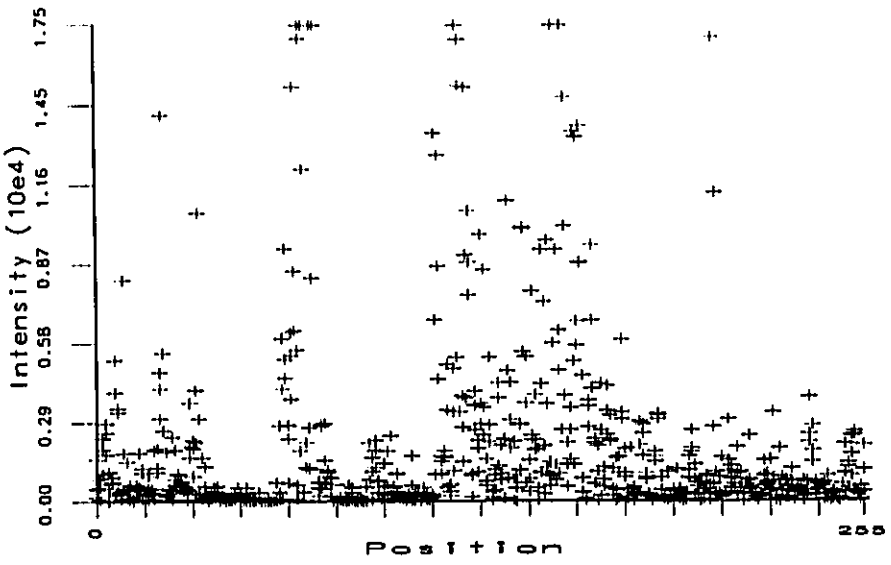

Figure 4.1: Scatter Plot of Three Adjacent rows from original Victoria image.

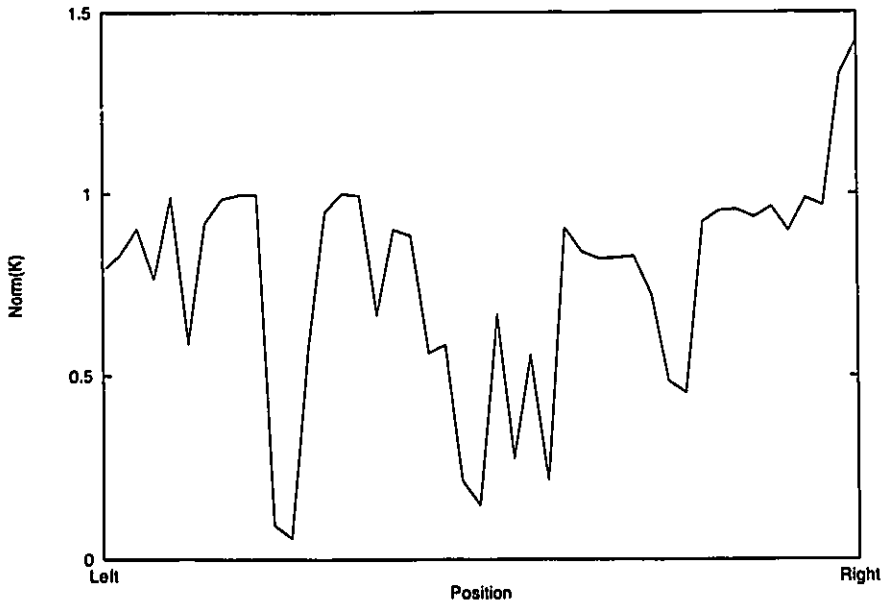

Figure 4.2: Plot of K_{norm} From Original ABKF on Victoria image.

λ was generated as a sequence using the formula

$$\lambda_k = \lambda_{ss} + \lambda_{rate}(\lambda_{k-1} - \lambda_{ss}) \tag{4.2}$$

In the original ABKF[5], the forgetting factor generating function was given as

$$\lambda_k = 0.99\lambda_{k-1} + 0.01 \tag{4.3}$$

which is equivalent to a λ_{ss} of 1.0 and a λ_{rate} of 0.99. The suggested λ_0 was 0.95. This form of the forgetting factor generating function applies to a time-invariant solution as given in [37]. If instead, a time-variant solution is allowed for the parameter estimation, the parameters will continue to change over the remaining image as the image properties vary over different regions. This may be achieved by simply setting λ_{ss} to a value less than 1.0. In most cases, setting λ_{ss} too low, will result in the parameters not converging. An appropriate value for λ_{ss} is between 0.95 and 0.99 for most time-variant cases. An initial condition of $\lambda_0 = 0.95$ is still suggested to be acceptable.

Since the filter is no longer assumed to reach a steady state solution, it is necessary to recalculate the Kalman gain for every iteration. This also requires the computation of the derivative of the Kalman gain κ for use in the parameter estimation. Calculating the derivative is, by far, the largest computational burden in the recursive parameter estimation. To calculate $\kappa_{i,j}$, the derivative of the gain equation given in (3.24) is needed. This in turn is dependent on the derivative of the *a priori* error covariance, $P_{i,j}^{(-)}$, given in (3.20) and $R_{z\ i,j}$, the covariance of the innovation process given in (3.23). The derivative of $P_{i,j}^{(-)}$ requires the derivative of past *a posteriori* covariances (3.27) and (3.21) as well as the derivative of each

of the state transition matrices: A_0, A_1, and B as detailed in (4.4) and (4.5). The resolution of the above variables involves as much calculation for the one $\kappa_{i,j}$ term as for the entire remainder of the Kalman filter. In order to reduce the complexity of the filter, this calculation must be simplified as much as possible.

$$\begin{aligned}
\frac{d}{d\Phi}K_k(\Phi) &= \mu_\gamma \frac{d}{d\Phi}(P_{i,j}^{(-)} C^T R_{z\,i,j}^{-1}) \\
&= \mu_\gamma \frac{dP_{i,j}^{(-)}}{d\Phi} C^T R_{z\,i,j}^{-1} + \mu_\gamma P_{i,j}^{(-)} C^T \frac{dR_{z\,i,j}^{-1}}{d\Phi} \qquad (4.4) \\
\frac{dP_{i,j}^{(-)}}{d\Phi} &= \frac{d}{d\Phi}[\mathbf{A}_0 P_{i,j-1}^{(+)} \mathbf{A}_0^T + \mathbf{A}_1 P_{i-1,j}^{(+)} \mathbf{A}_1^T + \\
&\quad \mathbf{A}_0 P_{i,j}^{(\times)} \mathbf{A}_1^T + \mathbf{A}_1 P_{i,j}^{(\times)T} \mathbf{A}_0^T + \\
&\quad \mathbf{B}\sigma_u^2 \mathbf{B}^T] \qquad (4.5)
\end{aligned}$$

Ljung and Söderström[37] show that the recursive parameter estimation(RPE) technique and the extended Kalman filter(EKF) are asymptotically equivalent in calculating the parameters of the state space model. Anderson and Moore[2] refer to models such as the RPE as an augmented innovations model of the extended Kalman filter. As well, the major differences between the two parameter estimation techniques are the cross-covariance terms, $P^{(\times)}$, and the coupling of the parameters Φ and the Kalman gain $K(\Phi)$ that results from the κ term in the RPE in (3.50). By removing the κ term from (3.50), the calculation of κ is no longer required and the computational requirements are greatly reduced. Based on [37], the filter should asymptotically converge to the same solution. However, the rate of convergence would be adversely affected [2],[37]. This results in a modified RPE equation as

given in (4.6).

$$\Sigma_{a(k)}(\Phi) = (\mathbf{I} - \mu_\gamma K_k(\Phi)C)\Sigma_{b(k)}(\Phi) \tag{4.6}$$

In order to avoid convergence problems with the recursive parameter estimation, the full RPE technique will be applied for the initial iterations of the filter. This will allow the parameters to quickly converge to those values appropriate for the initial portion of the image. Assuming that the parameters for different regions change relatively slowly, the EKF approximation of the RPE can then be used. It is also important to maintain the heuristic limitations on the parameter vector as specified on page 38 to ensure convergence [2]. Thus, the RPE from the ABKF is modified so that the initial parameter estimations are carried out using the full RPE, and that continued estimations are done with the derivative of the Kalman gain, κ, set to zero. This removes a large portion of the computational burden from the parameter estimation technique while having little affect on the performance of the filter. The value for the number of iterations to wait before switching from the full RPE to the extended Kalman filter approximation will be affected by the choice of the parameter estimation forgetting factors, λ_0, and λ_{rate}. The faster λ approaches λ_{ss}, the sooner the switch may be made from using (3.50) to using (4.6) in the parameter estimation process.

Since the filter is to be used for speckle reduction, the observation matrix, C, can be set to the identity matrix, $\mathbf{I}$. For the special case of no blur in the observation, i.e. $C = \mathbf{I}$, the calculation for the local state statistics, $\mu_{x\ i,j}$, and $\sigma^2_{x\ i,j}$, can be based

on the observed local statistics as detailed in (4.7) [5].

$$\sigma_{y\ i,j}^2 = \sigma_{\gamma\ i,j}^2 \mu_{x\ i,j}^2 + (\sigma_{\gamma\ i,j}^2 + \mu_{\gamma\ i,j}^2)\sigma_{x\ i,j}^2 + \sigma_v^2 \tag{4.7}$$

where

$$\begin{aligned} \mu_{x\ i,j} &= \mu_{y\ i,j}/\mu_{\gamma\ i,j} \\ \mu_{y\ i,j} &\quad \text{is the local mean for block i,j,} \\ \sigma_y^2 &\quad \text{is the local variance for block i,j.} \\ \sigma_{\gamma\ i,j} &\quad \text{is the local variance for} \\ &\quad \text{the multiplicative observation noise} \end{aligned} \tag{4.8}$$

This equation can be rearranged to give a calculation for the local state variance

$$\sigma_{x\ i,j}^2 = (\sigma_{y\ i,j}^2 - \sigma_{\gamma\ i,j}^2 \mu_{x\ i,j}^2 - \sigma_v^2)/(\sigma_{\gamma\ i,j}^2 + \mu_{\gamma\ i,j}^2) \tag{4.9}$$

It is important to realize that the blind application of these equations to determine the local state statistics can lead to errors involving the use of negative values for the variance, σ_x^2. The negative values are result from very homogeneous regions, where the variance of the observed image is very low and the speckle assumption is no longer valid. In order to avoid this and to better model the image based on its true statistics, the variance of the image σ_x^2 is set to zero and the multiplicative noise variance σ_γ^2 is recalculated as in (4.11) so that (4.7) remains true. Thus, the multiplicative noise variance will be reduced in regions with the homogeneity exceeding that of the original estimate of the multiplicative noise.

$$\sigma_{\gamma\ i,j}^2 = \sigma_{y\ i,j}^2 - \mu_{\gamma\ i,j}^2 \sigma_{x\ i,j}^2 - \sigma_v^2/(\mu_{x\ i,j}^2 + \sigma_{x\ i,j}^2) \tag{4.10}$$

Given that $\mu_\gamma = 1$ and for this special case, $\sigma_{x\ i,j} = 0$, (4.10) can be simplified to

$$\sigma^2_{\gamma\ i,j} = (\sigma^2_{y\ i,j} - \sigma^2_v)/\mu^2_{x\ i,j} \tag{4.11}$$

In examining the original implementation of the ABKF given by Azimi-Sadjadi [5] several simplifications and assumptions were made that are not valid for the processing of single look intensity SAR images. The forgetting factor generating function (4.3) for the time-invariant case as given in [5] was replaced with a time-variant version (4.2). The Kalman gain was assumed to be dependent on local statistics requiring updates for every iteration of the filter. To reduce the computational burden that was required by setting the gain to a non-constant value, the RPE technique used for parameter estimation was modified by removing the derivative of the gain, κ, from (3.50) after some number of initial iterations with the full ABKF. The inclusion of the κ term at the beginning allows the estimated parameters to converge to an initial value quickly. As well, a check was placed on the calculation of the local statistics in order to prevent inadvertent use of negative terms for the local variance, $\sigma^2_{x\ i,j}$. These changes should result in a filter with better performance than the original ABKF over single look intensity SAR images.

4.2 Adaptive Observation Multiplicative Noise Parameters

It has been shown by many [32],[15],[27] that, over homogeneous regions, the speckle statistics of SAR imagery remain stationary and close to the theoretical values of

$1/\sqrt{M}$; where M is the number of looks. However, in areas with strong point reflectors, such as urban regions, the assumption of fully developed speckle is no longer true. Consider the observation effected by a multiplicative noise as given in the relationship:

$$Y_{i,j} = C\Gamma_{i,j}X_{i,j} + V_{i,j} \quad observation \tag{4.12}$$

with the following multiplicative noise conditions:

$$\mathcal{E}[\Gamma_{i,j}] = \mu_\gamma \quad multiplicative\ noise \tag{4.13}$$

$$\mathcal{E}[\Gamma_{i,j}\Gamma^T_{i-k,j-l}] = \sigma^2_\gamma \mathbf{I}\delta_{k,l} + \mu^2_\gamma \mathbf{I} \tag{4.14}$$

If it is assumed that the statistics of the multiplicative noise are non-stationary over the entire image, then a variable value of σ^2_γ must be considered.

Lopes et al.[40] developed a criteria to assess the validity of the multiplicative noise assumption for use in many SAR imagery filters. This criteria, known as the coefficient of variation, C_o, is the ratio of the square root of the variance of a region to the mean of the region. For a homogeneous region, this coefficient is also known as the speckle index. This parameter can be used to modify the multiplicative noise term in the state observation equation (3.10).

$$C_o = \frac{\sigma_{y\ ij}}{\mu_{y\ i,j}} \tag{4.15}$$

For regions where the multiplicative noise assumption is valid, the algorithm may be left unchanged. For regions where the coefficient of variation exceeds a given

limit, the multiplicative noise assumption is deemed invalid and must be relaxed. Two values must be defined: σ_γ^2 is the value of the multiplicative noise variance over the majority of the image and is typically $\sim 1/\sqrt{M}$; $\sigma_{\gamma\ i,j}^2$ is a localized value of the multiplicative noise variance that is calculated for each iteration. For a smooth decrease in the effect of this variation a linear decay function, $f(C_o)$, is defined.

$$f(C_o) = \begin{cases} 1 & If\ C_o \leq C_{omax1} \\ \frac{C_{omax2} - C_o}{C_{omax2} - C_{omax1}} & if\ C_{omax1} < C_o < C_{omax2} \\ 0 & \text{otherwise} \end{cases} \tag{4.16}$$

The decay function may now be applied to the multiplicative noise term, $\sigma_{\gamma\ i,j}$ so that the value of the noise term will be decreased as the assumption becomes less likely, until the multiplicative noise parameter is set to zero at C_{omax2}.

$$\sigma_{\gamma\ i,j} = f(C_o)\sigma_\gamma \tag{4.17}$$

As well, the parameter estimation must be reduced or terminated for the iteration when the model assumptions no longer hold. This will prevent the parameters from being affected by the errors created by applying the model to localized regions of images that do not fit the model. Consequently, the calculation of the parameter vector in (3.48) must be modified as given in (4.18).

$$\Phi_k = [\Phi_{k-1} + f(C_o)\mathcal{L}_k Z_k]\mathfrak{D}_M \tag{4.18}$$

The effect of this modification can be determined by examining the formulation of the gain in (3.24) and (3.23). By setting the multiplicative noise variance term, σ_γ, to zero the value of the gain, K, will have a larger magnitude allowing the filter to better track the change in the image. The parameter estimation is halted so that any large transients are not introduced into the parameter vector.

The values for C_{omax} must be chosen so that the Kalman filter is capable of following the changes in the image over highly variable areas without under-smoothing more homogeneous regions. For an intensity image, the values should be larger than the expected value over a homogeneous region of $C_o = 1/\sqrt{M}$. Lopes et al.[40] suggest a value of $C_{omax} = \sqrt{1 + 2/M}$ for an intensity image. For a one-look intensity image, this results in a value of $C_{omax} = 1.73$.

Although there are various means of determining an optimal estimate of the multiplicative noise parameter, it is only required here to ascertain the effectiveness of varying the multiplicative noise parameter. This may lead to other methods in future work.

By combining the limitations of σ_γ^2 given here in (4.11), the multiplicative noise variance can be calculated as follows:

$$\sigma_{\gamma\ i,j}^2 = \begin{cases} (\sigma_{y\ i,j}^2 - \sigma_v^2)/\mu_{x\ i,j}^2 & \sigma_{y\ i,j}^2 - \sigma_v^2 < \sigma_{\gamma\ k}^2 \\ f(C_o)\sigma_\gamma & \text{otherwise} \end{cases} \tag{4.19}$$

The calculation of the variable σ_γ^2 term will effect the calculation of the R_z term (3.23) which in turn effects the value of the Kalman gain (3.24). The affected equations are given below.

$$R_{z\ i,j} = \mu_\gamma^2 C P_{i,j}^{(-)} C^T + \sigma_v^2 \mathbf{I} + \sigma_{\gamma\ i,j}^2 (\sigma_{x\ i,j}^2 + \mu_{x\ i,j}^2) C C^T \tag{4.20}$$

$$K_{i,j} = \mu_\gamma P_{i,j}^{(-)} C^T R_{z\ i,j}^{-1} \tag{4.21}$$

A block diagram of the resulting Kalman filter is given in Figure 4.3.

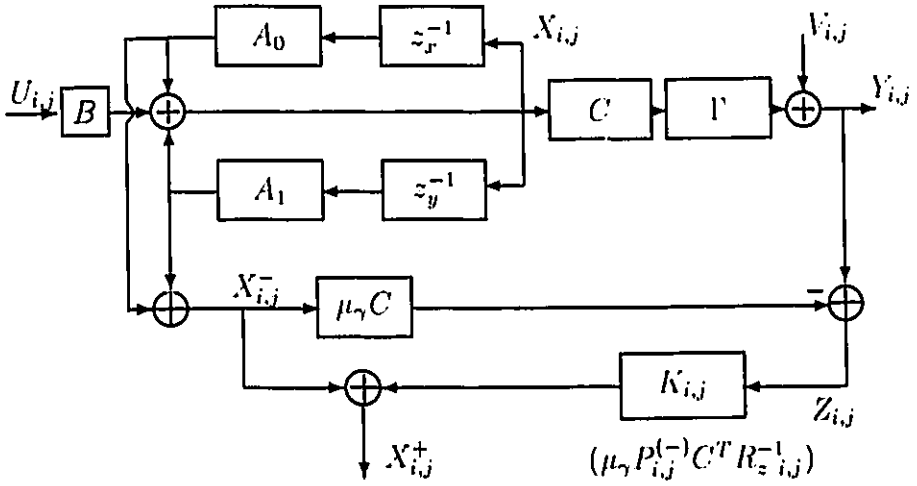

Figure 4.3: Block Diagram of Modified Block Kalman Filter.

The filter derived by combining both the modifications to the ABKF discussed in Section 4.1 and in this section were applied to the non-symmetric half plane region of support model detailed in Section 3.5 and the full plane model detailed in Section 3.6. In the tests of the filters, these will be referred to as the MABKF for the modified ABKF with the half plane region of support and the FABKF for the modified ABKF with the full plane region of support.

4.3 Adaptive Multiplicative Noise Parameters in the Dynamic Equations

In examining the image formation model of a SAR image and the nature of urban regions containing many strong reflectors, it has been proposed that the change in

the radar response between adjacent regions may be related using a multiplicative noise term in the state transition equation (3.8). This is a result of the property of radar in regions of strong returns that are due to point reflectors. Urban regions tend to consist of complicated regions that vary quickly from strong point reflectors to "dark" regions caused by building shadows or multi-path effects on the radar. The use of a multiplicative noise parameter in the dynamic equation would allow the filter to follow the image in regions of fast change such as sharp edges. These modified block dynamic equations would be expressed as

$$X_{i,j} = \mathbf{A}_0\Psi\mathbf{X}_{i,j-1} + \mathbf{A}_1\Psi\mathbf{X}_{i-1,j} + \mathbf{BU} \quad \textit{state transition} \tag{4.22}$$

$$Y_{i,j} = C\Gamma X_{i,j} + V \quad \textit{observation} \tag{4.23}$$

where the noise process Ψ is Gaussian with the following statistics:

$$\mathcal{E}[\Psi_{i,j}] = 1 \quad \textit{multiplicative state noise} \tag{4.24}$$

$$\mathcal{E}[\Psi_{i,j}\Psi^T_{i-k,j-l}] = \sigma^2_\psi \mathbf{I}\delta_{k,l} + \mathbf{I} \tag{4.25}$$

and the remaining noise parameters are

$$\mathcal{E}[U_{i,j}] = 0 \quad \textit{process noise} \tag{4.26}$$

$$\mathcal{E}[U_{i,j}U^T_{i-k,j-l}] = \sigma^2_u \mathbf{I}\delta_{k,l} \tag{4.27}$$

$$\mathcal{E}[V_{i,j}] = 0 \quad \textit{observation noise} \tag{4.28}$$

$$\mathcal{E}[V_{i,j}V^T_{i-k,j-l}] = \sigma^2_v \mathbf{I}\delta_{k,l} \tag{4.29}$$

$$\mathcal{E}[\Gamma_{i,j}] = \mu_\gamma \quad \textit{multiplicative noise} \tag{4.30}$$

$$\mathcal{E}[\Gamma_{i,j}\Gamma^T_{i-k,j-l}] = \sigma^2_\gamma \mathbf{I}\delta_{k,l} + \mu^2_\gamma \mathbf{I} \tag{4.31}$$

Note that the various noise parameters, u, and v, are independent of the signal, $\mathbf{X}$, and are uncorrelated to each other.

We also assume that the multiplicative noise parameters $\Psi_{\cdot}$ are independent of the signal, $\mathbf{X}$, and the other noise parameters, Γ, $U_{\cdot}$, and $V_{\cdot}$.

The local statistics of the image model are also defined for the state variable X as

$$\mathcal{E}[X] = \mu_{x\,i,j} \tag{4.32}$$

$$\mathcal{E}[X_{i,j}X^T_{i-k,j-l}] = \sigma^2_{x\,i,j}\mathbf{I}\delta_{k,l} + \mu^2_{x\,i,j}\mathbf{I} \tag{4.33}$$

The resulting dynamic model is given as a block diagram in Figure 4.4. Recall that the terms z_x^{-1} and z_y^{-1} are the shift operators in the x and y directions. The derivation of the required Kalman equations will be given next.

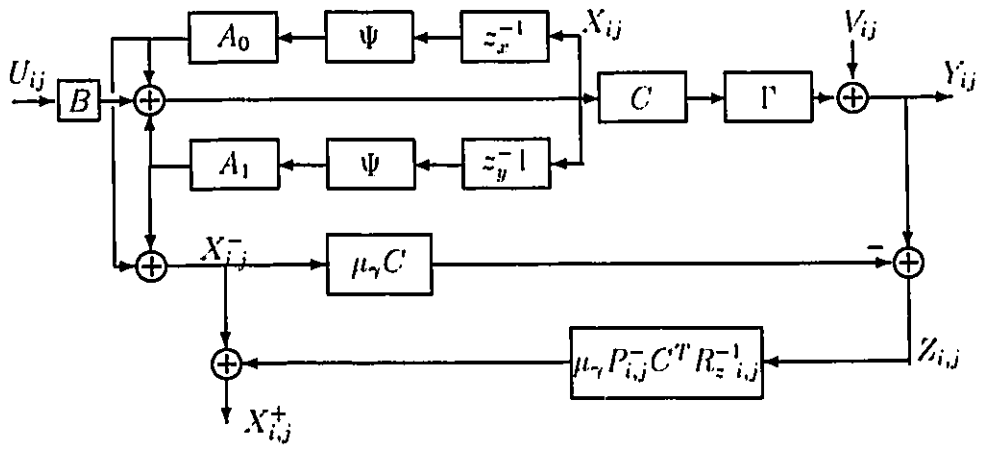

Figure 4.4: Block Diagram of State Space Model with State Transition Multiplicative Noise.

4.3.1 Derivation of Modified Kalman Equations

The derivation of the Kalman equations is done similarly to the derivation of the equations given in chapter 3. The re-evaluation of each of the Kalman equations is given here to determine the effects of including a multiplicative noise term, Ψ, in the state transition equation (4.22).

a priori estimate

$$\begin{aligned}
\mathbf{X}_{i,j}^{(-)} &= \mathcal{E}[\mathbf{X}_{i,j}|\mathbf{X}_{i-1,j}, \mathbf{X}_{i,j-1}] \\
&= \mathcal{E}[\mathbf{A}_0\Psi\mathbf{X}_{i,j-1} + \mathbf{A}_1\Psi\mathbf{X}_{i-1,j} + \mathbf{B}\mathbf{U}_{i,j}] \\
&\quad \Psi \text{ and } \mathbf{X} \text{ are independent, therefore} \\
\mathcal{E}[\Psi\mathbf{X}] &= \mathcal{E}[\Psi]\mathcal{E}[\mathbf{X}] = \mathcal{E}[\mathbf{X}] \\
&\quad \text{Recall } \mathcal{E}[U_{i,j}] = 0, \text{ giving} \\
\mathbf{X}_{i,j}^{(-)} &= \mathbf{A}_0\mathbf{X}_{i,j-1}^{(+)} + \mathbf{A}_1\mathbf{X}_{i-1,j}^{(+)} \qquad (4.34)
\end{aligned}$$

Assuming x and y are jointly Gaussian, then an optimal estimator may be expressed as a function of the *a priori* estimate, $X_{i,j}^{(-)}$, and the observation, $\mathbf{Y}$ in the form:

$$\mathbf{X}_{i,j}^{(+)} = K_k^1\mathbf{X}_{i,j}^{(-)} + \bar{K}_k\mathbf{Y}_{i,j} \qquad (4.35)$$

The orthogonality condition [20] must be met to determine the minimum mean squared error. This can be written as

$$\mathcal{E}[(\mathbf{X}_{i,j} - \mathbf{X}_{i,j}^{(+)})\mathbf{Y}_{k,l}^T] = 0 \qquad 1 \le k < i, 1 \le l < j \qquad (4.36)$$

Using this relationship and the fact that $\mathcal{E}[V_{i,j}Y_{k,l}] = 0$ for $k,l < i,j$, the expression for the factor K_k^1 may be derived.

$$\begin{aligned}
\mathcal{E}[X_{i,j}Y_{k,l}^T - X_{i,j}^{(+)}Y_{k,l}^T] &= 0 \\
&\text{substituting (4.35)} \\
\mathcal{E}[X_{i,j}Y_{k,l}^T - K_k^1 X_{i,j}^{(-)}Y_{k,l}^T - \bar{K}_k Y_{i,j}Y_{k,l}^T] &= 0 \\
&\text{substituting (4.23)} \\
\mathcal{E}[X_{i,j}Y_{k,l}^T - K_k^1 X_{i,j}^{(-)}Y_{k,l}^T - \bar{K}_k C\Gamma X_{i,j}Y_{k,l}^T - \bar{K}_k V_{i,j}Y_{k,l}^T] &= 0 \\
\mathcal{E}[X_{i,j}Y_{k,l}^T - K_k^1 X_{i,j}^{(-)}Y_{k,l}^T - \bar{K}_k C\Gamma X_{i,j}Y_{k,l}^T] &= 0 \\
\mathcal{E}[(\mathbf{I} - \bar{K}_k C\Gamma)X_{i,j}Y_{k,l}^T - K_k^1 X_{i,j}^{(-)}Y_{k,l}^T &= 0 \\
\mathcal{E}[(\mathbf{I} - \bar{K}_k C\Gamma - K_k^1)X_{i,j}Y_{k,l}^T - K_k^1((X_{i,j}^{(-)} - X_{i,j})Y_{k,l}^T] &= 0 \\
&\text{using (4.36)} \\
\mathcal{E}[(\mathbf{I} - \bar{K}_k C\Gamma - K_k^1)X_{i,j}Y_{k,l}^T] &= 0 \\
(\mathbf{I} - \bar{K}C\mathcal{E}[\Gamma] - K_k^1)\mathcal{E}[X_{i,j}Y_{k,l}^T] &= 0 \\
(\mathbf{I} - \bar{K}C\mu_\gamma - K_k^1)\mathcal{E}[X_{i,j}Y_{k,l}^T] &= 0 \qquad (4.37)
\end{aligned}$$

This restriction will remain true if the first portion of the expression is zero. Therefore

$$K_k^1 = \mathbf{I} - \bar{K}_k C\mu_\gamma \qquad (4.38)$$

where $\bar{K}_k$ is the Kalman gain and will be simplified to K_k from now on.

Now the estimator, $X_{i,j}^{(+)}$ is expressed as

$$\begin{aligned}
X_{i,j}^{(+)} &= (\mathbf{I} - K_k C\mu_\gamma)X_{i,j}^{(-)} + K_k Y_{i,j} \\
&= X_{i,j}^{(-)} + K_k(Y_{i,j} - C\mu_\gamma X_{i,j}^{(-)}) \qquad (4.39)
\end{aligned}$$

Using the definition of the innovation

$$Z_{i,j} = Y_{i,j} - C\mu_\gamma X_{i,j}^{(-)} \tag{4.40}$$

the *a posteriori* estimate now assumes the standard Kalman filter form

$$X_{i,j}^{(+)} = X_{i,j}^{(-)} + K_{i,j} Z_{i,j} \tag{4.41}$$

Using the orthogonality condition again, the two equations

$$\begin{aligned} \mathcal{E}[(X_{i,j} - X_{i,j}^{(+)})Y_{i,j}^T] &= 0 \\ \mathcal{E}[(X_{i,j} - X_{i,j}^{(+)})(C\mu_\gamma X_{i,j}^{(-)})^T] &= 0 \end{aligned}$$

may be combined to give

$$\mathcal{E}[(X_{i,j} - X_{i,j}^{(+)})(Y_{i,j} - C\mu_\gamma X^{(-)})^T] = 0 \tag{4.42}$$

This equation may be arranged using (4.39), (4.23), and the definition for $P_{i,j}^{(-)}$ given in (3.20) to determine an expression for the Kalman gain

$$\begin{aligned} 0 &= \mathcal{E}[(X_{i,j} - X_{i,j}^{(-)} - KY_{i,j} + KC\mu_\gamma X_{i,j}^{(-)})(Y_{i,j} - C\mu_\gamma X^{(-)})^T] \\ 0 &= \mathcal{E}[((X_{i,j} - X_{i,j}^{(-)}) - K(C\Gamma X_{i,j} + V_{i,j}) + KC\mu_\gamma X_{i,j}^{(-)}) \\ &\quad (C\Gamma X_{i,j} + V_{i,j} - C\mu_\gamma X^{(-)})^T] \\ 0 &= \mathcal{E}[(X_{i,j} - X_{i,j}^{(-)}){X_{i,j}}^T \Gamma^T C^T - \\ &\quad (X_{i,j} - X_{i,j}^{(-)})(X_{i,j}^{(-)})^T \mu_\gamma C^T + \\ &\quad (X_{i,j} - X_{i,j}^{(-)}){V_{i,j}}^T - \\ &\quad KC(\Gamma X_{i,j} - \mu_\gamma X_{i,j}^{(-)}){X_{i,j}}^T \Gamma^T C^T + \end{aligned}$$

$$
\begin{aligned}
& KC(\Gamma X_{i,j} - \mu_\gamma X_{i,j}^{(-)})(X_{i,j}^{(-)})^T \mu_\gamma C^T - \\
& KC(\Gamma X_{i,j} - \mu_\gamma X_{i,j}^{(-)}) V_{i,j}{}^T - \\
& KV_{i,j} X_{i,j}{}^T \Gamma^T C^T + KV_{i,j}(X_{i,j}^{(-)})^T \mu_\gamma C^T - KV_{i,j} V_{i,j}^T] \qquad (4.43)
\end{aligned}
$$

$$
\begin{aligned}
0 \;=\; & \mathcal{E}[(X_{i,j} - X_{i,j}^{(-)})(X_{i,j} - X_{i,j}^{(-)})^T]\mu_\gamma C^T + \mathcal{E}[(X_{i,j} - X_{i,j}^{(-)})]\mathcal{E}[V_{i,j}] - \\
& KC\mathcal{E}[\Gamma X_{i,j} X_{i,j}{}^T \Gamma^T - \mu_\gamma X_{i,j}^{(-)} X_{i,j}{}^T \Gamma^T - \\
& \Gamma X_{i,j} X_{i,j}^{(-)}{}^T \mu_\gamma + \mu_\gamma X_{i,j}^{(-)} X_{i,j}^{(-)}{}^T \mu_\gamma] C^T - \\
& KC\mathcal{E}[\Gamma X_{i,j} - \mu_\gamma X_{i,j}^{(-)}]\mathcal{E}[V_{i,j}{}^T] - \\
& K\mathcal{E}[V_{i,j}]\mathcal{E}[X_{i,j}{}^T \Gamma^T] C^T + K\mathcal{E}[V_{i,j}][(X_{i,j}^{(-)})^T]\mu_\gamma C^T - K\mathcal{E}[V_{i,j} V_{i,j}^T] \qquad (4.44)
\end{aligned}
$$

Simplifying the expectation expressions and substituting for the expression of $P_{i,j}^{(-)}$ gives

$$
\begin{aligned}
0 \;=\; & P_{i,j}^{(-)} \mu_\gamma C^T - \\
& KC\mathcal{E}[\Gamma X_{i,j} X_{i,j}{}^T \Gamma^T] C^T - \\
& KC\mu_\gamma P_{i,j}^{(-)} \mu_\gamma C^T + \\
& KC\mu_\gamma \mathcal{E}[X_{i,j} X_{i,j}^T] \mu_\gamma C^T - \\
& K\mathcal{E}[V_{i,j} V_{i,j}^T] \qquad (4.45)
\end{aligned}
$$

$$
\begin{aligned}
0 \;=\; & \mu_\gamma P_{i,j}^{(-)} C^T - \\
& KC((\sigma_\gamma^2 + \mu_\gamma^2)(\sigma_x^2 + \mu_x^2)) C^T - \\
& KC\mu_\gamma^2 P_{i,j}^{(-)} C^T + \\
& KC(\mu_\gamma^2(\sigma_x^2 + \mu_x^2)) C^T \\
& -K\sigma_v^2 \qquad (4.46)
\end{aligned}
$$

$$
0 \;=\; \mu_\gamma P_{i,j}^{(-)} C^T - K(C\sigma_\gamma^2(\sigma_x^2 + \mu_x^2) C^T + \mu_\gamma^2 C P_{i,j}^{(-)} C^T + \sigma_v^2 \mathbf{I}) \qquad (4.47)
$$

Rearranging for the Kalman gain results in

$$K = P_{i,j}^{(-)} C^T \mu_\gamma [\mu_\gamma^2 C P_{i,j}^{(-)} C^T + C\sigma_\gamma^2(\sigma_x^2 + \mu_x^2)C^T + \sigma_v^2 \mathbf{I}]^{-1} \tag{4.48}$$

To derive the *a posteriori* error covariance,

$$\begin{aligned}
P_{i,j}^{(+)} &= \mathcal{E}[(X_{i,j} - X_{i,j}^{(+)})(X_{i,j} - X_{i,j}^{(+)})^T] \\
&\text{substituting in (4.39)} \\
P_{i,j}^{(+)} &= \mathcal{E}[(X_{i,j} - (\mathbf{I} - KC\mu_\gamma)X_{i,j}^{(-)} - KY_{i,j})(X_{i,j} - (\mathbf{I} - KC\mu_\gamma)X_{i,j}^{(-)} - KY_{i,j})^T] \\
&= \mathcal{E}[X_{i,j}(X_{i,j}^T - (X_{i,j}^{(-)})^T(\mathbf{I} - \mu_\gamma CK)^T - (K(C\Gamma X_{i,j} + V_{i,j})^T)] - \\
&\quad \mathcal{E}[(\mathbf{I} - KC\mu_\gamma)X_{i,j}^{(-)}(X_{i,j}^{(-)})^T(\mathbf{I} - \mu_\gamma CK)^T - (K(C\Gamma X_{i,j} + V_{i,j})^T)] - \\
&\quad \mathcal{E}[KC\Gamma X_{i,j}^{(-)}(X_{i,j}^{(-)})^T(\mathbf{I} - \mu_\gamma CK)^T - (K(C\Gamma X_{i,j} + V_{i,j})^T)] - \\
&\quad \mathcal{E}[KV_{i,j}(X_{i,j}^{(-)})^T(\mathbf{I} - \mu_\gamma CK)^T - (K(C\Gamma X_{i,j} + V_{i,j})^T)] \qquad (4.49) \\
&= \mathcal{E}[(\mathbf{I} - KC\Gamma)X_{i,j}X_{i,j}^T(\mathbf{I} - KC\Gamma)^T] - \\
&\quad \mathcal{E}[(\mathbf{I} - KC\mu_\gamma)X_{i,j}^{(-)}X_{i,j}^T(\mathbf{I} - KC\Gamma)^T] - \\
&\quad \mathcal{E}[(\mathbf{I} - KC\mu_\gamma)X_{i,j}^{(-)}X_{i,j}^T(\mathbf{I} - KC\Gamma)^T] + \\
&\quad \mathcal{E}[(\mathbf{I} - KC\mu_\gamma)X_{i,j}^{(-)}(X_{i,j}^{(-)})^T(\mathbf{I} - KC\mu_\gamma)^T] + \\
&\quad \mathcal{E}[KV_{i,j}V_{i,j}^T K^T] \qquad (4.50)
\end{aligned}$$

Now adding extra terms to complete the expression for $(X_{i,j} - X_{i,j}^{(-)})(X_{i,j} - X_{i,j}^{(-)})^T$, the equation becomes

$$\begin{aligned}
P_{i,j}^{(+)} &= (\mathbf{I} - KC\mu_\gamma)\mathcal{E}[(X_{i,j} - X_{i,j}^{(-)})(X_{i,j} - X_{i,j}^{(-)})^T](\mathbf{I} - KC\mu_\gamma) + \\
&\quad KC\mathcal{E}[\Gamma X_{i,j}X_{i,j}^T\Gamma^T]C^TK^T - KC\mu_\gamma\mathcal{E}[X_{i,j}X_{i,j}^T]\mu_\gamma C^TK^T + \\
&\quad K\mathcal{E}[V_{i,j}V_{i,j}^T]K^T
\end{aligned}$$

The expression for $P_{i,j}^{(-)}$ may now be substituted, and the expectations replaced by their values so that

$$\begin{aligned} P_{i,j}^{(+)} &= (\mathbf{I} - \mu_\gamma KC) P_{i,j}^{(-)} (\mathbf{I} - \mu_\gamma KC)^T + \\ &\quad KC(\sigma_\gamma^2(\sigma_x^2 + \mu_x^2))C^T K^T + \\ &\quad K\sigma_v^2 K^T \qquad (4.51) \\ &= (\mathbf{I} - \mu_\gamma KC) P_{i,j}^{(-)} - \mu_\gamma P_{i,j}^{(-)} C^T K^T + \\ &\quad KC(\sigma_\gamma^2(\sigma_x^2 + \mu_x^2))C^T K^T + \\ &\quad K(C P_{i,j}^{(-)} C^T + \sigma_v^2 \mathbf{I}) K^T \qquad (4.52) \end{aligned}$$

By substituting the expression for $\mu_\gamma P_{i,j}^{(-)} C^T$ from (4.47) into the above equation, the expression simplifies to

$$P_{i,j}^{(+)} = (\mathbf{I} - \mu_\gamma KC) P_{i,j}^{(-)} \qquad (4.53)$$

The expression for the *a priori* error covariance

$$P_{i,j}^{(-)} = \mathcal{E}[(X_{i,j} - X_{i,j}^{(-)})(X_{i,j} - X_{i,j}^{(-)})^T]$$

is now determined by substituting the expressions for $X_{i,j}$ and $X_{i,j}^{(-)}$ and expanding the resulting expression.

$$\begin{aligned} P_{i,j}^{(-)} &= \mathcal{E}[(\mathbf{A}_0 \Psi X_{i,j-1} + \mathbf{A}_1 \Psi X_{i-1,j} + BU - \mathbf{A}_0 X_{i,j-1}^{(+)} + \mathbf{A}_1 X_{i-1,j}^{(+)}) \\ &\quad (\mathbf{A}_0 \Psi X_{i,j-1} + \mathbf{A}_1 \Psi X_{i-1,j} + BU - \mathbf{A}_0 X_{i,j-1}^{(+)} + \mathbf{A}_1 X_{i-1,j}^{(+)})^T] \qquad (4.54) \\ &= \mathcal{E}[\mathbf{A}_0 \Psi X_{i,j-1} X_{i,j-1}^T \Psi^T A_0^T + \mathbf{A}_0 \Psi X_{i,j-1} X_{i-1,j}^T \Psi^T \mathbf{A}_1^T + \mathbf{A}_0 \Psi X_{i,j-1} U^T B^T - \\ &\quad \mathbf{A}_0 \Psi X_{i,j-1} X_{i,j-1}^{(+)T} \mathbf{A}_0^T - \mathbf{A}_0 \Psi X_{i,j-1} X_{i-1,j}^{(+)T} \mathbf{A}_1^T + \end{aligned}$$

$$\mathbf{A}_1\Psi X_{i-1,j}X_{i,j-1}^T\Psi^T\mathbf{A}_0^T + \mathbf{A}_1\Psi X_{i-1,j}X_{i-1,j}^T\Psi^T\mathbf{A}_1^T + \mathbf{A}_1\Psi X_{i-1,j}U^TB^T -$$
$$\mathbf{A}_1\Psi X_{i-1,j}X_{i,j-1}^{(+)^T}\mathbf{A}_0^T - \mathbf{A}_1\Psi X_{i-1,j}X_{i-1,j}^{(+)^T}\mathbf{A}_1^T +$$
$$BUX_{i,j-1}^T\Psi^T\mathbf{A}_0^T + BUX_{i-1,j}^T\Psi^T\mathbf{A}_1^T + BUU^TB^T -$$
$$BUX_{i,j-1}^{(+)^T}A_0^T - BUX_{i-1,j}^{(+)^T}A_1^T -$$
$$\mathbf{A}_0X_{i,j-1}^{(+)^T}X_{i,j-1}^T\Psi^T\mathbf{A}_0^T - \mathbf{A}_0X_{i,j-1}^{(+)^T}X_{i-1,j}^T\Psi^T\mathbf{A}_1^T - \mathbf{A}_0X_{i,j-1}^{(+)^T}U^TB^T +$$
$$\mathbf{A}_0X_{i,j-1}^{(+)^T}X_{i,j-1}^{(+)^T}\mathbf{A}_0^T + \mathbf{A}_0X_{i,j-1}^{(+)^T}X_{i-1,j}^{(+)^T}\mathbf{A}_1^T -$$
$$\mathbf{A}_1X_{i-1,j}^{(+)^T}X_{i,j-1}^T\Psi^T\mathbf{A}_0^T - \mathbf{A}_1X_{i-1,j}^{(+)^T}X_{i-1,j}^T\Psi^T\mathbf{A}_1^T - \mathbf{A}_1X_{i-1,j}^{(+)^T}U^TB^T +$$
$$\mathbf{A}_1X_{i-1,j}^{(+)^T}X_{i,j-1}^{(+)^T}\mathbf{A}_0^T + \mathbf{A}_1X_{i-1,j}^{(+)^T}X_{i-1,j}^{(+)^T}\mathbf{A}_1^T] \tag{4.55}$$

Substituting the expressions for the earlier $P^{(+)}$ in both the x and y directions and the cross covariance term, the equation now becomes

$$\begin{aligned} P_{i,j}^{(-)} &= \mathbf{A}_0P_{i,j-1}^{(+)}\mathbf{A}_0^T + \mathbf{A}_0\mathcal{E}[\Psi X_{i,j-1}X_{i,j-1}^T\Psi^T]\mathbf{A}_0^T - \mathbf{A}_0\mathcal{E}[X_{i,j-1}X_{i,j-1}^T]\mathbf{A}_0^T + \\ &\quad \mathbf{A}_1P_{i-1,j}^{(+)}\mathbf{A}_1^T + \mathbf{A}_1\mathcal{E}[\Psi X_{i-1,j}X_{i-1,j}^T\Psi^T]\mathbf{A}_1^T - \mathbf{A}_1\mathcal{E}[X_{i-1,j}X_{i-1,j}^T]\mathbf{A}_1^T + \\ &\quad \mathbf{A}_0P_{i,j}^{(\times)}\mathbf{A}_1^T + \mathbf{A}_0\mathcal{E}[\Psi X_{i,j-1}X_{i-1,j}^T\Psi^T]\mathbf{A}_1^T - \mathbf{A}_0\mathcal{E}[X_{i,j-1}X_{i-1,j}^T]\mathbf{A}_1^T + \\ &\quad \mathbf{A}_1P_{i,j}^{(\times)}\mathbf{A}_0^T + \mathbf{A}_1\mathcal{E}[\Psi X_{i-1,j}X_{i,j-1}^T\Psi^T]\mathbf{A}_0^T - \mathbf{A}_1\mathcal{E}[X_{i-1,j}X_{i,j-1}^T]\mathbf{A}_0^T + \\ &\quad B\mathcal{E}[UU^T]B^T \end{aligned} \tag{4.56}$$

Since the multiplicative noise, Ψ, and the original image, X, are independent, the result of the combined expectation can be expressed as

$$\mathcal{E}[\Psi X_{i,j-1}X_{i,j-1}^T\Psi^T] = \sigma_\psi^2(\sigma_x^2 + \mu_x^2) + \sigma_x^2 + \mu_x^2 \tag{4.57}$$

Recall that

$$\mathcal{E}[X_{i,j-1}X_{i,j-1}^T] = \sigma_x^2 + \mu_x^2 \tag{4.58}$$

resulting in the final expression for the *a priori* error covariance of

$$\begin{aligned} P_{i,j}^{(-)} &= \mathbf{A}_0 P_{i,j-1}^{(+)} \mathbf{A}_0^T + \mathbf{A}_1 P_{i-1,j}^{(+)} \mathbf{A}_1^T + \\ & \mathbf{A}_0 P_{i,j}^{(\times)} \mathbf{A}_1^T + \mathbf{A}_1 P_{i,j}^{(\times)T} \mathbf{A}_0^T + \\ & \mathbf{A}_0(\sigma_\psi^2(\sigma_x^2 + \mu_x^2))\mathbf{A}_0^T + \mathbf{A}_1(\sigma_\psi^2(\sigma_x^2 + \mu_x^2))\mathbf{A}_1^T + \\ & \mathbf{A}_0(\sigma_\psi^2(\sigma_x^2 + \mu_x^2))\mathbf{A}_1^T + \mathbf{A}_1(\sigma_\psi^2(\sigma_x^2 + \mu_x^2))\mathbf{A}_0^T + \\ & \mathbf{B}\sigma_u^2\mathbf{B}^T \end{aligned} \tag{4.59}$$

The above derivations show that only the *a priori* error covariance term changes when the multiplicative noise mean of one is included into the model. The formulation of the recursive parameter estimation remains the same as in [18], with only the derivative of *a priori* covariance changing to reflect the new equations. The effect of these new terms will be that the Kalman gain value will become more sensitive to local statistics. The *a priori* covariance will become larger as a result of these new terms, while the gain will become marginally larger as the covariance term is present in the Kalman gain equation as a multiplicative term and as part of the inverse of R_z, as shown in (4.48). In homogeneous regions and regions of low mean value, the effect of the multiplicative noise term in the state transition matrix will be negligible, and the effects should only become noticeable in regions of greater variance and mean. Currently, there is no proven method of estimating the desired value of the multiplicative noise term, but values less than one are recommended in order to maintain filter stability.

Using these derivations, the Kalman filter using multiplicative state transition

noise was applied to the NSHP model given in Section 3.5 and tests involving this filter will be referred to as the multiplicative modified ABKF (MMABKF).

At this point the derivation of the various modified Kalman filters has been given. The following chapter details the results of applying these filters to a series of test images and an actual SAR image. These results are compared with the original ABKF and other SAR speckle processing techniques.

Chapter 5

Results and Performance Evaluation

It is important to compare the performance of the modified filters to the original filters in terms of the variation of many of the parameters and Kalman gain during the use of the filters. The evaluation of the effectiveness of a filter is highly dependent on the final use of the output.

Shi and Fung [50] developed a series of criteria to compare the processing of SAR imagery by different filters. These criteria will be adapted in order to compare the performance of the modified non-symmetric half-plane and the full-plane ABKF filters developed in this thesis to the original ABKF filter and the Lee statistical filter. The criteria for filters for SAR imagery include: the speckle reduction capability, the change in the average mean of the image, the edge handling capability, point target capability, and distortion of angular structures. The filters will also be

evaluated using actual images, and the performance will be monitored by both the filter output and the behaviour of various filter parameters extracted from the test of the filter.

5.1 Implementation Considerations

The four Kalman filters used in the tests are: the original ABKF as described by Azimi-Sadjadi et al[5]; the modified ABKF(MABKF) as developed in chapter 4 with the same image model as the ABKF; the full-plane modified ABKF(FABKF) is the same as the MABKF but modified to use the semi-causal full-plane region of support as outlined in [11]; and the multiplicative modified ABKF(MMABKF) that includes the multiplicative noise terms in the model with the modifications outlined in the latter portion of chapter 4. The form of the MMABKF uses the same non-symmetric half-plane region of support as the ABKF and MABKF.

All of the Kalman filters use a region of support of 5 pixels in the x direction. The filters using the half-plane region of support, ABKF, MABKF, and MMABKF, use a region of support of only 3 pixels in the y direction, while the FABKF uses a 5x5 region of support for its final estimate for block 8. These values correspond to the dimension parameters of the filters as given in chapter 3 of $m = n = 2$. These values were chosen since the results of Azimi-Sadjadi in [5] suggested that this was the best choice for the ABKF. Although the performance of the original full-plane Kalman filter in [11] suggested an optimal size of $m = n = 1$, the dimension was

kept at $m = n = 2$ for comparison purposes.

In the implementation of the FABKF, it was found that attempting parameter estimation on the A_{66} matrix, ie. block 6, was highly sensitive to initial conditions, and parameter estimates were consequently highly untrustworthy. This was determined to be caused by the relatively small region of support that was used for the filter estimation of the parameters in matrix A_{66}. This small region of support did not allow sufficient statistical information for proper parameter estimation. In order to rectify this problem, the A_{66} matrix was removed from the parameter estimation and set constant as a Gaussian smoothing function. The Gaussian smoothing function was chosen as an approximation to a decaying weighting function such as the Frost filter that is often used in SAR speckle filters. The remaining parameters were still estimated using the RPE and EKF approximation to the RPE as given in chapter 4.

In order to simplify the implementation of the coefficient of variation cutoff, as derived in Section 4.2, the algorithm was implemented so that the user entered in one parameter, Cr_{max}. The relationship of Cr_{max} to the values of C_{omax1} and C_{omax2} found in (4.16) are as follows:

$$\begin{aligned} C_{omax1} &= C_{max} - 0.5 \\ C_{omax2} &= C_{omax1} + 1 \end{aligned}$$

In the implementation of each of the filters tested, it is necessary to determine the most effective values of the parameters. Those input values in the Kalman filters

that have been fixed are listed below.

λ_0	0.95	Initial forgetting factor
λ_{rate}	0.99	Forgetting factor convergence rate
h	0.1	Initial estimate of Hessian of quadratic norm N = hI
$\Sigma_a(0)$	0	Initial estimate of Estimation Derivative
Φ_o	1/p	Initial Parameter Vector (Equal weights)
$Y_{-i,-j}$	μ_y	Observations outside image boundaries.
$P^{(+)}(0)$	σ_y^2I	Initial Error Covariance

The input parameters that are used are listed below.

σ_u^2	State transition variance: $U = \sigma_u^2$I
λ_{ss}	Steady state forgetting factor
Cr_{max}	Maximum Coefficient of variation parameter
σ_ψ^2	MMABKF only, Multiplicative state transition variance
k	Iteration to switch from full RPE to approximate EKF method

5.2 Evaluation of Modified Kalman Filters

The performance of the Kalman filters to reduce speckle will be evaluated using four criteria as given by Shi and Fung [50]. The first criterion is the speckle reduction capability. This consists of comparing the image variance of a homogeneous region before and after filtering to determine the improvement in the SNR. The bias of the mean of the image that the filter introduces is also measured. The second criterion involves the distortion introduced to a straight edge or step response in the image. The third criterion examines the filters' ability to preserve large point

responses without distorting the surrounding image. The rounding of sharp two-dimensional structures in the image is the final criterion that is used with the special test images. In general, the filters should be able to reduce the effective level of speckle while maintaining the average mean of the image and without displacing edges or distorting the image. The effects of varying the input noise parameters on each filter will also be demonstrated. The filters are used on single look intensity images, so the correct level of multiplicative observation noise input, σ_γ^2, equals one. This value was verified to be approximately correct for all speckle test images since the actual values were between 0.98 and 1.05. The additive observation noise input, σ_v^2, is set very low since this type of noise has very little impact on SAR imagery. The additive state transition noise input, σ_u^2, is dependent on both the original scene and the level of noise excursions. Since there are large excursions of the data expected in SAR imagery, it is often the practice to limit the data to a threshold, to reduce the effect of these large values that occur at the tail of the probability distribution [5]. In Kalman filtering, it is often required to set σ_u^2 higher, so that the filter will recover from unexpected noise excursions [20]. If this value is too low, the filter will diverge. If it is too high, the filter will not remove any speckle, as the speckle noise will be within the range of noise associated with the error in the state transition. The value of Cr_{max} is also allowed to vary for the modified Kalman filters.

5.2.1 Speckle Reduction Capability

The evaluation of speckle reduction is carried out by determining the performance of each of the filters, by measuring the induced bias and equivalent number of looks over homogeneous regions. The test images are two statistically homogeneous single-look intensity sub-images of 64x64 pixels, extracted from an ERS-1 image. The filter results in terms of output image mean and variance are given in Table 5.1. The bias terms are calculated as the proportion of change, (mean filter output)/(mean original), and are given in dB. The equivalent number of looks(ENL) is based on (2.14).

$$ENL = \mu_y^2/\sigma_y^2 \tag{5.1}$$

$$\begin{aligned} Bias &= 20\log(\mu_y/\mu_{original}) \\ &= 20\log(\mu_y/942) \end{aligned} \tag{5.2}$$

The data indicates that the Lee statistical filters result with the least change in the average of the image. When using any of the Kalman filters, the bias is higher. For the cases where the additive state transition noise is set low, $\sigma_u^2 = 3.0e4$, the filter diverges and the output values becomes unpredictable. For all other cases, the mean is reduced by an amount usually proportional to the amount of smoothing done by the filter. This is due to the Gaussian noise assumption in the derivation of the Kalman filter. The filter smoothes the low probability, higher intensity pixels in the image so that they fit within the envelope of the given Gaussian noise distribution.

Filter	Image A				Image B			
	Mean	Variance	Bias(dB)	ENL	Mean	Variance	Bias(dB)	ENL
None	942	9.18e5		0.97	2537	6.699e6		0.96
Lee, 5x5	938	1.23e5	-3.7e-2	7.1	2530	9.47e5	-2.4e-2	6.8
Lee, 7x7	939	6.79e4	-2.7e-2	12.0	2536	5.74e5	-3.4e-3	11.0
ABKF, σ_u^2 = 3.0e4	936	5.2e4	-5.5e-2	16	3020	4.87e5	1.5	18
ABKF, σ_u^2 = 3.0e5	922	1.49e5	-1.8e-1	5.7	2313	2.376e5	-8.0e-1	22
ABKF, σ_u^2 = 3.0e6	927	5.33e5	-1.4e-1	1.6	2347	1.15e6	-6.8e-1	4.8
MABKF, σ_u^2 = 3.0e4	817	3.30e4	-1.2	20	3492	9.11e5	2.7	13.4
MABKF, σ_u^2 = 3.0e5	909	1.83e5	-3.1e-1	4.5	2595	4.52e5	9.53e-2	14.6
MABKF, σ_u^2 = 3.0e6	929	5.8e5	-1.2e-1	1.5	2376	1.44e6	-5.7e-1	3.9
MMABKF, σ_u^2 = 3.0e4	850	6.88e4	-8.9e-1	10.5	2351	4.74e5	-6.6	11.7
MMABKF, σ_u^2 = 3.0e5	922	1.91e5	-1.9e-1	1.5	2394	6.0e5	-5.0e-1	9.55
MMABKF, σ_u^2 = 3.0e6	927	5.72e5	-1.4e-1	1.5	2417	1.54e6	-4.2e-1	3.8
FABKF, σ_u^2 = 3.0e4	877	8.99e4	-6.2e-1	8.6	2703	8.65e5	5.5e-1	8.4
FABKF, σ_u^2 = 3.0e5	843	1.85e5	-9.6e-1	3.8	2753	1.17e6	7.1e-1	6.5
FABKF, σ_u^2 = 3.0e6	896	5.54e5	-4.3e-1	1.4	2543	2.07e6	2.1e-2	3.1

Table 5.1: Speckle Reduction Performance of Filters

Since most SAR imagery is re-mapped for display in such a way that these points are compressed into a smaller dynamic range, this bias will have little effect on image clarity but may negatively affect various classification algorithms. From Table 5.1, the data shows that the higher the noise parameter, σ_u^2, the lower the bias that the image suffers, and the lower degree of smoothing that takes place. The very large ENL values, $\geq$ 18, typically correspond to those tests where the Kalman filter diverges from the image.

The effect of the tested filters on a left to right cross section of the image are shown in Figure 5.1. For a value of σ_u^2 of 3.0e5, the MABKF and the FABKF give results similar to the 5x5 Lee statistical filter. Figure 5.2 illustrates the effect of varying the noise parameter in the MABKF. The MABKF result with σ_u^2 equal to 3.0e6 closely follows the original image. The MABKF result diverges from the image

when σ_u^2 equals 3.0e4. When the filters are applied to an image having a low mean value this dependence on the transition noise parameter is much reduced.

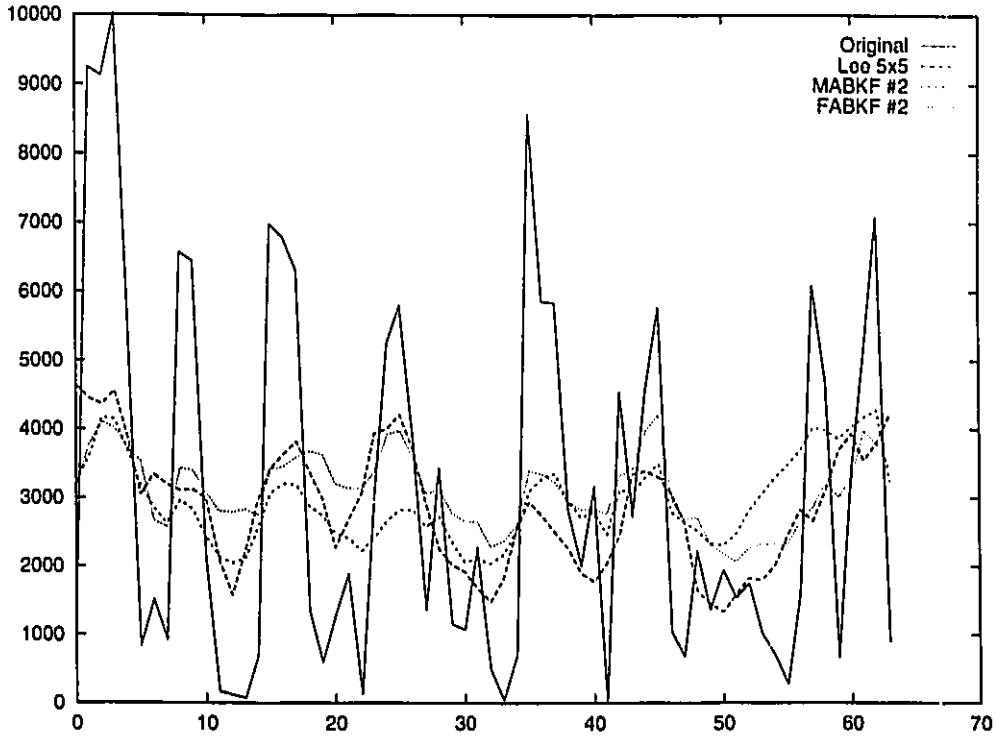

Figure 5.1: Cross Section of Results of Filters on High Mean Intensity Image.

5.2.2 Step Response

The step response is measured by determining the ability of the filter to locate the boundary between two homogeneous regions. Two sub-images from the original ERS-1 test image are placed together in one image. The result is a 64x64 image with a statistically homogeneous region left of the edge with a mean of 1192, and another statistically homogeneous region right of the edge with a mean of 2107. Following Shi and Fung [50], the performance of the filters will be evaluated on the

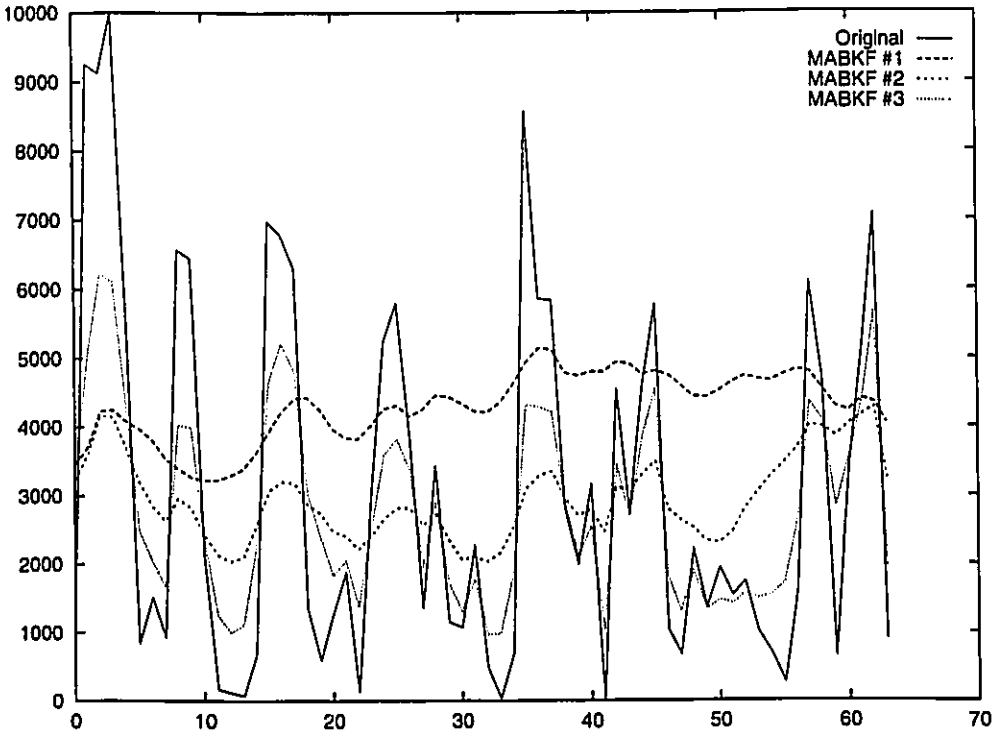

Figure 5.2: Effect of Transition Noise Parameter, σ_v^2.

displacement of the edge and the slope of the edge. The displacement is determined by the location of the nearest point to the midpoint level near the edge boundary. The slope is calculated as the change in intensity between the 20% upward and 10% downward points in the slope. These terms are defined in Figure 5.3 using the Lee statistical filter results and the original image for comparison. The values avg_{lo} and avg_{hi} are the low and high nominal values of the step. The process $x(i)$ is defined as the nominal value of the image from left to right. The equations for calculating the midpoint and slope are therefore given as:

$$Midpoint = i|\min(x(i) - (avg_{hi} + avg_{lo})/2) \quad (5.3)$$

$$UpperPosition = i|\min(x(i) - (avg_{hi} - 0.1(avg_{hi} - avg_{lo}))) \quad (5.4)$$

$$UpperValue = x(i)|\min(x(i) - (avg_{hi} - 0.1(avg_{hi} - avg_{lo}))) \quad (5.5)$$

$$LowerPosition = i|\min(x(i) + (avg_{lo} + 0.2(avg_{hi} - avg_{lo}))) \quad (5.6)$$

$$LowerValue = x(i)|\min(x(i) + (avg_{lo} + 0.2(avg_{hi} - avg_{lo}))) \quad (5.7)$$

$$Slope = \frac{(UpperValue - LowerValue)}{(UpperPosition - LowerPosition)} \quad (5.8)$$

The results are given in Table 5.2. The multiplicative noise reacts slightly faster to changes in the input images, which is most likely due to the larger error covariance matrix. A decrease in the maximum coefficient of variation, Cr_{max}, has little affect on the ability of the filter to track the test edge, since the statistics do not vary greater than expected using the multiplicative noise model. The magnitude of the step is locally lost within the speckle noise.

5.2.3 Point response

The test image for the point response was generated by taking a 64x64 statistically homogeneous region from an ERS-1 image and inserting a 3x3 point with similar SAR statistics($\mu^2 = \sigma^2$). Each of the filters was run using a state transition noise value of 3.0e5, and the modified filters used a Cr_{max} of 2.5. The MABKF was also run against the point target with a Cr_{max} of 2.0 and 3.5. The results are given in Figures 5.4 and 5.5.

All of the filters, greatly reduce the level of noise in the original image. The Lee statistical filter smoothes out the image, but also severely reduces the values of the point target. The ABKF completely removes the point target, while the three mod-

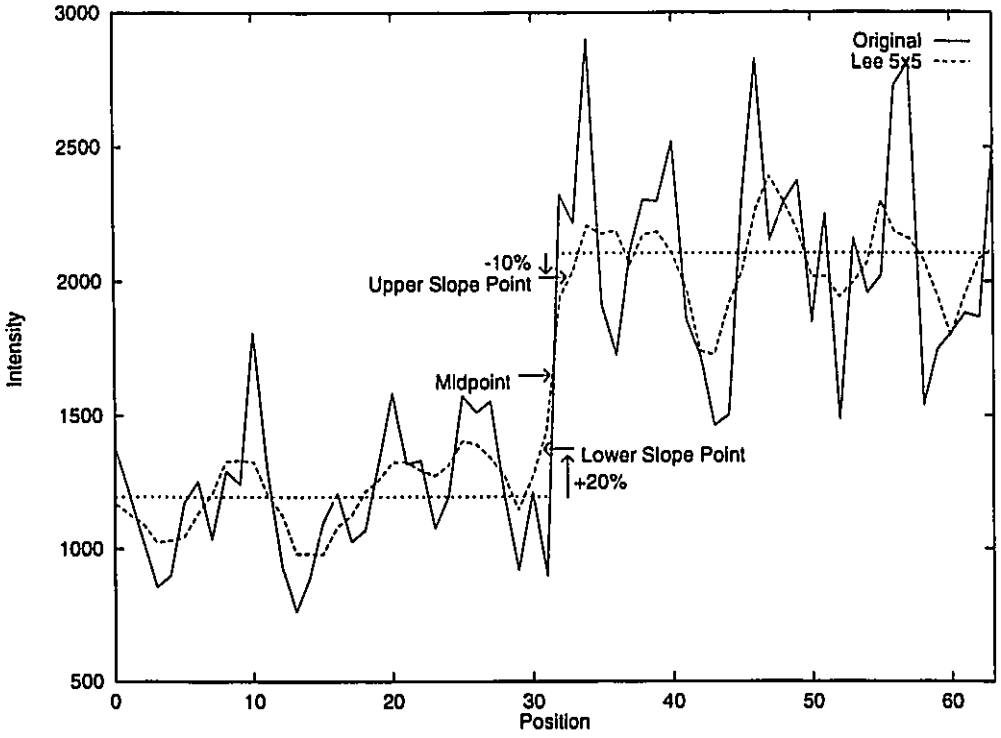

Figure 5.3: Measurement of Step Response

ified Kalman filters all preserve the point target at values near the original. Of the modified Kalman filters, the FABKF results are the best compromise of smoothing the homogeneous region while maintaining the point target. The MMABKF smoothes the homogeneous region the least while maintaining the point target.

It is interesting to note that increasing the state transition noise, σ_u^2, in the image is not the best means to bring out point targets. The ABKF did not preserve the point target at all. The maximum coefficient of variation was the determining factor in the ability of the modified Kalman filters to detect the point target within the clutter. This is demonstrated in Figure 5.5 where the results of the MABKF with various coefficient of variation threshold values, Cr_{max}, are given. When Cr_{max}

Filter	Midpoint	Slope
Lee, 5x5	31	165.3
Lee, 7x7	31	151.2
ABKF, $\sigma_v^2 = 3.0e4$	34	34.8
ABKF, $\sigma_v^2 = 3.0e5$	32	82.5
ABKF, $\sigma_v^2 = 3.0e6$	32	756
MABKF, $\sigma_v^2 = 3.0e4$	34	32.3
MABKF, $\sigma_v^2 = 3.0e5$	32	80.4
MABKF, $\sigma_v^2 = 3.0e6$	32	811
MMABKF, $\sigma_v^2 = 3.0e4$	31	82.3
MMABKF, $\sigma_v^2 = 3.0e5$	32	136.7
MMABKF, $\sigma_v^2 = 3.0e6$	32	831
FABKF, $\sigma_v^2 = 3.0e4$	34	61.6
FABKF, $\sigma_v^2 = 3.0e5$	33	98.5
FABKF, $\sigma_v^2 = 3.0e6$	32	390

Table 5.2: Step Response Values for Filters.

is set to 3.5 or higher, the entire point is filtered out as with the ABKF.

5.2.4 Distortion of an angular object

The distortion of an angular object is measured by evaluating the output of a filter after processing a parallelogram with no noise. The parallelogram is the equivalent to a two-dimensional step function. From the results of the four filters tested, it is obvious that the ABKF and the other NSHP filters suffer from block effects that cause undesirable local distortions in the image. The fullplane filter, the FABKF,

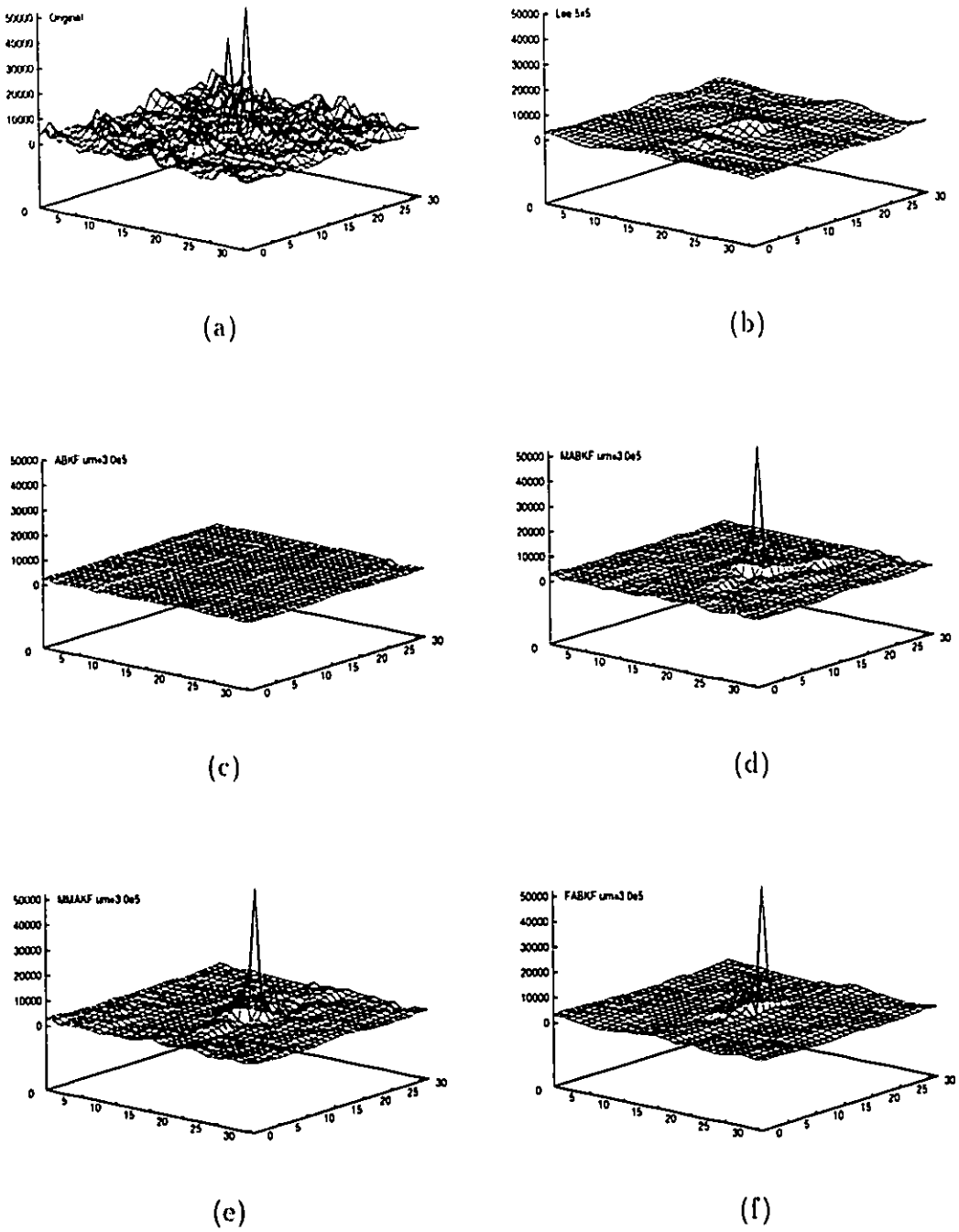

(a) (b) (c) (d) (e) (f)

Figure 5.4: Comparison of Results of Filters on Noisy Point Target.

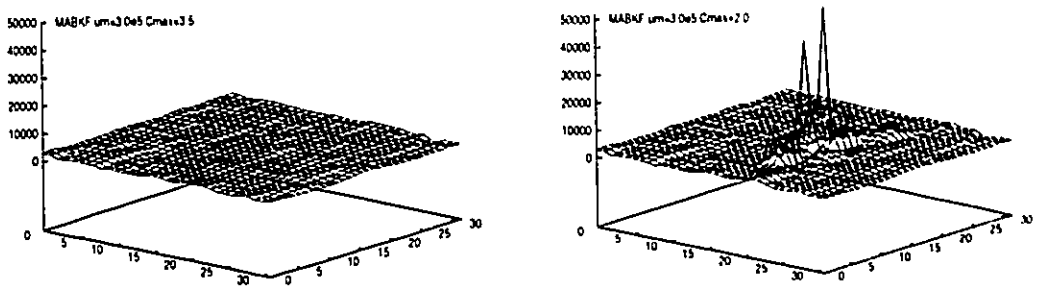

(a) (b)

Figure 5.5: Comparison of Results of MABKF Filter with Varying Cr_{max} on Noisy Point Target.

does not suffer from these distortions due to the different arrangement of the block and the smaller region over which the same parameters are applied. The effect of varying the state transition noise is analagous to a damping factor, where the smaller the value of σ_u^2, the slower the filter responds to the change. In processing the homogenous region, a value of σ_u^2 set too low causes the filter to diverge from the actual image value creating invalid output. As the value is increased, the filter responds much quicker, but it becomes more susceptible to an increase in the noise. The inclusion of the multiplicative term in the state transition matrix in the MMABKF seems not to have very much effect. This image contains no noise, so that the error covariance matrix will be very small resulting in little difference achieved by changing the multiplicative state transition noise term. However, varying the maximum coefficient of variation, Cr_{max}, results in much improved response to sharp edges and points.

The box results are illustrated by the contour lines at ±1% around the maximum and minimum values and at 10% and 90% between the maximum and minimum values. This indicates the degree of overshoot and undershoot in the filter output and it is shown in Figure 5.6.

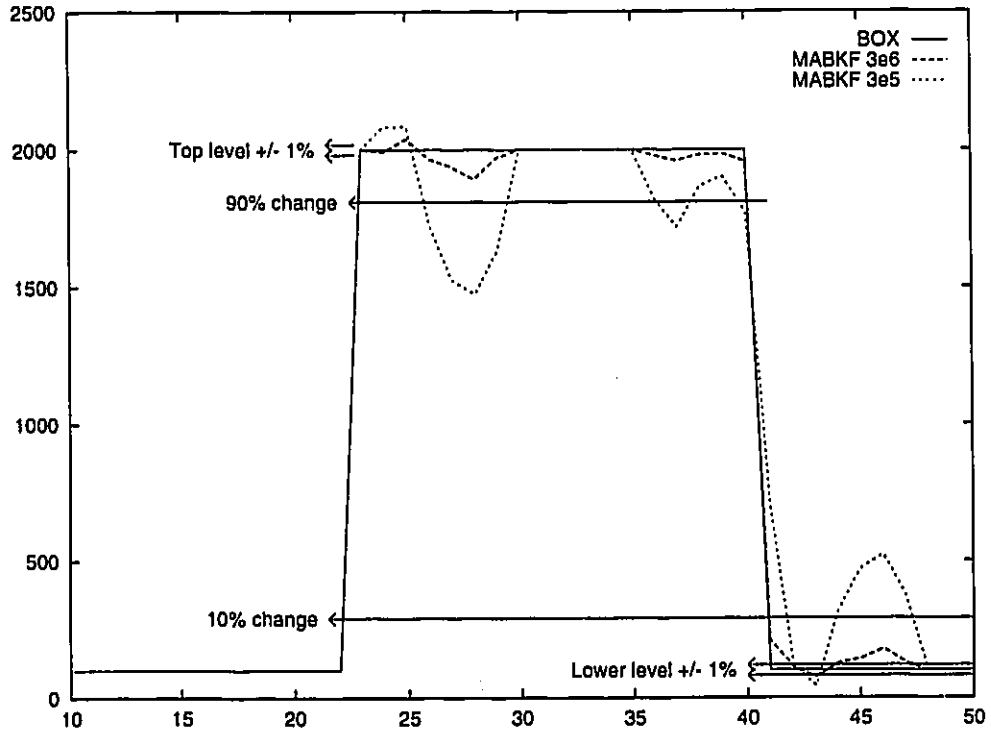

Figure 5.6: Levels of Contour Indicators for Angular Object Results.

5.3 Results of Filters on an Image of Victoria B.C

The test image was taken from the ERS-1 satellite data of Victoria, BC. taken in August, 1993. The test data is a single look intensity image and is shown in Figure 2.1 corresponding to the highlighted region in Figure 2.2. The test data is given

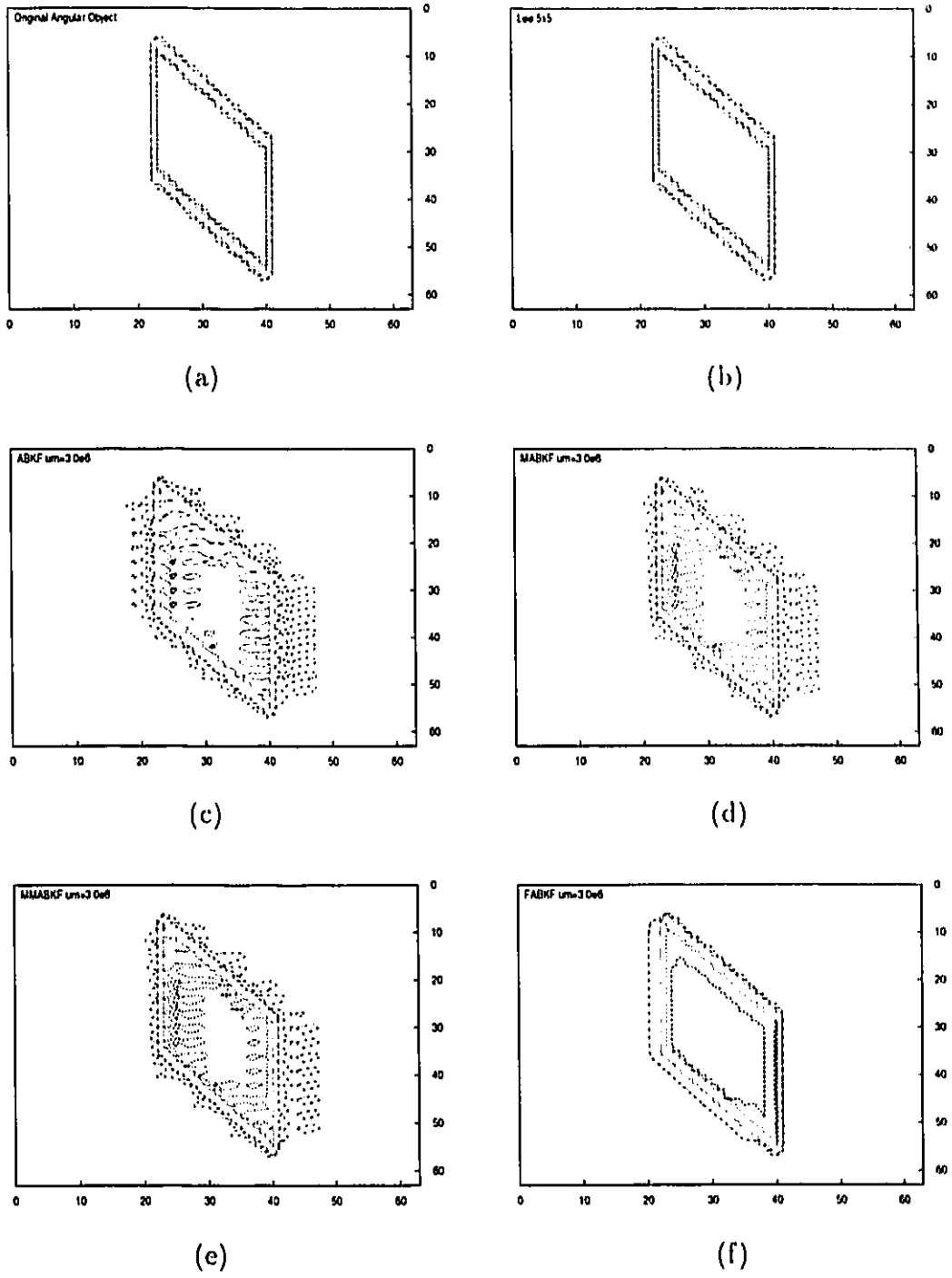

Figure 5.7: Comparison of Results of Filters on Angular Objects

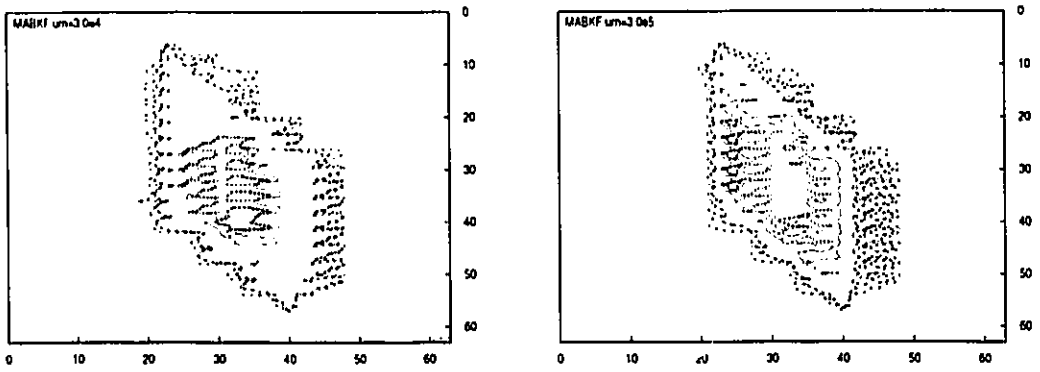

(a) (b)

Figure 5.8: Effects of Different Transistion Noise Values on Angular Object

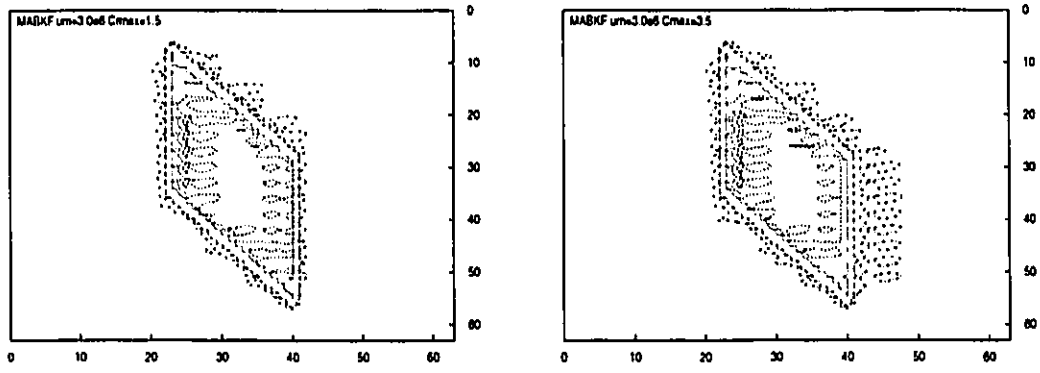

(a) (b)

Figure 5.9: Effect of Different Maximum Coefficient of Variations on Angular Object

again in Figure 5.10 displaying the pixels with equal dimensions in both the cross-track and along-track directions. This image was chosen because of the different classes of data that is present. It includes very low intensity regions that correspond to the harbour region juxtaposed with the high intensity dock and city regions. The image also contains large regions that fall between these two extremes.

Due to the use of the quadratic noise reduction criterion (3.29), the Kalman filters will be sensitive to large changes in the image process. This is very common in SAR imagery, and these statistical outliers must be removed. The tests were run using an image with the upper 2% of the image compressed to 5 values at the peak of the image intensity level. This reduces the mean value of the image to some degree, but does not greatly affect the distribution of the image intensity data.

It was found during testing that attempting to run the ABKF on images with less than the upper 2% of the image compressed, the filter would often become numerically unstable. The modified filters, the MABKF, the MMABKF, and the FABKF all maintained stability operating on images with only 1% of the image compressed.

In analysing the results of the various filters on the image of Victoria, we will consider in turn the filter output, the behaviour of the Kalman gain, and the behaviour of the parameter vectors.

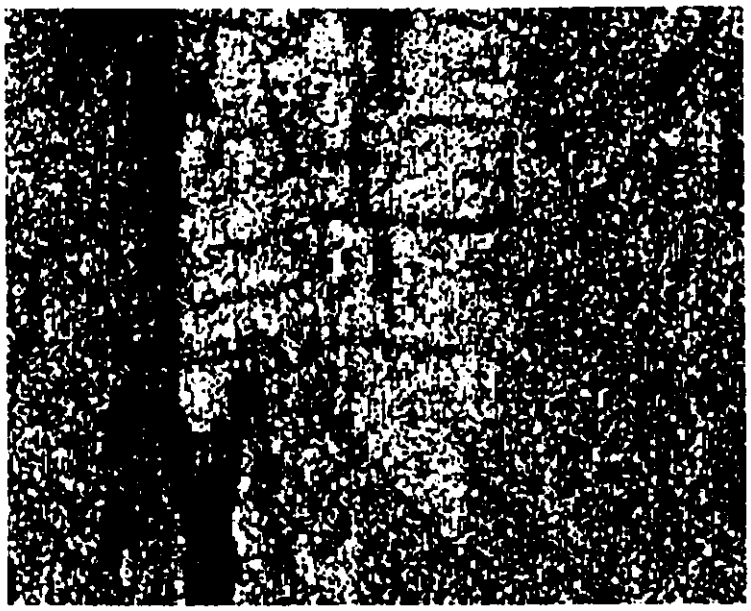

Figure 5.10: Single-Look Intensity Image of Victoria, B.C. from ERS-1.

5.3.1 Analysis of Kalman Filter Output

The output of the test runs of the filter are given in Figures 5.11 - 5.13. Figure 5.11 shows the results of all four Kalman filters with $\sigma_u^2 = 3.0e5$ and $Cr_{max} = 2.5$. This value of the state transistion noise parameter, σ_u^2, was found to give satisfactory results over both the high intensity urban area in the centre of the image and the regions at the left and right of the image. The maximum coefficient of variation value, Cr_{max}, was chosen so as to affect regions where the multiplicative noise assumption is no longer true, ie. $C_o > 2.0$. The MMABKF result in Figure 5.11d uses a value of the state transition multiplicative noise parameter, $\sigma_\psi = 0.25$. The NHSP filters shown in a, c, and d all suffer from the asymmetric distortions due to the use of the half-plane region of support. The MABKF and ABKF results

are indistinguishable over the homogenous regions at the left and right of the image. However, the major improvement in the MABKF is identifiable in the high intensity urban region. Here the filter distorts the dark lines and edges of the intense region much less. The MMABKF was run with a value of $\sigma_\psi = 0.25$ and the results show a slight improvement in the edge regions as well as some improvement in image contrast. Currently there is no theoretical means of determining the ideal value of σ_ψ for such complex images. Experimentation suggests that 0.25 is acceptable but that a value too large, ie. > 0.5 results in very little improvement in the image over the input image. The FABKF results given in Figure 5.11b indicate a slight reduction in the smoothing of homogenous regions for the same value of σ_u^2 but lack the asymmetric distortion that is prevalent in the NHSP based filters.

The effect of varying the additive state transition noise parameter, σ_u^2, is shown in Figure 5.12. The MABKF filter was chosen for these demonstrations because of its faster execution time with respect to the FABKF. Figure 5.12a was processed with $\sigma_u^2 = 3.0e4$. This image is highly oversmoothed in the urban region, while the smoothing may be acceptable in the lower intensity regions. Processing the image with $\sigma_u^2 = 3.0e6$ resulted in very little reduction in the speckle noise over the lower intensity images, but an acceptable level of smoothing with less distortion over the high intensity region in the centre of the image.

The maximum coefficient of variation parameter, Cr_{max}, is designed to affect the filter most in the high intensity urban regions where the multiplicative noise assumption does not hold due to large numbers of strong reflectors. The effect of

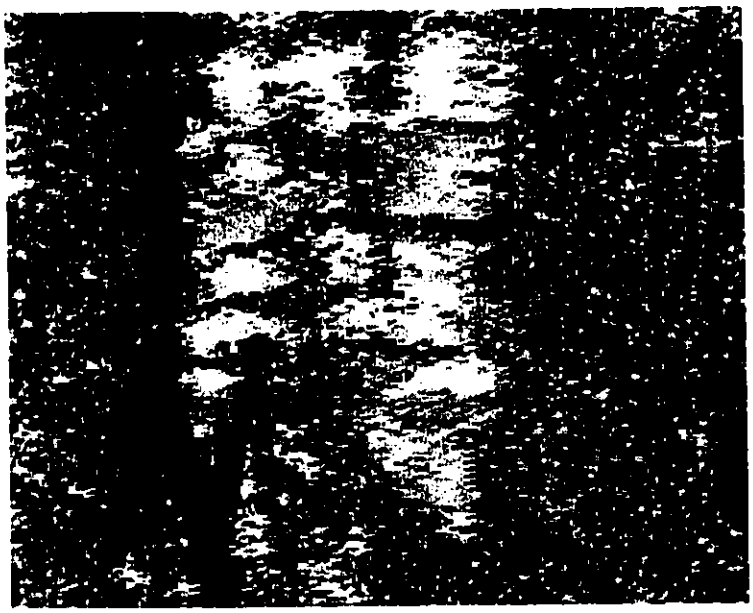

(a)

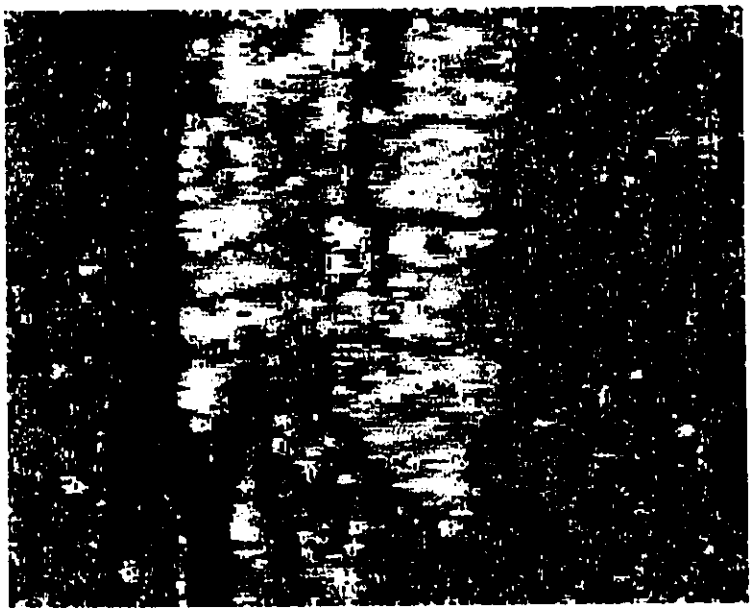

(b)

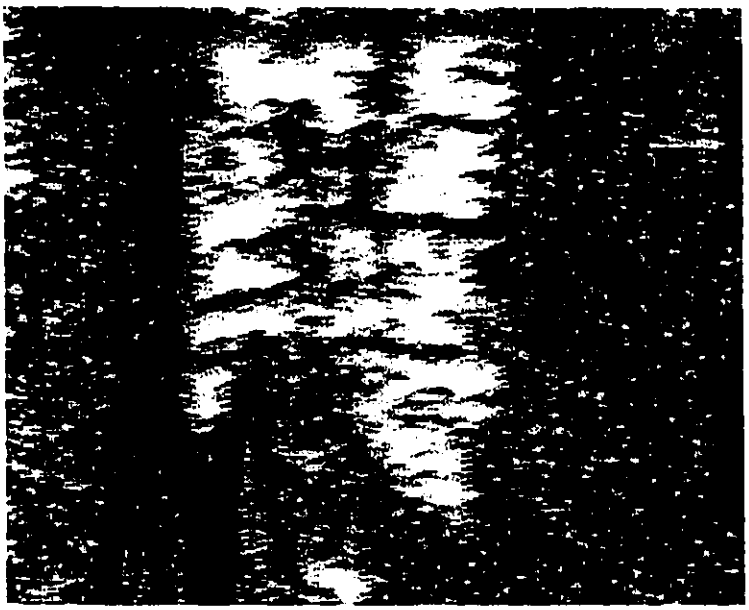

(c)

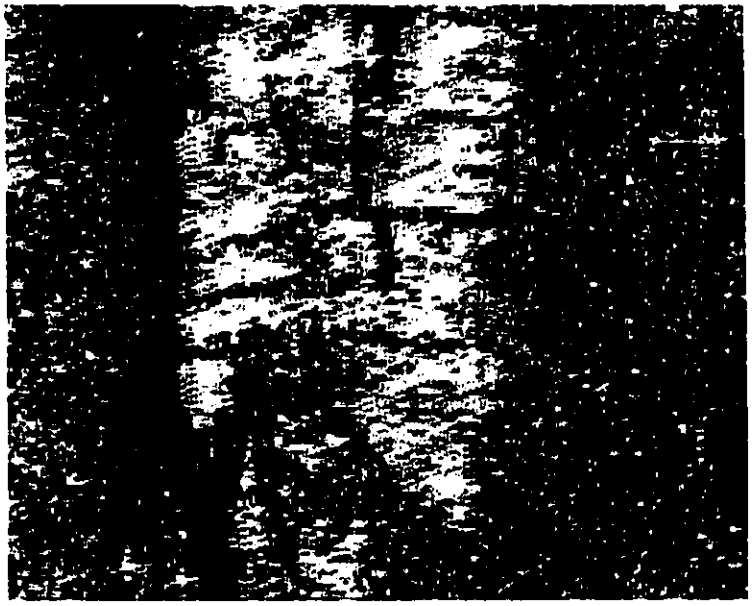

(d)

Figure 5.11: Results of Kalman Filters Applied to SAR Image a) MABKF, b)FABKF, c)ABKF, d) MMABKF , $\sigma_\psi^2 = 0.25$. The state transistion covariance, σ_u^2, is set to 3.0e5 for all images.

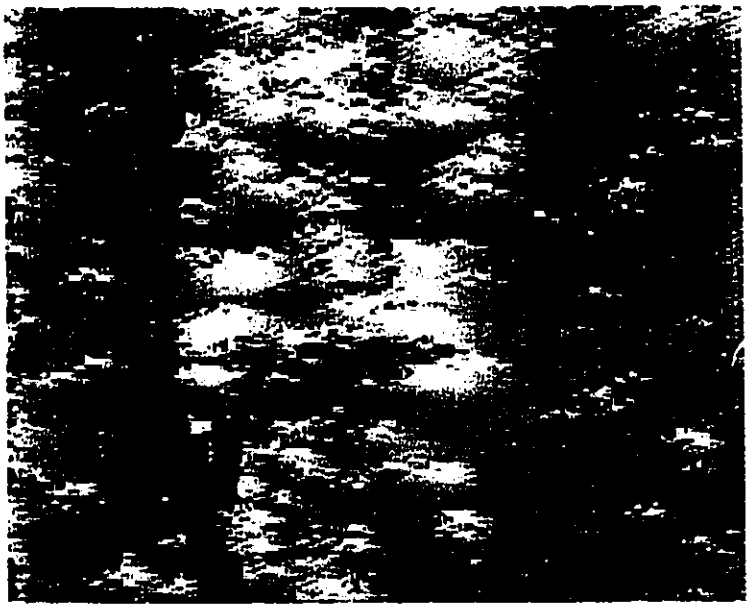

(a)

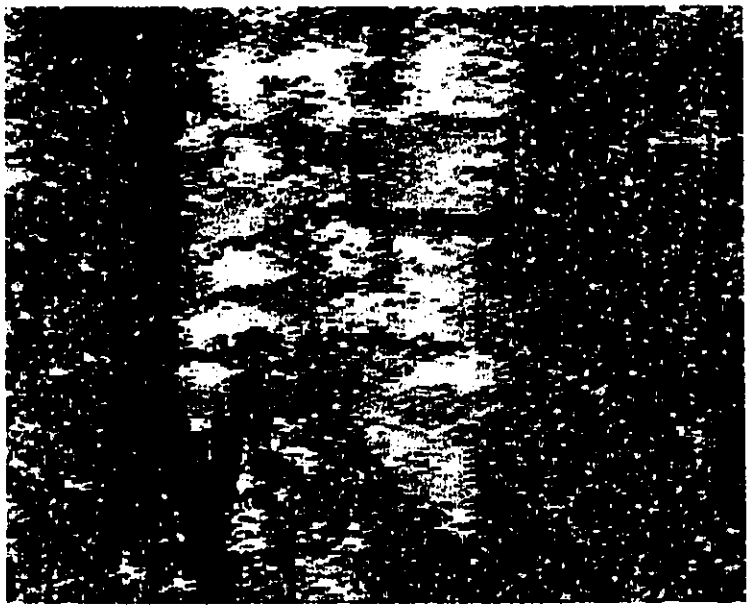

(b)

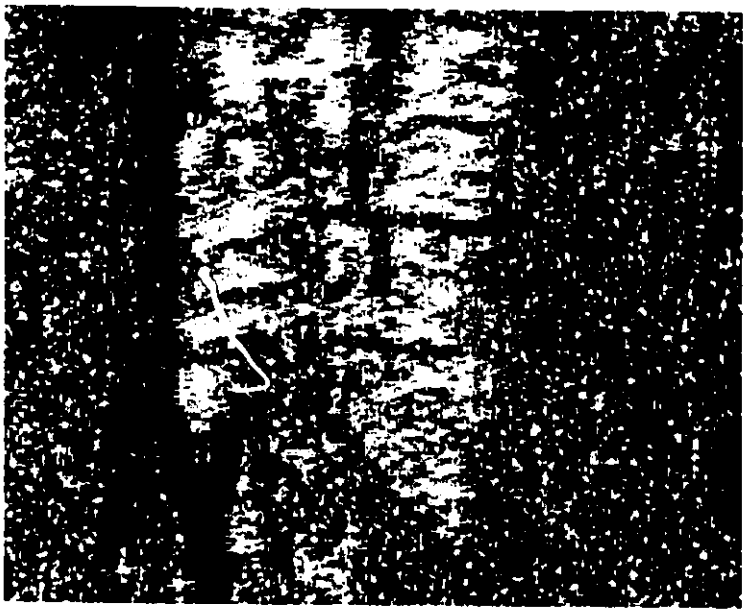

(c)

Figure 5.12: Comparison of MABKF with varying State Transition Variance on a SAR image a) $\sigma_u^2 = 3.0e4$, b) $\sigma_u^2 = 3.0e5$, c) $\sigma_u^2 = 3.0e6$,

processing the image with a lower maximum threshold is seen in Figure 5.13. As in Section 4.2 the suggested C_{omax} is approximately 1.73. A Cr_{max} value of 2.0 begins the detuning of the Kalman filter at a local coefficient of variation of 1.5, just below the value suggested by Lopes et al. [40]. The results indicate that this factor is very important in the use of the Kalman fitler as the high intensity region suffers from much less distortion using the lower value of Cr_{max}.

5.3.2 Evaluation of Kalman Filter Gain Behaviour

Although the final test of the utility of a filter is to visually inspect the output, the evaluation of the filter should also be based on performance measures that are

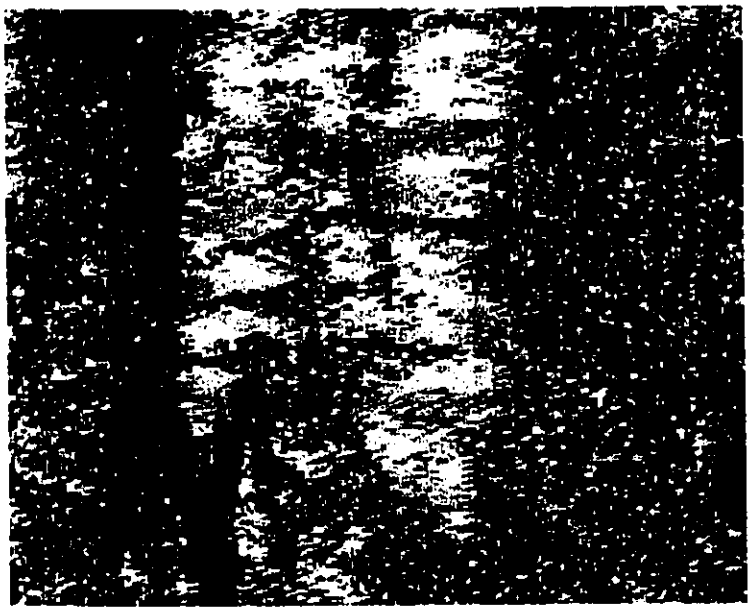

Figure 5.13: Effect of Changing Threshold Coefficient of Variation on a SAR image, $Cr_{max} = 2.0$, Using MABKF.

identifiable within the filter. The behaviour of the Kalman gain is determined by monitoring the norm of the Kalman gain matrix. The norm used is defined below in (5.9) and is taken from [8]. Although this is only a partial indicator of the state of the filter it allows the easy display of the information [5].

$$K_{norm} = \| A \|_{\infty} = \max_{1 \le i \le N} \sum_{j=1}^{N} | a_{ij} | \tag{5.9}$$

The Adaptive Block Kalman Filter (ABKF) was developed by Azimi-Sadjadi [5] assuming a steady state Kalman gain and space-invariant parameters in the state transition matrix. When processing the single-look intensity or single-look amplitude SAR images over targets such as urban regions, these assumptions are

unacceptable. The assumption of a steady state Kalman gain after as few as 20 iterations was shown to be invalid in Section 4.1, due to the signal dependent term (3.23) in the Kalman gain equation (3.24). The actual performance of the Kalman gain using the Modified ABKF (MABKF), the multiplicative MABKF (MMABKF), and the Fullplane ABKF (FABKF) on the image of Victoria, B.C. is shown in Figure 5.14. This Figure illustrates the norm of the gain matrix for the first 10 rows of the test image for each filter.

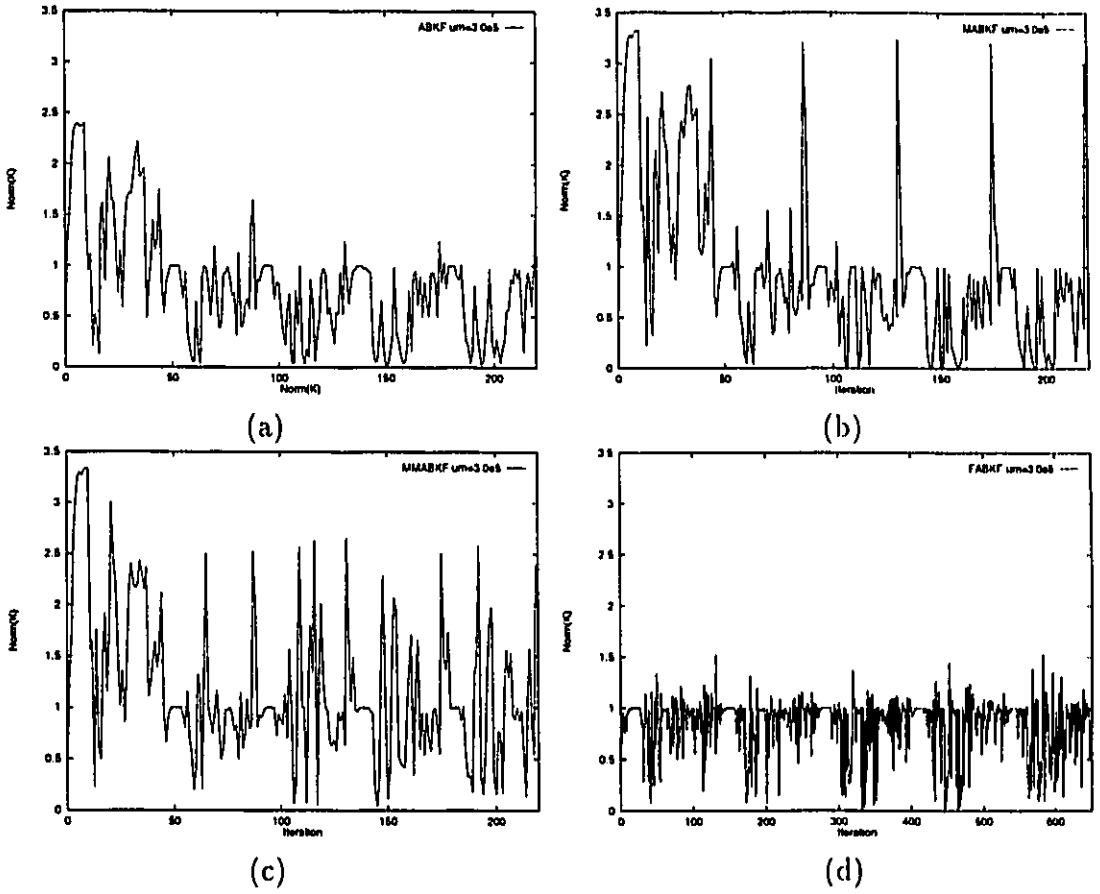

Figure 5.14: Comparison of K_{norm} for Adaptive Block Kalman Filters. a) ABKF b) MABKF c) MMABKF d) FABKF

From inspecting the norms of the K matrix in Figure 5.14, the Kalman gain for the ABKF converges to a repetitive sequence that is dependent on the local image statistics. The large peaks that exceed the value of one are due to the image edges, where the error covariance is greatly reduced. Recall that points outside of the image boundaries were assigned to the image mean value so that the covariance of these regions approaches zero. The repetitive cycle can be seen to be true for the MABKF and the MMABKF as well. The FABKF, because of its different block structure, requires a greater number of iterations to cover the same area of the image. The Kalman gain for the FABKF is closer to a value of one, indicating less smoothing for these points. The value of the gain falls often enough below one that some degree of smoothing is evident. The variation of the gain of the MMABKF indicates the faster rate that this model can follow changes in the image. However, the Kalman gain of the MMABKF diverges greatly from the pattern seen in the other NSHP filters. This may indicate that the filter is more likely to become unstable.

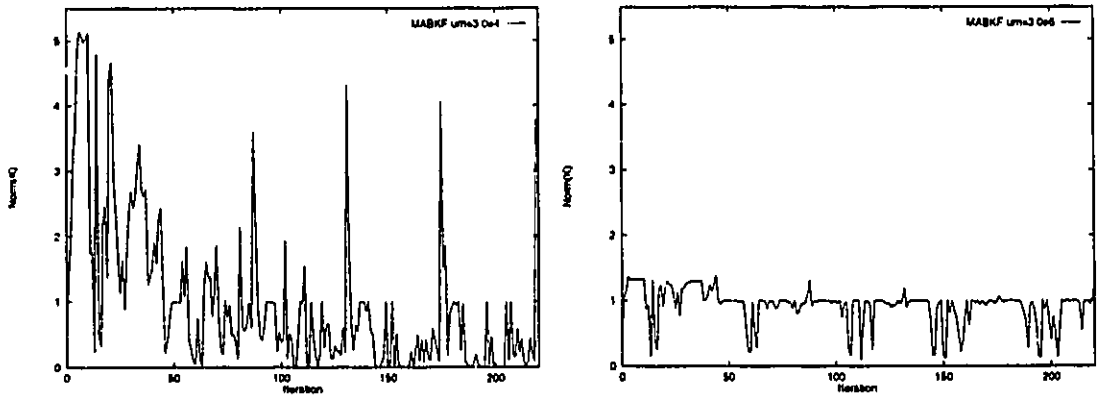

(a) (b)

Figure 5.15: Comparison of Gain Variation Relative to Noise Parameter, σ_u^2. a) MABKF with $\sigma_u^2 = 3.0e4$, b) MABKF with $\sigma_u^2 = 3.0e6$.

The effect of modifying the state transition noise parameter, σ_u^2, can be seen in Figure 5.15, where the norm of the Kalman gain is given for the case of the MABKF with $\sigma_u^2 = 3.0e4$ and $\sigma_u^2 = 3.0e6$. For $\sigma_u^2 = 3.0e4$, the filter gain is highly variable, often reaching values greater than 1.0. The low values of the gain indicate that the filter is not following the image values, and that the filter is oversmoothing. The output image may therefore be well removed from the input image, as shown for the homogenous image in Figure 5.2. For the increased noise parameter, $\sigma_u^2 = 3.0e6$, the value of the filter gain is consistently near one. This indicates that little smoothing is carried out by the filter, and that the observed image is within the specified noise values of the values calculated. In this case, the output image is very similar to the input image, and very little gain in SNR has been achieved. The ideal value for the state transistion noise parameter is between these two extremes.

5.3.3 Evaluation of Kalman Filter Parameter Behaviour

The variation of the parameter values is also useful in determining the performance of the filters. Parameters that change too often indicate difficulty with convergence over the image while parameters that do not change at all over a highly variable image indicate an inability of the filter to follow the changes in the image. Figure 5.16 shows the beginning of the convergence of the parameter values and subsequent variation for each of the ABKF, MABKF, and MMABKF. Figures 5.18 - 5.20 show the parameter variation for the FABKF. These are displayed separately as the processing differs in the number of parameters and iterations required to process the

image.

The variation of the twelve parameters used in each of the NSHP based filters is given in Figure 5.16. The ABKF parameters change rapidly, with the $a_{0,0}$ parameter quickly becoming predominant. This indicates a very narrow correlation with the surrounding pixels. As well, the parameters change very little after the initial 1000 iterations. This is due to the value of the forgetting factor approaching one and reducing the weighting of any new information to almost nothing. The MABKF filter with a $Cr_{max} = 2.5$ converges to a different set of values for the parameters with much less dependency on any one single parameter. Since the forgetting factor, λ_{ss}, has a value of 0.99, the parameters continue to change throughout the processing of the image. The exceptionally large change in the parameters, approximately 60% of the way through the image, is due to local change in the structure of the image near the bridge over the Victoria Arm, indicated in Figure 2.2. The parameter values of the MABKF filter with a $Cr_{max} = 2.0$ change somewhat slower than the run of the MABKF with $Cr_{max} = 2.5$. Evaluating the effect of the coeffecient of variation on these filters it is shown that the rapid change of the parameters in the ABKF is due to those regions of the image where the multiplicative model of the image is invalid. The removal of these regions from the calculation of the parameter estimation results in a better estimate of the parameters that is not overly dependent on single terms. The MMABKF filter behaves very similarly to the MABKF filter, with some regions of greater variability evident in the latter portion of the image.

The effect of varying the steady state forgetting factor λ_{ss} is demonstrated in

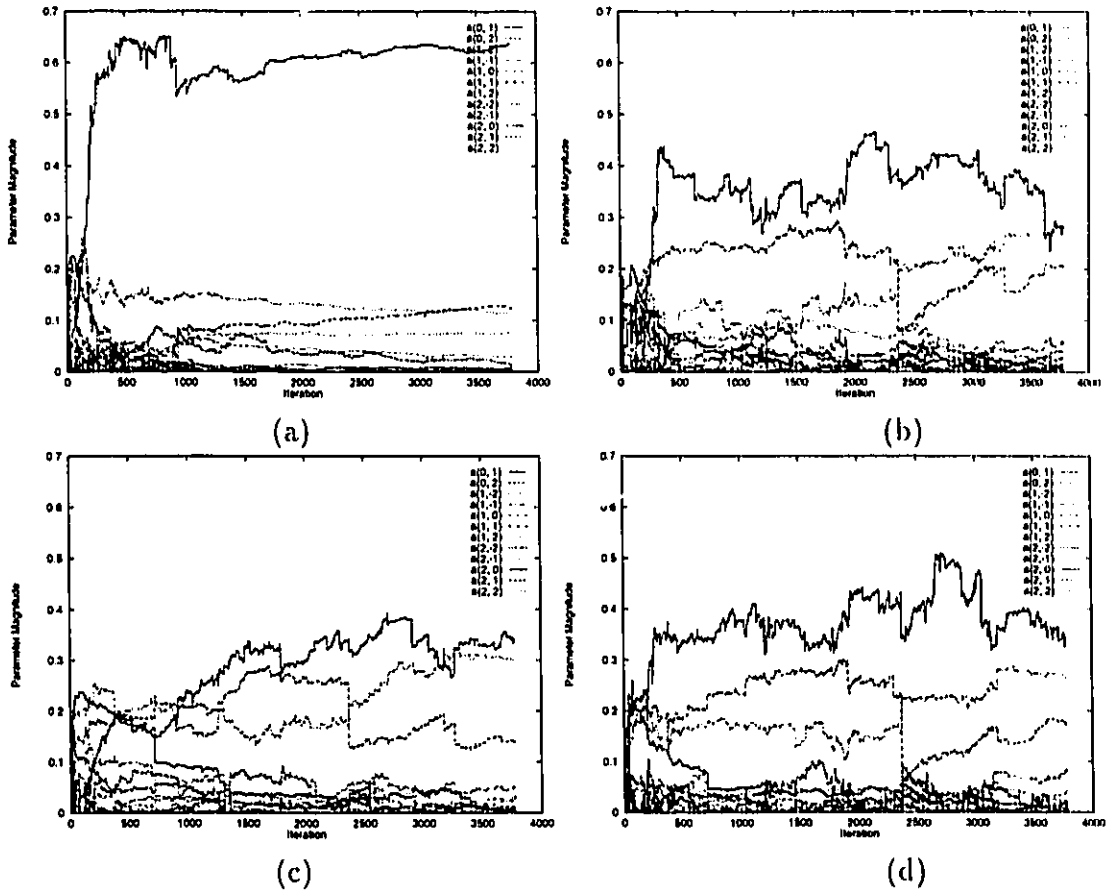

Figure 5.16: Comparison of Parameter Variation for NSHP Adaptive Block Kalman Filters. a) ABKF $\sigma_u^2 = 3.0e5$, b) MABKF $\sigma_u^2 = 3.0e5$, $Cr_{max} = 2.5$, c) MABKF $\sigma_u^2 = 3.0e5$, $Cr_{max} = 2.0$, d) MMABKF $\sigma_u^2 = 3.0e5$, $Cr_{max} = 2.5$, $\sigma_\psi^2 = 0.25$.

Figure 5.17 using the MABKF. With a low steady state forgetting factor of 0.95 there is great variation in the parameters. Such variation does not give the filter an opportunity to adjust the Kalman gain to the new parameter values, so that the filter will remain unstable and not converge to give good performance. The higher value of 0.995 results in a smoothing of the parameter estimation processes, ensuring that the Kalman filter running in parallel may adjust to maintain optimal estimates

for the new parameter values. A compromise of adaptability and damping of the parameter estimation process is achieved for the Victoria BC. image using a λ_{ss} of 0.99.

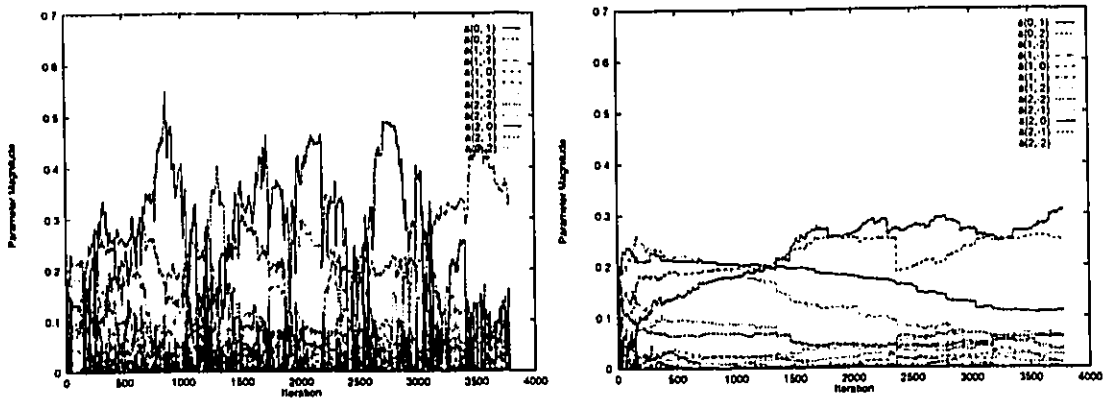

(a) (b)

Figure 5.17: Comparison of Effect of Forgetting Factor, λ_{ss} for MABKF Filter. a) Large parameter variation occurs with $\lambda_{ss} = 0.95$ while a larger value, b) $\lambda_{ss} = 0.995$ reduces parameter variation.

The FABKF requires many more iterations than the NSHP based Kalman filters to process the same image. As well, for a block size parameter of m=2, the number of parameters for the FABKF is 40, much greater than the 12 used for the NSHP based filters for a similar sized region of support. Thus the parameter variation for the FABKF is very different from the NSHP-based filters examined above. The parameters for block 6 in the FABKF were set to approximate a Gaussian average, due to the lack of statistical support for a small region compared to the region of support for blocks 5, 7, and 8. When the above parameters were included in the parameter estimation, the values were found to be extremely unstable because of the effect of large errors caused by the remaining statistical outliers on the parameter

estimation. For a block size value of m=2, the parameters in block six were calculated using a region of only 4 elements of the original image. Some of the parameters from the upper leading edge, block 5, are given in Figure 5.18. This figure indicates that the parameters have converged locally by the 500th iteration and change much less after the 4000th iteration. The remaining figures for the FABKF will only show the parameters for the first 4000 iterations to illustrate the convergence and steady state variation of the parameters.

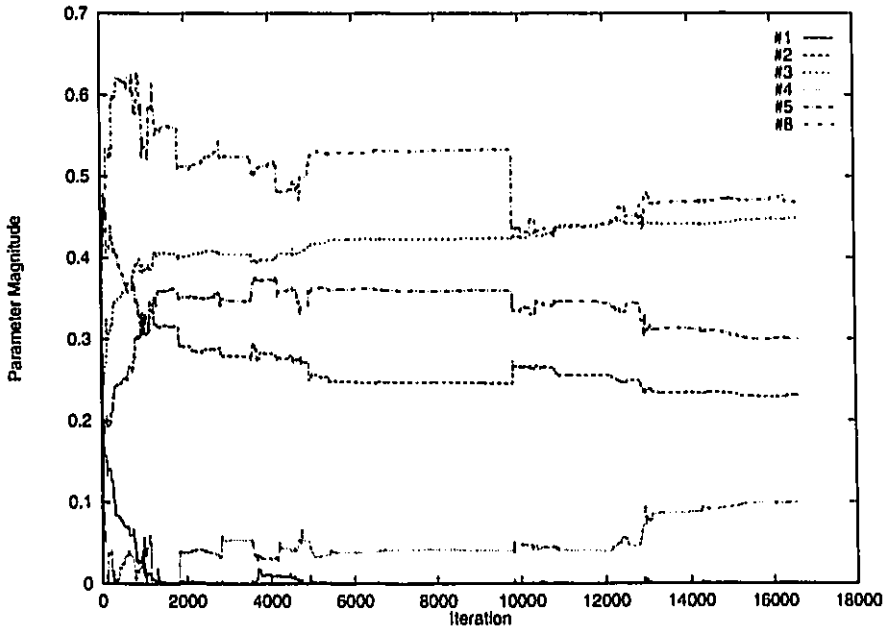

Figure 5.18: Parameter Variation for Block 5 in FABKF.

The FABKF was implemented so that the leading block, block 6, uses a Gaussian smoother for its initial estimate. The other leading edge blocks, blocks 5 and 7, use a NSHP region of support much like that used by the ABKF. Each one of these blocks has 8 parameters, which are displayed in Figure 5.19. In comparing the two iterations of the FABKF with different Cr_{max} values, it is evident that the

lower Cr_{max} values result in fewer parameter "jumps" and a smoother change in the estimation process. As well, there tend to be fewer large parameters then there are in the ABKF and MABKF filters. The 24 parameters for the final fullplane portion of the filter are divided among the three graphs in Figure 5.20. The first graph consists of the eight neighbours of the center pixel, while the remaining graphs are the upper left and lower right regions of the filter mask used. These figures indicate that the filter depends more heavily on values outside the nearest neighbours to calculate the smoothed estimate.

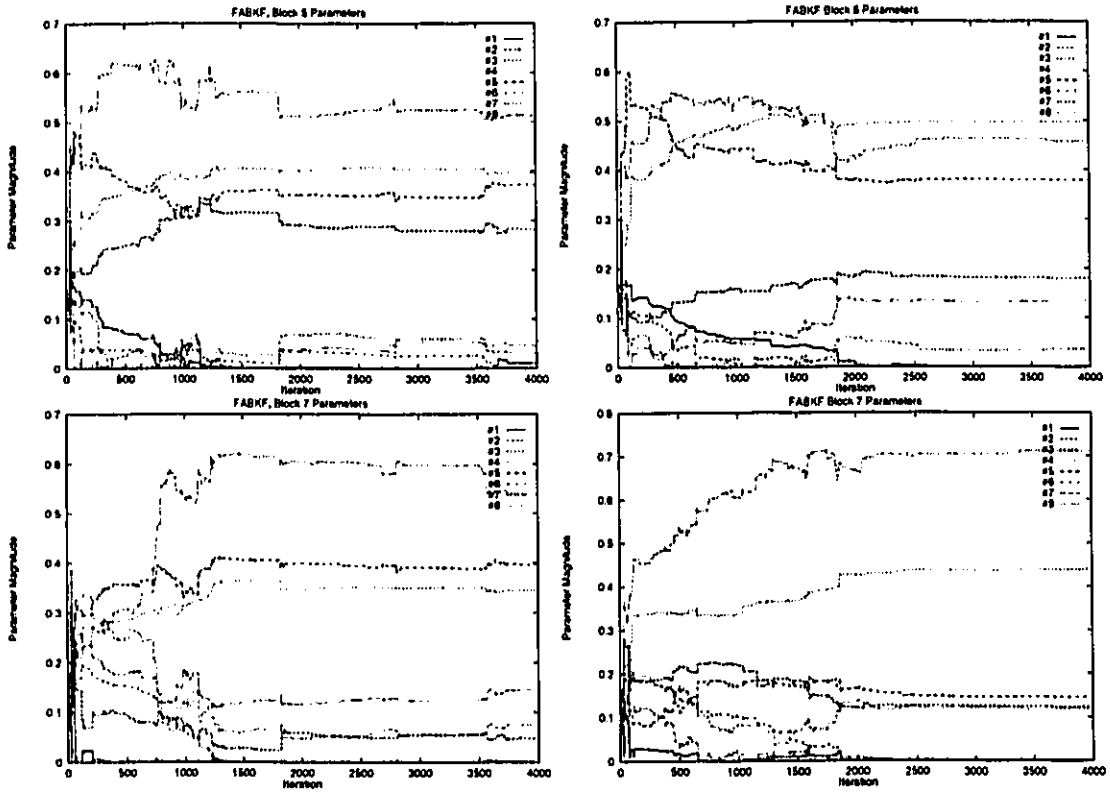

Figure 5.19: Comparison of Parameter Variation in Blocks 5 and 7 of FABKF with varying Cr_{max}. a) $Cr_{max} = 2.5$, b) $Cr_{max} = 2.0$.

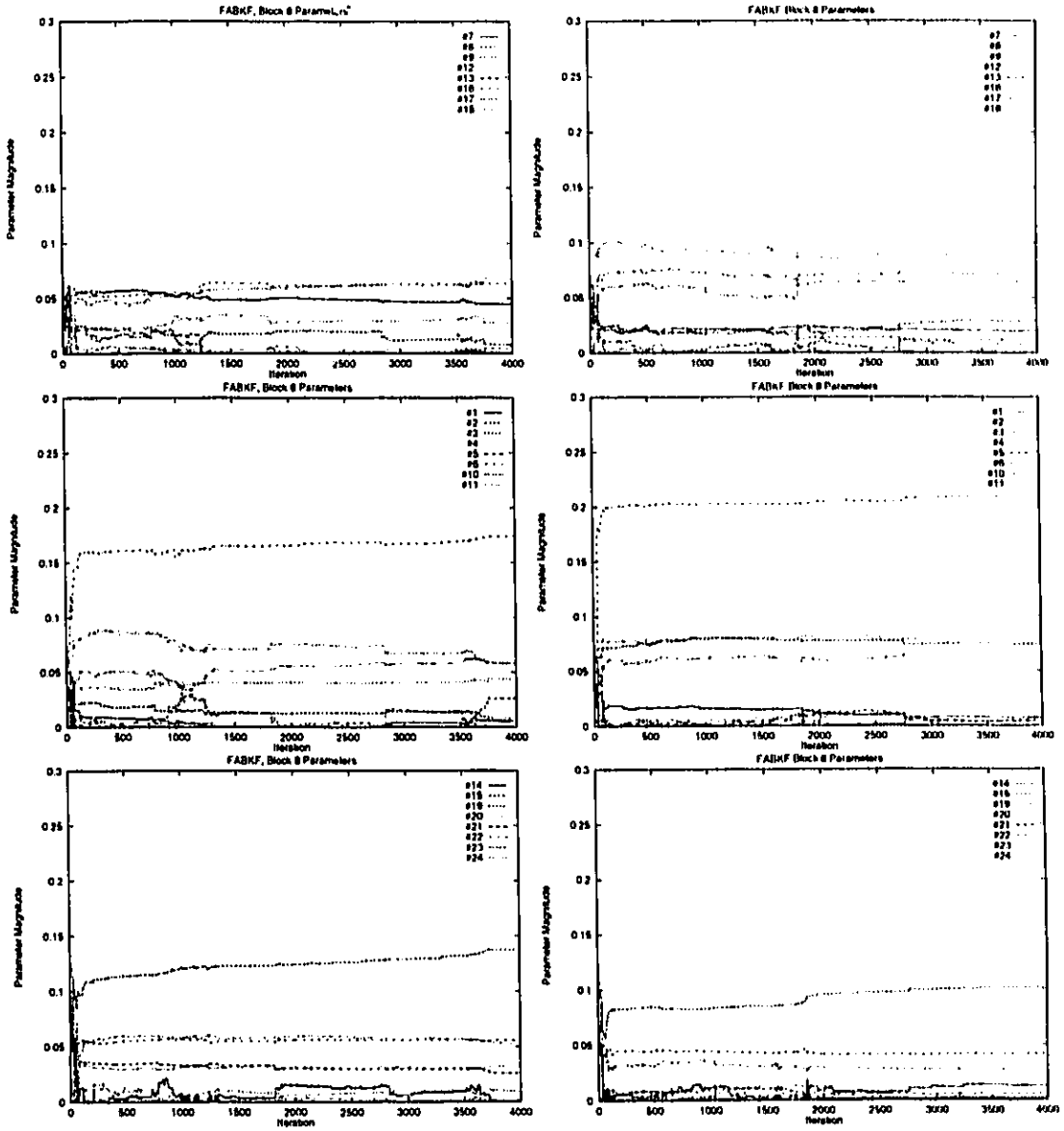

Figure 5.20: Comparison of Parameter Variation in Block 8 of FABKF with varying Cr_{max}. a) $Cr_{max} = 2.5$, b) $Cr_{max} = 2.0$.

5.4 Execution Complexity Issues

An analysis of the filtering issues would not be complete if execution complexity were not addressed. The original ABKF was designed to use special fast convolution techniques in order to reduce computational complexity. For the purpose of evaluating the test filters, these methods were not used. The greatest reduction in the complexity of the ABKF was in the assumption of a steady state Kalman gain value, which removed the requirement to calculate both the Kalman gain and its derivative. Even with the simplification of the filter by using the EKF approximation of the RPE, the MABKF filter is still complex and requires approximately 30 minutes on a Sun Sparcstation 2 for the 256x256 test images used for this thesis. The FABKF has another order of magnitude increase in the filter complexity. As the filter actually consists of four filters, two of which are similar to the MABKF filter, the computational load is overwhelming. Since the FABKF calculates a smaller block than the MABKF(2x2 square vs 3x6 diagonal), the number of iterations to process the same region is greater. The execution time of this filter was approximately five hours on a Sun Sparcstation 2. Efforts could be taken to reduce these times significantly, but the filters would still be orders of magnitude more complex than such filters as the Lee statistical filter. The Lee filter calculates the local mean and variance to determine the filter output while these values are used as inputs to the modified Kalman filters to calculate the much larger covariance and gain matrices. Then these values are used to calculate both the output vector and the new parameter vector for the next iteration of the filter. As well, the Lee filter requires

only the local window to process the image while the NSHP-based filters all require a large history to process the data in two-dimensions.

5.5 Summary of Results

Overviewing the results given in this chapter, several conclusions on the performance of Kalman filtering for SAR can be reached. The use of the quadratic norm criterion severly limits the utility of the Kalman filtering without first preprocessing the image by thresholding the large magnitude statistical outliers. By using the coefficient of variation threshold, Cr_{max}, the Kalman filter can detect point targets, follow sharp edges with a minimum of distortion, and reduce the effect of the remaining outlier values on the parameter estimation process. The selection of a proper forgetting factor is also important. The most effective values have been demonstrated to start at 0.99 for space variant problems, and range up to 1.0 for the spatially invariant problem. Determining the value of the state transistion noise parameter is also critical. In non-homogenous regions such as the Victoria image, a value of σ_u^2 between 10 and 20 times less than the image variance appears to work very well. Overall, the FABKF gives the best performance of all the other tested Kalman filters. It does not suffer from the asymmetric distortion that the NSHP based methods have. In addition, it uses a larger region of support for its estimates, resulting in better statistical support and better filter performance in terms of parameter estimation.

Chapter 6

Conclusions

In this thesis, Kalman filtering methods have been applied to SAR images in order to reduce the speckle noise. Kalman filtering techniques have been applied to SAR imagery before[5]. However, these filters were developed for largely homogeneous images. Images of urban regions and higher resolution images that are becoming possible with newer satellites such as Radarsat and Envisat [56], and more advanced imaging techniques [41], do not preserve the homogeneous regions and the multiplicative noise assumption required by many existing speckle noise filters.

To correct these deficiencies in existing Kalman filters that have been applied to SAR imagery, the derivation of these filters was re-examined and those areas involving incorrect assumptions were addressed. This involved the evaluation of the multiplicative noise assumption during the processing of the image and the detuning of the filter in those regions where the filter assumptions were no longer valid. As

well, the derivation of the parameter estimation technique used was also re-evaluated and modified so that the parameters continue to be adaptive over the entire image. This process led to the development of the modified adaptive block Kalman filter (MABKF) in this thesis.

When applied to complex images such as those involving high intensity urban regions, it was determined that the MABKF gave improvement over the original ABKF. The improvement of the MABKF over the ABKF is evident in very homogeneous regions where the multiplicative noise effect is not present, and over complex scenes where the image changes rapidly due to the presence of strong radar reflectors. The MABKF was also found be be superior in the preservation of strong point targets. Much of the improved response of the MABKF can be attributed to the inclusion of the coefficient of variation test to detune the filter when the filter assumptions were invalid. There is some increase in execution time of the MABKF with respect to the ABKF due to the calculation of the Kalman gain. However, the removal of the calculation of the derivative of the Kalman gain after a predetermined number of iterations reduces this increase greatly without any discernible negative effects on the capability of the filter.

To address the requirement for greater filter flexibility over complex urban regions the image formation model was re-examined. This resulted in the derivation of the Kalman filter equations for a system involving multiplicative noise in the state transition equations and a multiplicative MABKF (MMABKF). The MMABKF filter resulted in greater parameter variation over the image and marginal improve-

ment in the response of the filter when the noise level was exceedingly high. The MMABKF allows greater filter flexibility but may result in filter instability in some cases. Overall, the performance of the MMABKF was slightly better in complex urban regions offering some improvement in contrast. As well, the difficulty in determining an acceptable value for σ_ψ precludes easy usage of this form of the Kalman filter.

The primary problem with the Kalman filters based on the non-symmetric half plane region of support was asymmetric distortions. Both the MABKF and ABKF suffer from asymmetric distortion of the image due to block effects when strong reflectors are encountered in the image. This issue was addressed by the conversion of a non-adaptive full plane region of support Kalman filter into an adaptive Kalman filter similar in form the the MABKF. This FABKF filter was the combination of three casual Kalman filters feeding a fourth semi-causal full-plane Kalman filter. Although this filter was much more complicated than the MABKF, the FABKF gave much better performance than all the other Kalman filters examined in this thesis and did not suffer from the asymmetric distortions attributed to those filters.

In comparing the results of these filters with the Lee statistical filter it is seen that improvements are seen near edges and strong reflectors such as the two point targets that are located in the harbour that are blurred by the Lee filter as shown in Figure 2.5. However, if the modified Lee filter proposed by Lopes et al. [40] is used as a comparison, the point targets are resolved separately. Due to the greater simplicity of the modified Lee filter, it would be better suited for routine use for

speckle reduction on SAR imagery. However, as SAR images become more complex at higher resolutions, methods such as those defined here may have greater utility.

6.1 Summary of Contributions

As a summary of the above conclusions, the contributions of this thesis are:

- The development of a modified adaptive block Kalman filter encorporating local statistics measures to further control filter behaviour. This MABKF filter was shown to perform better than the ABKF on complex SAR images such as urban regions.
- The derivation of the Kalman filter and parameter estimation equations for a state transition equation including multiplicative state transition noise. This enhanced the ability of the Kalman filter to follow the variations common in SAR images of complex urban environments while having a reduced effect on homogeneous regions.
- The adaptation of the modified adaptive block Kalman filtering paradigm to an auto-regressive process utilizing a full plane region of support. The use of a Kalman filter based on a full plane model removed the asymmetric distortions encountered when using Kalman filters based on non-symmetric half plane models. This resulted in improved results over the other Kalman filters developed in this thesis.

6.2 Further Work

In the implementation of these filters, many options presented themselves that were not taken. These include a modified parameter estimation scheme, speed optimization of the full plane filter, statistical estimation of the multiplicative noise parameters, and statistical estimation of the additive noise in the state equations.

The parameter estimation scheme used in the development of the Kalman filters in this thesis is based on the recursive parameter estimation(RPE) technique by Ljung and Söderström [37]. This system offered such advantages as fast and enforced convergence of the parameters. However, the method requires the determination of an approximation of the gradient of the Kalman filter which is computationally expensive. Tekalp et al. [52] developed a fast implementation of an extended Kalman filter for parameter estimation for the reduced update Kalman filter(RUPK) developed by Woods et al. [60]. This system used reduced memory and calculated the parameter vector in a much less complicated manner than the the RPE. There is some promise in improved speed performance if such a method were adapted to the MABKF or FABKF.

The full-plane adaptive block Kalman filter, used the semi-causal full-plane model developed by Azimi-Sadjadi and Bannour[11]. The original derivation used constant parameters for all filters based on *a priori* determination of the filter parameters. Thus the filter was not optimized for fast parameter estimation. Future work could concentrate on rearranging the input vectors and the associated param-

eters so that faster techniques such as those given in [1] and [43] could be used. As well, the filter problem could be rearranged so that scalar operations could be used rather than the matrix operations for this thesis.

In implementing the modified Kalman filters, the value of the multiplicative noise variance, $\sigma_{\gamma\ i,j}$, is calculated *a priori* based on the assumed statistics of the image given its formation, ie. intensity or amplitude image and the number of looks. This value is then modified using a linear decay function based on the validity of the multiplicative noise function. A more accurate means of modeling the image would be to use statistical measures to determine the multiplicative noise parameter, $\sigma_{\gamma\ i,j}$, locally within the image as it is processed. A model for this determination is currently being investigated as a subject in a Ph.D. thesis by K.B. Fung and may result in further improvements.

Recalling the evaluation of the Kalman filter output for the Victoria BC image in Section 5.3.1, it is seen that a value of σ_u^2 that gives the desired results for a medium intensity region over-smoothes in high intensity regions. This implies that an adaptive additive noise parameter in the state transition equation (6.1) would be desirable. This value could also be used so that the multiplicative noise term used in the MMABKF would not be necessary as the noise in the Ψ term could be encorporated into the adaptive $U_{i,j}$ term as in (6.2) [45].

$$X_{i,j} = \mathbf{A}_0\Psi\mathbf{X}_{i,j-1} + \mathbf{A}_1\Psi\mathbf{X}_{i-1,j} + \mathbf{B}\mathbf{U}_{i,j} \tag{6.1}$$

$$\mathbf{U}_{i,h} = U_{i,j} + (\Sigma_k A_k \Psi_k X_k)_{i,j} \tag{6.2}$$

Tekalp et al. approached this problem, by deriving, *a priori*, the steady state Kalman gain values required for eight different edge models [53] and applying the model which best fit the data at each point. A texture parameter is defined, T, that is dependent on the local image statistics. As the image statistics change, the value of T is modified to allow the state dynamic noise, U, to be modified.

Another approach to this problem is to calculate the U_i, j term based on the local image statistics and the history of the Kalman filter. This approach is being investigated as a subject in a Ph.D. thesis by K.B. Fung.

A suggestion for much more complicated work is the application of Kalman filtering to process polarimetric SAR images. Polarimetric radars record multiple polarizations of the radar beam and can give more information for the same region of image space [61]. Much current work is going into the development of such polarimetric radars, the SIR-C/X SAR used by the shuttle program being the latest example. Kalman filtering could be used to greatly enhance such SAR images as they become more prevalent.

Bibliography

[1] R.C. Agarwal and J.W. Cooley. New algorithms for digital convolution. *IEEE Transactions on Acoustics, Speech, and Signal Processing*, ASSP-25(5):392-410, October 1977.

[2] B.D.O. Anderson and J.B. Moore. *Optimal Filtering*. Information and Systems Science Series. Prentice-Hall, Inc., Englewood Cliffs, N.J., 1979.

[3] H.H. Arsenault and M. Levesque. Combined homomorphic and local-statistics processing for restoration of images degraded by signal-dependent noise. *Applied Optics*, 23(6):845–850, March 1984.

[4] M.R. Azimi-Sadjadi. Speckled image restoration by adaptive block Kalman filtering. In *Proceedings of IGARSS 87 Symposium*, pages 1449–1455, Ann Arbor, Michigan, May 18-21 1987.

[5] M.R. Azimi-Sadjadi and S. Bannour. Two dimensional adaptive block Kalman filtering of SAR imagery. *IEEE Transactions on Geoscience and Remote Sensing*, 29(5):742–753, September 1991.

[6] M.R. Azimi-Sadjadi and S. Bannour. Two-dimensional recursive parameter identification for adaptive Kalman filtering. *IEEE Transactions on Circuits and Systems*, 38(9):1077–1081, September 1991.

[7] M.R. Azimi-Sadjadi and R.A. King. Two-dimensional block processors: Structures and implementations. *IEEE Transactions on Circuits and Systems*, CAS-33(1):42–50, January 1986.

[8] R. Bellman. *Introduction to Matrix Analysis.* McGraw-Hill Book Company, Toronto, Canada, second edition, 1970.

[9] K. R. Carver, C. Elachi, and F. T. Ulaby. Microwave remote sensing from space. *Proceedings of the IEEE*, 73(6):970–994, June 1986.

[10] R.G. Caves, P.J. Harley, and S. Quegan. Edge structure in ERS-1 and airborne SAR data. In *Proceedings of IGARSS 92 Symposium*, pages 1117–1119, Houston, Texas, May 26-29 1992.

[11] S. Citrin and M.R. Azimi-Sadjadi. A full plane block Kalman filter for image restoration. *IEEE Transactions on Image Processing*, 1(4):488–495, October 1992.

[12] T.R. Crimmins. Geometric filter for speckle reduction. *Applied Optics*, 24(10):1438–1443, May 1985.

[13] John C. Curlander and Robert N. McDonough. *Synthetic Aperture Radar: Systems and Signal Processing.* John Wiley & Sons, Inc, 1991.

[14] F. Dewaele, P. Wambacq, and A. Oosterlinck. Comparison of some speckle reduction techniques for SAR images. In *Proceedings of IGARSS 90 Symposium*, pages 2417–2422, College Park, Maryland, May 20-24 1990.

[15] J.M. Durand, B.J. Gimonet, and J.R. Perbos. SAR data filtering for classification. *IEEE Transactions on Geoscience and Remote Sensing*, GE-25(5):629 637, September 1987.

[16] V.S. Frost, J.A. Stiles, K.S. Shanmugan, and J.C. Holtzman. A model for radar images and its application to adaptive digital filtering of multiplicative noise. *IEEE Transactions on Pattern Analysis and Machine Intelligence*, PAMI-4(2):157–165, March 1982.

[17] G. Geling and D. Ionescu. An edge detection operator for SAR images. In *Proceedings of CCECE 93*, pages 707–709, Vancouver, Canada, September 14-17 1993.

[18] G. Geling and D. Ionescu. A Kalman filter for speckle reduction in SAR data. In *Proceedings of CCECE 94*, pages 405–408, Halifax, Canada, September 24-27 1994.

[19] J.W. Goodman. Some fundamental properties of speckle. *Journal of the Optical Society of America*, 66(11):1145–1149, Nov. 1976.

[20] M.S. Grewal and A.P. Andrews. *Kalman Filtering: Theory and Practice*. Prentice Hall, Englewood Cliffs, New Jersey, 1993.

[21] A. Habibi. Two-dimensional bayesian estimate of images. *Proceedings of the IEEE*, 60(7):878–883, July 1972.

[22] A. Hendry, S. Quegan, and J. Wood. The visibility of linear features in SAR images. In *Proceedings of IGARSS 88*, pages 1517–1520, Edinburgh, U.K., Sept 12-16 1988.

[23] D. Ionescu and G. Geling. Automatic detection of large object features from SAR data. In *Proceedings of IGARSS 93 Symposium*, pages 1225–1227, Tokyo,Japan, August 18-21 1993.

[24] Bernd Jähne. *Digital Image Processing: Concepts, Algorithms, and Scientific Applications*. Springer-Verlag, Berlin,Germany, 1991.

[25] A.K. Jain. *Fundamentals of Digital Image Processing*. Prentice-Hall, Englewood Cliffs, New Jersey, 1989.

[26] H. Kaufman, J.W. Woods, S. Dravida, and A. M. Tekalp. Estimation and identification of two-dimensional images. *IEEE Transactions on Automatic Control*, AC-28(7):745–756, July 1983.

[27] D.T. Kuan, A.A. Sawchuk, T.C. Strand, and P. Chavel. Adaptive noise smoothing filter for images with signal dependent noise. *IEEE Transactions on Pattern Analysis and Machine Intelligence*, PAMI-7(2):165–177, March 1985.

[28] D.T. Kuan, A.A. Sawchuk, T.C. Strand, and P. Chavel. Adaptive restoration of images with speckle. *IEEE Transactions on Acoustics, Speech, and Signal Processing*, ASSP-35(3):373–383, March 1987.

[29] J.E. Kurek. The general state-space model for a two-dimensional linear digital system. *IEEE Transactions on Automatic Control*, AC-30(6):600–602, June 1985.

[30] J. S. Lee. Refined filtering of image noise using local statistics. *Computer Graphics and Image Processing*, 15:380–389, 1981.

[31] J. S. Lee and I. Jurkevich. Coastline detection and tracing in SAR images. *IEEE Transactions on Geoscience and Remote Sensing*, 28(4):662–668, July 1990.

[32] J.S. Lee. Digital image enhancement and noise filtering by use of local statistics. *IEEE Transactions on Pattern Analysis and Machine Intelligence*, PAMI 2(2):165–168, March 1980.

[33] J.S. Lee. A simple speckle smoothing algorithm for synthetic aperture radar images. *IEEE Transactions on Systems, Man, and Cybernetics*, SMC-13(1):85–89, Jan/Feb 1983.

[34] J.S. Lee. Speckle suppression and analysis for synthetic aperture radar images. *Optical Engineering*, 25(5):636–643, May 1986.

[35] J.S. Lee and I. Jurkevich. Segmentation of SAR images. *IEEE Transactions on Geoscience and Remote Sensing*, 27(6):674–680, November 1989.

[36] J.S. Lee, I. Jurkevich, P. Dewaele, P. Wambacq, and A. Oosterlinck. Speckle filtering of synthetic aperture radar images: A review. *Remote Sensing Reviews*, 8:313–340, 1994.

[37] L. Ljung and T. Söderström. *Theory and Practice of Recursive Identification.* MIT Press, Cambridge, Massachussetts, 1983.

[38] A. Lopes, E. Nezry, R. Touzi, and H. Laur. Maximum a posteriori filtering and first order texture models in SAR images. In *Proceedings of IGARSS 90 Symposium*, pages 2409–2412, College Park, Maryland, May 20-24 1990.

[39] A. Lopes and R. Touzi. Adaptive speckle filtering for SAR imagery. In *Proceedings of IGARSS 88 Symposium*, volume 3, pages 1263–1266, Edinburgh Scotland, September 13-16 1988.

[40] A. Lopes, R. Touzi, and E. Nezry. Adaptive speckle filters and scene heterogeneity. *IEEE Transactions on Geoscience and Remote Sensing*, 28(6):992–1000, November 1990.

[41] D.L. Mensa. *High Resolution Radar Imaging.* Artech House Inc., Norwood, Mass., 1981.

[42] E. Nezry, A. Lopes, and D. Ducros-Gambart. Supervised radiometric and textural segmentation of SAR images. In *Proceedings of IGARSS 93 Symposium*, pages 1426–1428, Tokyo,Japan, August 18-21 1993.

[43] H.J. Nussbaumer and P. Quandalle. Computation of convolutions and discrete fourier transforms by polynomial transforms. *IBM Journal of Research and Development*, 22(2):134–144, March 1978.

[44] A. Papoulis. *Probability, Random Variables, and Stochastic Processes.* McGraw-Hill Inc, New York, third edition, 1991.

[45] Y.A. Phillis. Estimation and control of systems with unknown covariance and mulitplicative noise. *IEEE Transactions on Automatic Control*, 34(10):1075-1078, October 1989.

[46] H.Ch. Quelle and J.M. Boucher. Combined use of parametric spectrum estimation and frost algorithm for radar speckle filtering. In *Proceedings of IGARSS 90 Symposium*, pages 295–297, College Park, Maryland, May 20-24 1990.

[47] R.K. Raney and G.J. Wessels. Spatial considerations in SAR speckle simulation. *IEEE Transactions on Geoscience and Remote Sensing*, GE-26(5):666–672, September 1988.

[48] R. P. Roesser. A discrete state-space model for linear image processing. *IEEE Transactions on Automatic Control*, AT-20(1):1–10, February 1975.

[49] R. Samadani and J.F. Vesecky. Finding curvilinear features in speckled images. In *Proceedings of IGARSS 89 Symposium*, pages 1198–1202, Vancouver, Canada, July 10-14 1989.

[50] Zhenghao Shi and K.B. Fung. A comparison of digital speckle filters. In *Proceedings of IGARSS 94 Symposium*, pages 10–11, Pasadena, California, August 1994.

[51] E.R. Sudibjo, G.D. Lodwick, and S.H. Paine. Digital enhancement of STAR-1 SAR imagery for linear feature extraction. In *Proceedings of IGARSS 89*, pages 2242–2245, Vancouver, Canada, July 10-14 1989.

[52] A.M. Tekalp, H. Kaufman, and J.W. Woods. Fast recursive estimation of the parameters of a space-varying autoregressive image model. *IEEE Transactions on Acoustics, Speech, and Signal Processing*, ASSP-33(2):469–472, April 1985.

[53] A.M. Tekalp, H. Kaufman, and J.W. Woods. Edge-adaptive Kalman filtering for image restoration with ringing suppression. *IEEE Transactions on Acoustics, Speech, and Signal Processing*, ASSP-37(6):892–899, June 1989.

[54] R. Touzi, A. Lopes, and P. Bousquet. A statistical and geometrical edge detector for SAR images. *IEEE Transactions on Geoscience and Remote Sensing*, 26(6):764–773, Nov 1988.

[55] F. T. Ulaby, R. K. Moore, and A.K. Fung. *Microwave Remote Sensing: Active and Passive*, volume III, from theory to applications. Artech House Inc., Dedham, Maryland, 1986.

[56] A. Wilson, editor. *Jane's Space Directory, 1994-1995.* Jane's Information Group Limited, Surrey, U.K., tenth edition, 1994.

[57] J.W. Woods. Correction to "Kalman filtering in two dimensions". *IEEE Transactions on Information Theory*, IT-25(5):628, September 1979.

[58] J.W. Woods and J. Biemond. Comments on "A model for radar images and its application to adaptive digital filtering of multiplicative noise". *IEEE Transactions on Pattern Analysis and Machine Intelligence*, PAMI-6(5):658–659, September 1984.

[59] J.W. Woods and V.K. Ingle. Kalman filtering in two dimensions: Further results. *IEEE Transactions on Acoustics, Speech, and Signal Processing*, ASSP-29(2):188–197, April 1981.

[60] J.W. Woods and C.H. Radewan. Kalman filtering in two dimensions. *IEEE Transactions on Information Theory*, IT-23(4):473–482, July 1977.

[61] Howard. A. Zebker and Jakob J. vanZyl. Imaging radar polarimetry: A review. *Proceedings of the IEEE*, 79(11):1583–1606, November 1991.

[62] Jin Yun Zhang and William Steenaart. High speed Kalman filtering for image restoration. *SPIE Visual Communications and Image Processing IV*, 1199:125-135, 1989.